SOUND GENERATION BY FLOW OVER MULTIPLE SHALLOW CAVITIES

Sound Generation By Flow Over Multiple Shallow Cavities

By

AYMAN SHAABAN, M.SC.

A Thesis

Submitted to the School of Graduate Studies

In Partial Fulfillment of the Requirements

for the Degree

Doctor of Philosophy

McMaster University

DOCTOR OF PHILOSOPHY (2018) McMaster University

(Mechanical Engineering) Hamilton, Ontario, Canada

TITLE: Sound Generation By Flow Over Multiple Shallow Cavities

AUTHOR: Ayman Shaaban, M.Sc. (Cairo University)

SUPERVISOR: Professor Samir Ziada

NUMBER OF PAGES: xxiii, 186

ABSTRACT

Corrugated pipes are widely used in offshore gas and oil fields for their flexibility while offering local rigidity. However, self-sustained pressure pulsations associated with the flow in corrugated pipes results in a noisy environment, high running costs and eventually structure fatigue failure upon long exposure. Recent literature has addressed either the flow over a single cavity or the global oscillations. The current research aims at understanding the flow over multiple cavities as a first step to correlate the rich single cavity literature and the actual corrugated pipe problem with the ultimate goal of predicting oscillations amplitude in corrugate pipes.

The standing wave method (SWM), which is an efficient experimental tool, has been successfully adapted in the first phase of the project to measure the source of multiple cavity configurations. One, two and three-cavity configurations have been investigated by means of the SWM. The source non-linearly becomes more pronounced as the number of cavities increases. The cavity length (L) is still found to be the appropriate length scale to define the oscillation dimensionless frequency (the Strouhal number). The measured source data have been successfully employed in a semi-empirical model to predict the amplitude of the self-excited oscillations. Accurate model performance is achieved for the single, double and triple cavity configurations. Including the absorption losses at the cavity corners has been found to be crucial for the model prediction accuracy.

The separation distance (L_p) effect on the generated source is investigated for two and three-cavity configurations using the SWM over a practical range of

spacing ratios. At extremum spacing ratios of (L_p/L) 0.5 and 1.375, constructive hydrodynamic interference associated with strong sources has been observed. At high excitation levels the source consistently becomes weaker upon increasing the spacing ratio. The reported trends are consistent for both the double and triple cavity configurations. However, the destructive interference spacing ratio is found to depend on the number of cavities indicating a relatively more complicated interaction mechanism. The different interaction patterns have been analytically interpreted based on the synchronization of the hydrodynamic cycle of the cavity shear layer and the disturbance convection along the pipe spacing between the cavities. Moreover, the three-cavity constructive interference cases have been visualized using Particle Image Velocimetry (PIV). The source evaluated based on the PIV data and applying Howe's analogy revealed each cavity share of the global source, which fairly agrees with the SWM measured source.

The source contribution due to gradually increasing the number of cavities is investigated using the SWM up to a six-cavity configuration. The source contribution reaches asymptotically a consistent value starting from the fourth cavity. This persistent contribution defines a building unit cavity source which is representative of a general cavity in a long corrugated pipe. The building unit source fairly agrees with the ninth-cavity source in a twelve-cavity configuration extracted by means of the PIV technique. Finally, a predication model, based on the building unit source, successfully predicts the oscillations amplitude of a twelve-cavity configuration, which serves as a model for a corrugated pipe section.

ACKNOWLEDGEMENTS

Firstly, I would like to thank Almighty ALLAH, whom I owe everything, for His generousness and support through all my life.

I would like to extend my gratitude for my supervisor and mentor Prof. Samir Ziada for his unremitting co-operation and guidance throughout the PhD journey. He has always been available providing technical support and precious advice. I am also very grateful to my committee members Dr. Arthurs and Dr. Tullis for their constructive feedback and fruitful suggestions during the research.

I am very grateful to the whole aeroacoustic research group who created a friendly environment for ultimate productivity and offered aid whenever required. I would like to thank Saber for the technology transfer in the early phase of the project. The machine-shop technicians; Ron, Michael, John, Mark, Joe and Dan, provided very insightful consultations while developing the experimental facility. I would like also to thank the mechanical engineering staff for all the administrative assistance they offered throughout the program.

Finally, words fall short to express how grateful I am to my parents who encouraged me to travel to Canada and pursue my PhD. Their support never stopped while inspiring me to achieve my goals. I would like to thank my brother and sister as well, and wish them all the best in their bright future life.

NOMENCLATURE

A	Pipe cross-sectional area (m^2)
a, R_{pipe}	Pipe radius (m)
c	Speed of sound (m/s)
D	Pipe diameter (m)
f	Resonance frequency (Hz)
H	Cavity depth (m)
I	Inductance upon area change (Pa s/m^3)
k	Wave number (m^{-1})
L	Cavity length (m)
L_p	Separation plateau distance between cavities (m)
M	Mach number
P	Acoustic pressure (Pa)
ΔP	Acoustic pressure difference across the cavity section (Pa)
Q	Acoustic flux (m^3/s)
R	Acoustic wave reflection coefficient
S	Normalized aeroacoustic source

S_{loss}	Normalized aeroacoustic loss or sink term
St	Strouhal number based on the cavity length
St_a	Strouhal number based on the pipe radius
St_θ	Strouhal number based on the momentum thickness
U	Flow velocity (m/s)
v	Acoustic particle velocity (m/s)
Y_0	Characteristic acoustic impedance (Pa s/m^3)
ΔZ	Acoustic impedance difference across the cavity section (Pa s/m^3)
Z_{abs}	Absorption impedance loss at the cavity edges (Pa s/m^3)
ρ_0	Air density (kg/m^3)
α	Pipe diameter ratio
λ	Area change ratio
θ	Momentum boundary layer thickness (m)
ω	Flow vorticity (1/s)
β	Complex wave number (m^{-1})
Π	Acoustic power (W)
Π_{loss}	Acoustic power losses (W)

TABLE OF CONTENTS

LIST OF FIGURES

LIST OF TABLES

CHAPTER 1
INTRODUCTION

1.1 Self-sustained Oscillations

Self-sustained oscillations are instabilities which are capable of maintaining themselves upon occurrence through a closed loop feedback mechanism. Oscillations in pipe flows can pose potential danger and eventually lead to system failure. Several recent incidents have been reported in various industrial applications because of self-excited oscillations produced in piping systems. Lafon et al. (2003) investigated tonal noise and excessive vibration of a steam pipeline in a nuclear power station caused by a fully open gate valve. The noise was found to be similar to that generated by flow over cavities. A similar phenomenon had been reported earlier by Ziada et al. (1989) who studied tonal noise generation by control valves.

Steam pipe failure in Gentilly Nuclear Power Station was caused by acoustic fatigue as reported by Michaud et al. (2001), where several cracks were observed in the steam dump piping system. Control valve acoustic excitation at high frequencies was found to be the main cause of this problem and modification of the valve stem design reduced the dynamic stresses below the fatigue limit. In a recent review by Ziada and Lafon (2014), acoustic resonance in the standpipes of relief valves was found to be the cause of the steam dryer failure in Quad Cities nuclear

power plant according to the incident report by the US Nuclear Regulatory Commission (NRC) (2002) and the investigation by DeBoo et al. (2007).

Corrugated pipes represent a typical industrial example of free shear layer flows inside ducts. Corrugated pipes are commonly used in offshore gas fields because of their global flexibility while offering high stiffness as a result of the corrugations. The corrugations can be modelled as a series of consecutive shallow cavities. Belfroid et al. (2007) stated that acoustic pressure pulsations in corrugated pipes used in high pressure gas installations may attain a value in the order of bars. This is clearly a serious issue regarding the system integrity upon long exposure time. The high noise level also contributes to a poor working environment. Moreover, the energy consumed in sustaining the acoustic resonance adds to the hydrodynamic losses upon pumping the fluid in corrugated pipes which is already substantial when compared with regular ducts (Stel et al., 2010; Popiel et al., 2013).

1.2 Scope of the Work

Recent literature on corrugated pipes oscillations focused on understanding the phenomenon by investigating either the global system oscillations or the sound generation by a single cavity. Limited research addressed the flow over multiple cavities and the hydrodynamic interaction that occurs between them as an essential link to comprehend the global oscillations of corrugated pipes in terms of individual cavity contributions. The current research is concerned with investigating the flow over multiple cavities and the corresponding acoustic power generated and how it

can eventually be used to predict the oscillations amplitude of actual corrugated pipes.

Quantifying the acoustic power generated as a result of the flow-sound interaction is a vital tool in the design stage of a piping system housing cavities. Knowing the acoustic power expected to be generated and through proper modelling of the system, resonance conditions can be detected together with the expected amplitude of pressure pulsation. This is necessary to judge whether these resonance conditions lie within the system operating range, and if so, assess whether the pulsation amplitude can be tolerated or design modifications should be considered. The current investigation relies on the standing wave method (SWM) which has been proven to be an efficient experimental methodology to measure the acoustic power generated by cavity configurations. The method is based on analyzing the acoustic standing wave in the duct and measuring the acoustic pressure discontinuity as a result of the cavity aeroacoustic compact source.

The current study investigates at first the non-linear growth of the aeroacoustic source associated with multiple cavity configurations. This early phase of the project adapted the SWM for multiple-cavity configurations and highlighted the existence of hydrodynamic coupling between the neighbouring cavities. Prediction models are developed, which utilize the measured source data, to estimate the amplitude of self-excited oscillations in piping systems housing multiple cavities. The effect of the separation distance between consecutive cavities

is investigated augmented with flow visualizations to help understanding the hydrodynamic interaction mechanism. The separation distance is a new parameter distinctive to multiple cavity configurations and plays an essential role whether the hydrodynamic coupling being constructive or destructive. Eventually, the source behaviour when increasing the number of multiple cavities is assessed until the source strength reaches a fully developed state defining a building unit cavity source. The building unit source is validated by comparison with a general downstream cavity source extracted using Particle Image Velocimetry (PIV). The building unit source is then employed in a model to predict the pressure pulsation amplitude for long multiple-cavity section, as a model for a corrugated pipe.

1.3 Thesis Outline

This thesis is prepared in a sandwich thesis format encompassing three journal publications. **Chapter 2** presents a detailed literature review covering the basic phenomenon of free shear layer instability with the main focus on cavity flows. Different approaches to estimate the aeroacoustic source, numerically and experimentally, are discussed. Recent research investigating corrugated pipes along with the limited research on multiple cavities is also presented and the chapter is concluded with the current research proposal.

Chapter 3 investigates the aeroacoustic source of one, two and three-cavity configurations using the SWM. The source trends are compared with the general characteristics of the measured self-excited resonance of corresponding multiple

cavity configurations. A semi-empirical prediction model is developed based on the measured source to estimate the amplitude of the self-excited oscillations. This is an essential step which proves the applicability of the measured source to another cavity in a piping system different from the one used to measure the source.

Chapter 4 assesses the effect of the separation distance on the source of multiple cavities. The separation distance is a new geometrical parameter associated with multiple cavity configurations that was by default absent in the single cavity studies. Both double and triple cavity configurations are tested over a practical range of separation distances using the SWM. The hydrodynamic interference is further investigated by flow visualization using PIV technique.

Chapter 5 investigates the development of individual cavity source as the number of cavities is increased in multiple cavity configurations. The tested cases include up to a six-cavity configuration tested using the SWM seeking the fully developed source contribution per added cavity, i.e. building unit cavity source. The building unit cavity source is compared with the source obtained by PIV method for a downstream cavity in a long multiple-cavity section. A prediction model, based on the building unit cavity source, is then developed to predict the oscillations amplitude of a twelve-cavity configuration.

Chapter 6 summarizes the work that has been accomplished in the current research project and the corresponding conclusions that have been drawn. The

chapter aims at tying the work together and emphasizing the novel contributions achieved. Moreover, suggestions for potential future work are included.

1.4 Note to the Reader

As a result of the sandwich thesis format, an overlap is inevitable in the introduction and experimental setup sections of each paper presented in chapters 3 – 5. Thus, a separate chapter on literature review is included, as pointed earlier in the thesis outline, which should be sufficient to provide the reader with a comprehension of the relevant literature with even more details as compared to the concise introduction of the papers. However, the reader is still encouraged to read the introduction of each paper as it is tailored towards its topic and specifically the last paragraph that illustrates the scope of each publication. Also, the last paragraph of the experimental setup of each paper is distinctive as it describes the relevant experimental matrix that has been accomplished during the investigation.

CHAPTER 2
LITERATURE REVIEW

In this chapter, a literature survey is conducted aiming at shedding light on the current understanding of the acoustic oscillations of ducted shallow cavities and corrugated pipes. First, the basic phenomenon of free shear layer instability is introduced along with the disturbances growth mechanism. Focus is then dedicated to the self-sustained oscillations associated with flow over cavities with more attention directed towards fluid resonant oscillation, which is the category that encompasses oscillations in corrugated pipes. Different approaches to estimate the generated aeroacoustic source, both numerically and experimentally, are described in details while reflecting their corresponding advantages and limitations. Moreover, recent research on different geometries and configurations of corrugated pipes is addressed. Eventually, the limited research effort which investigated the flow over multiple cavities, as a model for corrugated pipes, is presented. At the end of this chapter, the current research proposal is summarized, stating the main objectives.

2.1 Basic Phenomenon

2.1.1 Shear Layer Instability

Flow over ducted cavities represents an example of free shear layer flows. The free shear layer is situated after the boundary layer separation and mixing

occurs between the main flow in the duct and the stagnant flow within the cavity. Jet flows and flows over valves, orifices and pipe closed side-branches are other common examples of free shear layer flows. The instability of free shear layers was first addressed in the 19th century by Rayleigh (1879). Michalke (1965) developed a linearized inviscid spatial growth model of disturbances in free shear layers based on the two-dimensional Helmholtz vorticity equation. The model is linearized as it deals only with small disturbances at the early stages of its growth. Neglecting the viscosity was justified by the findings of Freymuth (1966) where the disturbance data gathered from a jet free shear layer collapsed for different values of Reynolds number. Michalke (1965) performed the stability analysis for a hyperbolic-tangent velocity profile. The choice of the velocity profile was justified by being analogous to jet flows and also the presence of an inflection point as a sufficient condition for flow instability. The computed spatial growth rates agreed with the experimental values of Freymuth as shown in Figure 2.1. For high values of Strouhal number based on the momentum thickness ($St_\theta = f\theta/U$), the spatial model failed to predict the growth rates accurately. This was attributed to the fact that in this frequency range, the linear region is very limited after the leading edge and the non-linearity effects dominate. One interesting phenomenon is that the disturbance growth rate strongly depended on the oscillation frequency and there should be a characteristic frequency where maximum amplification would occur. The experiments done by Freymuth failed to excite the jet at high values of Strouhal numbers (above 0.025) as predicted theoretically.

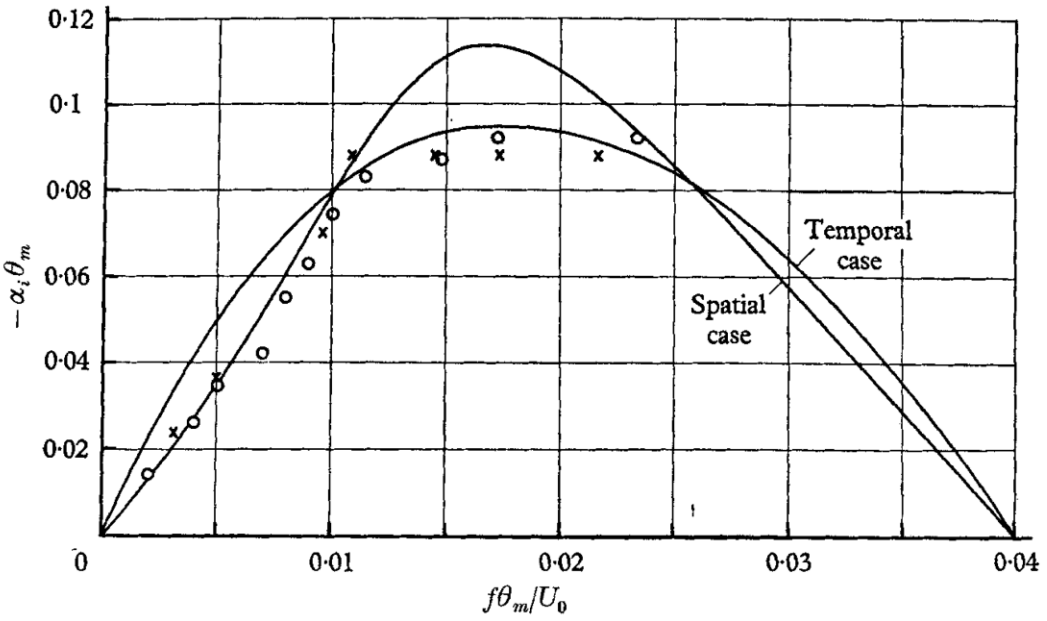

Figure 2.1. Disturbance growth rate vs. Strouhal number: ○, axisymmetric nozzle; x, plane nozzle (Freymuth, 1966)

Miksad (1972) performed an experimental study on the growth of free shear layer instabilities. At first, the disturbance followed exponential growth agreeing with the linearized model previously discussed at the fundamental frequency. As the disturbance propagates spatially, harmonics and subharmonics starts to appear and grow exponentially. The fundamental mode growth rate starts to deviate from the exponential behaviour at disturbance amplitudes in the order of 10^{-2} of the mean flow velocity. The disturbance then non-linearly saturates at a certain downstream distance and afterwards decays and coherent vortical structures start to roll. Eventually the structures breakdown into three-dimensional turbulence and transition is completed. No phase relationship at this point could be established with the upstream flow.

2.1.2 Flow over Cavities

Flow over cavities includes an interaction between the free shear layer and the cavity walls, i.e. flow-structure interaction. Rockwell and Naudascher (1978) classified oscillations of fluid flows past cavities into three main categories: fluid dynamic, fluid elastic and fluid resonant oscillations. For all these three categories, the instability of the free shear layer must be maintained by means of a feedback loop. The feedback, in all the different categories, sustains an initial instability for the free shear layer. The growth of the hydrodynamic instability in return transfers energy to the feedback element and thus self-sustaining oscillations can occur. The close feedback look is depicted in Figure 2.2.

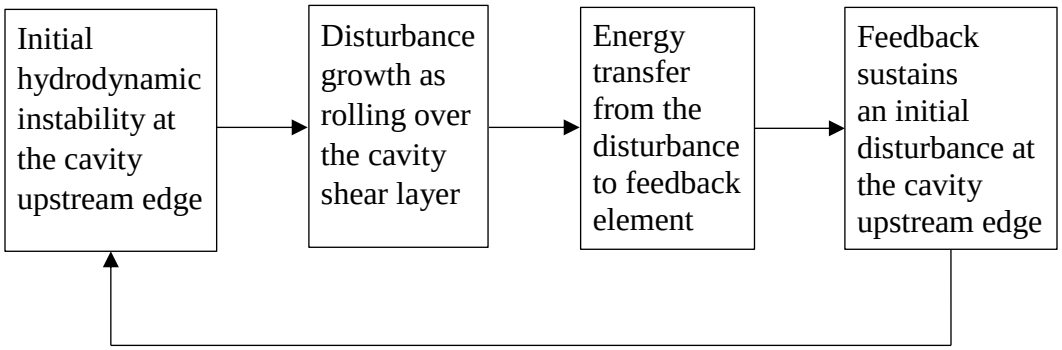

Figure 2.2. Schematic of the closed feedback look for cavity self-sustained oscillations

In the case of fluid dynamic oscillations, the flow impingement on the downstream edge of the cavity provides the feedback role, where the acoustic characteristics are analogous to that of the jet-edge impingement. A back pressure wave, as a result of impingement, travels upstream to disturb the free shear layer at the upstream corner of the cavity. The presence of the cavity downstream edge and its geometry crucially affects the oscillations of the fluid dynamic category. The

associated oscillation wavelength is usually much longer than the cavity wave length (e.g. Rockwell, 1977).

The second category of cavity oscillations is the fluid elastic oscillation which involves elastic vibration of the cavity boundaries interacting with the free shear layer instabilities, such as the case of metal bellows. The frequency of the vibration mode of the elastic boundary should match that of the hydrodynamic cycle along the cavity shear layer. Harrington and Dunham (1960) applied external actuation of the bottom wall of the cavity to simulate a vibrating elastic boundary. Such boundary oscillations excited fluctuation velocity component along the shear layer and affected the vortex formation.

The third category is the fluid resonant oscillation, which represents the current research case, where the hydrodynamic instabilities are sustained through an acoustic resonance such as a standing sound wave. The acoustic standing wave acts as a band-pass filter. A strong resonance will occur only when the free shear layer instability is in phase with the acoustic particle velocity at the cavity mouth, i.e. at specific combinations of flow velocities and acoustic resonance frequencies. Coherent vortical structures are formed along the cavity span. The essential condition for the acoustic resonance to be self-maintained is that the acoustic energy generated must overcome the associated piping system acoustic losses (radiation, visco-thermal, etc).

The energy of fluid resonant oscillations is normally concentrated around a distinct frequency, i.e. pure tone. Consequently, the amplitude of oscillations in presence of resonators can be two orders of magnitude higher than free oscillators (Rockwell, 1983). Tam and Block (1978) investigated cavity oscillation frequencies reported in the literature by plotting the Strouhal number vs. the Mach number for various experimental data points as shown in Figure 2.3. The data are clearly clustered in three bins representing different shear layer oscillation modes. The shear layer mode indicates the number of vortices travelling at any instant along the cavity shear layer as has been demonstrated by flow visualization investigations (Mohamed and Ziada, 2014). For each shear layer mode, the Strouhal number of oscillation is slightly higher at low Mach number flows.

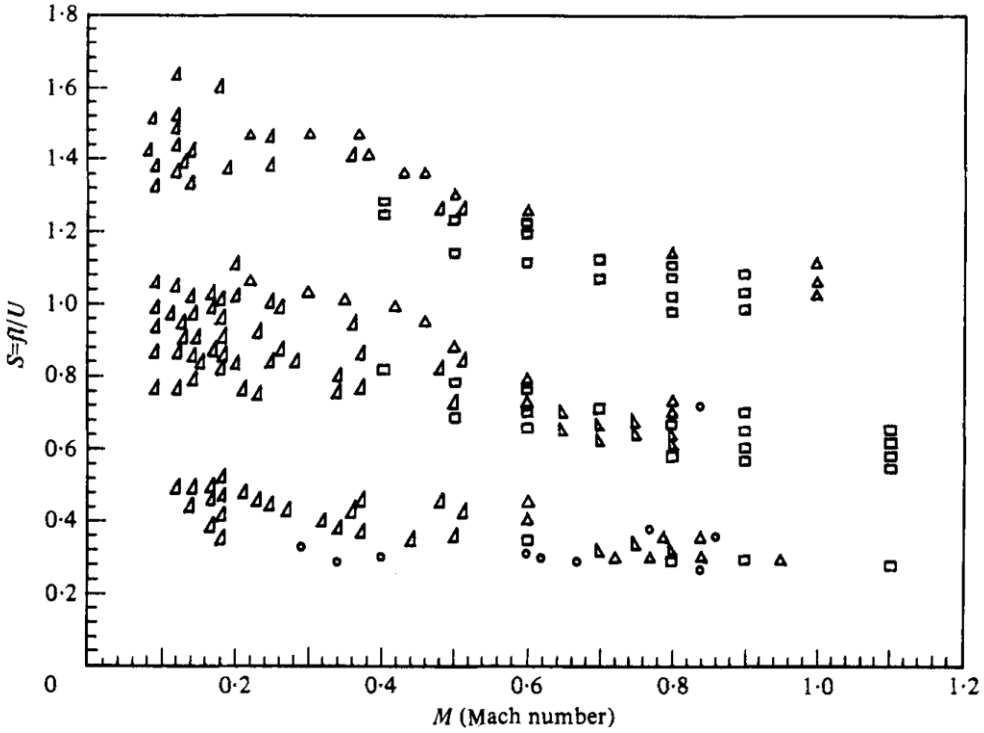

Figure 2.3. Different experimental data points for cavity resonance Strouhal number vs Mach number (Collected by Tam and Block, 1978)

Fluid resonant oscillations in cavities vary based on the nature of the acoustic standing wave. Transverse acoustic wave can be excited within the cavity volume with minimal energy dissipated to the associated duct, i.e. trapped modes (e.g. Aly and Ziada, 2010; Bolduc et al., 2016). The amplitude of oscillations for trapped modes are typically high because the energy of the waves is localized and concentrated. The cut-off frequency for the transverse waves in the presence of the cavity is lower than that of the duct and consequently the waves are only excited in the cavity vicinity. The wavelength in this case is the same order of magnitude of the cavity dimensions.

The other category of oscillations occurs when the cavities interact with a longitudinal plane acoustic wave along the main duct. This category varies depending whether the cavity being deep or shallow. A typical example of deep cavities is closed side-branches where the cavity depth to length ratio exceeds unity. An acoustic mode is excited along the side branch and interacts with a standing wave along either the upstream or the downstream ducts or both of them (e.g. Bruggeman et al., 1991; Ziada, 1994). The wavelength of the acoustic wave and the cavity depth are of the same order of magnitude. The acoustic particle velocity at the branch mouth is perpendicular to the main flow velocity as depicted in Figure 2.4 (a). For the case of shallow cavities, the acoustic particle velocity along the shear layer is parallel to the main flow velocity as shown in Figure 2.4 (b) (e.g. Nakiboglu et al., 2012; Mohamed et al., 2018). The acoustic wavelength along the main duct in such a case is much longer than the cavity length. Flow in corrugated

pipes lies in the last category and will be the main concern of the current research. The flow-structure interaction is quite different for deep and shallow cavities as a result of the acoustic particle velocity orientation as compared to the main flow field. This affects the aeroacoustic source and sink distributions along the shear layer.

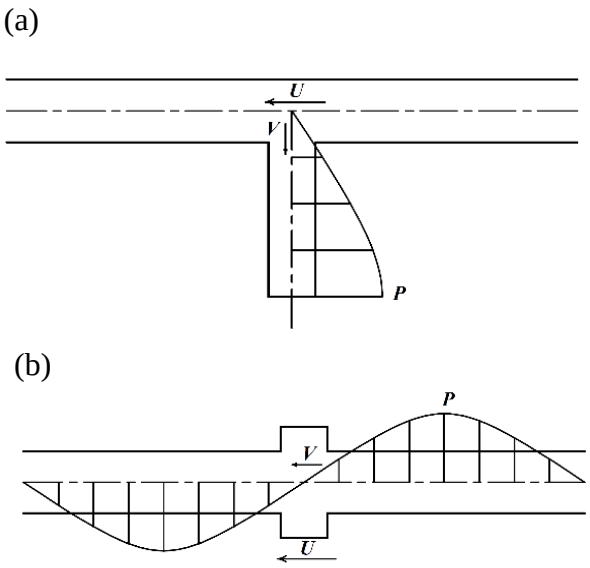

Figure 2.4. Two different configurations of cavity flow-sound interaction: (a) Deep cavity resonance for a closed side-branch, (b) Plane wave along a ducted shallow cavity. *U* is the mean velocity in the main pipe; *v* is the particle velocity of the acoustic mode; *P* is the acoustic pressure of the sound wave.

2.2 Aeroacoustic Source Estimation

Self-sustained oscillations associated with flow past cavities and corrugated pipes have been extensively studied in the literature (e.g. Petrie and Huntley, 1980; Davies, 1981; Rockwell and Schachenmann, 1982). However, these early studies were only concerned with the basic features of the lock-in phenomenon and reporting the self-excited oscillations at the tested flow velocities. Lock-in hereby

refers to self-excited oscillations which occur over a range of flow velocities corresponding to virtually the same resonance frequency. Fundamental understanding of the shear layer instability and the phasing between the hydrodynamic and acoustic cycles was established. On the other hand, the predictions of the critical Strouhal number ($St = f L/U$) for the onset of resonance and the amplitude of associated acoustic pressure pulsations were still not clearly resolved. These parameters are essential in the design stage of any system housing ducted cavities to know in advance whether self-sustained oscillations would occur or not. Moreover, in the case where the occurrence of such instabilities is inevitable, the evaluation of the resonance amplitude allows assessing the capability of the design to withstand such oscillations and the expected impact on the working environment. Resolving the onset Strouhal number and the corresponding oscillations amplitude is a challenging non-linear problem which requires the knowledge of the aeroacoustic source (i.e. the dimensionless acoustic power generated by flow over the cavities). In this section, the different approaches reported in the literature to determine the aeroacoustic source, both numerically and experimentally, are discussed in detail.

2.2.1 Numerical Approach

2.2.1.1 Analytical Models

Earlier numerical models were analytical in nature because of the relatively limited computational power at the time. Analytical models usually did not

accurately predict the aeroacoustic source. However, it was characterized by its simplicity and capturing the fundamental physics of the phenomenon. Analytical approaches were based on solving the flow field and coupling it to the acoustic field using Howe's analogy (1980) to evaluate the acoustic energy generation. Howe's analogy aims at quantifying the rate of energy exchange between both the acoustic and flow fields. The acoustic power (Π) is defined by equation (2.1), where ω and U are the flow vorticity and velocity, respectively, while v stands for the acoustic particle velocity. This equation is derived from Navier-Stokes equations and the first law of thermodynamics while applying the definition of entropy. The two basic assumptions are the flow being incompressible and inviscid which are justified by the encountered flow conditions of low Mach number but high Reynolds number, respectively. The flow was divided into a mean value and a periodic acoustic fluctuating component. The rate of unsteady kinetic energy is used to define the acoustic power in the final form shown by equation (2.1).

$$\Pi = -\rho \int \omega . (U \times v) \, \mathrm{dV} \tag{2.1}$$

Bruggeman et al. (1991) proposed an analytical model for the vorticity field over the mouth of a side-branch similar to the approach used by Nelson et al. (1983) in a study of Helmholtz resonator. A line vortex was assumed with a convection velocity (U_c) of 0.4 U, where U is the main flow speed. The circulation at the upstream edge is calculated based on Kutta condition. The circulation then increases with a linear rate of 0.5 U^2. The generated acoustic power must balance

with losses at the resonance condition. The acoustic amplitude was estimated based on the balance point. The radiation losses were measured while the visco-thermal losses were modelled. The acoustic pressure pulsations were over estimated by a factor of five. This may be attributed to the simplified assumptions of the model. In reality, the convection speed of the vortex is not constant through the hydrodynamic cycle but rather increases as the coherent structure travels downstream. Dealing with the distributed vorticity cloud as a single point vortex may have led to stronger flow-sound interaction and consequently overestimation of the acoustic pulsations.

Dequand et al. (2003) were inspired by the simplicity of this analytical model and tried to improve its performance. The problem of the singularity point at the downstream edge was addressed. The downstream edge was replaced by a wall during the conformal mapping of the potential flow. The model was also tested for side-branches with rounded edges. The model performance improved especially for the rounded edges case and the best case overestimated the pulsations by about 30%. However, the model failed to accurately predict the lock-in Strouhal range at which the resonance occurs.

Kreisels et al. (1995) introduced vortex blob method to analyze the closed side-branches resonance problem. The vortex sheet is simplified as a row of vortex blobs with uniform vorticity distribution. Flow visualization upon solving the potential flow field agreed with Schlieren pictures captured for the same problem.

The acoustic velocity ratio (ratio of acoustic particle velocity to mean flow velocity) was imposed as a boundary condition in this model. The simulation is performed for a certain Strouhal number and the generated acoustic power is computed. The simulations were repeated for different acoustic velocity ratios until a match is obtained between the generated energy and system losses. This was associated with a considerable computation cost that even some recent models still suffer from as long as the acoustic velocity is required as an input boundary condition rather than being an output of the simulation. The model tended to underestimate the pulsation amplitude by a factor of two as was later reported by Dequand et al. (2003) by comparing the model estimation to their experimentally measured acoustic oscillations amplitude.

2.2.1.2 CFD Models

Computational fluid dynamics (CFD) models have been extensively used in the literature to estimate the aeroacoustic source of flow over cavities. An earlier attempt was done by Radavich el al. (2001) to simulate the flow over closed side-branches. Unsteady two-dimensional compressible Navier-Stokes equations were solved including viscous terms. Turbulence was modeled using the standard k-ε model. The oscillations were triggered via initial conditions of out of phase pressure for the top and bottom side-branches. These initial perturbations were damped by viscous effects and numerical dissipation outside the lock-in resonance range. The estimated acoustic pressure was factor of two different from the experimental results. Radavich el al. acknowledged that increasing the spatial and temporal

resolution in the model may have enhanced the predictions, but it was hindered by the excessive computational time.

Dequand et al. (2003) proposed an Euler-based model, which relied on two-dimensional Euler's compressible inviscid equations to solve the flow field using finite volume method. The compressibility allows for resolving the acoustic waves in the computational domain. The experimentally measured acoustic profile was used as an initial condition for the solver. The number of the cells in the source region at the shear layer were only 80×80 cells in the finest applied grid. Grid refinement analysis still showed some dependence on the mesh size, but further refinement might have been limited by the computational facility at the time. The pulsation amplitude for a side-branch was overestimated by 30-40%. This overestimation may be attributed to the visco-thermal losses being absent by default in the inviscid Euler equations. Moreover, the simulated vortex path deviated slightly from the experimentally visualized one.

All the computational effort discussed so far was dedicated to the flow over closed-side branches which represents deep cavity resonance. Recently, Nakiboglu et al. (2012) proposed a numerical model to compute the aeroacoustic power of a single shallow cavity confined in a pipe. The CFD model was based on incompressible fluid simulation using commercial finite volume Fluent software. The incompressibility assumption was justified by the encountered low Mach number flows that resembles many industrial applications. Additionally, the flow

was assumed to be laminar and the acoustic fluctuating component was superimposed on the velocity profile entering the solution boundary. The model was capable of predicting the Strouhal number corresponding to the maximum amplitude of oscillations reasonably well. However, the aeroacoustic power was overestimated by a factor of two as shown in Figure 2.5.

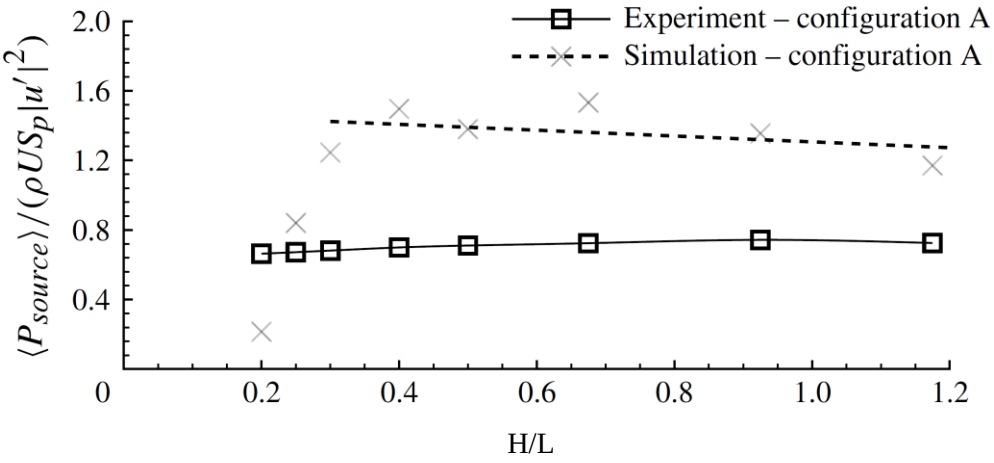

Figure 2.5. Measured and predicted acoustic power from the CFD model for different cavity depth to length ratios (Nakiboglu et al., 2012)

Golliard et al. (2013), in a later investigation, improved the CFD simulations by using URANS K-ω turbulence solver instead of the previous laminar solver. The estimation of the aeroacoustic power improved and the error was in the range of 20%. This improvement is logical as the turbulence fluctuations inherently exist in the actual flow field. However, the study was only limited to a single case of a relatively deep cavity rather than a shallow cavity which represents the practical case of corrugated pipes. Moreover, the methodology still suffers from the fact that the acoustic periodic oscillation is forced at the cavity entrance. Consequently, the

simulations should be repeated at each flow condition for multiple acoustic excitation levels until reaching the point where the energy balance takes place, i.e. resonance conditions. The numerical approach was described in the study to be computationally heavy and the simulations were restricted to the peak whistling Strouhal number, which was determined experimentally, rather than covering the whole lock-in range.

Using more sophisticated turbulence models, such as Large Eddy Simulations (LES), has shown some success in replicating the flow field parameters over an open cavity in a recent study by Nair and Sarkar (2016). The validation of the model relied on the predicted velocity profiles rather than the pulsations amplitude. Rajavel and Parasad (2014) used commercial code Ansys Fluent where the turbulent flow field was solved using Large Eddy Simulation (LES) and the solver was coupled to acoustics based on Ffowcs Williams and Hawkings (FW-H) analogy (1969). The flow field data obtained using CFD is used to predict the aeroacoustic sources within the flow and the corresponding pulsations amplitude in case they occur. The aim of the numerical work is to simulate the fully coupled flow-sound interaction phenomenon and predict the frequency and amplitude of the self-excited resonance in a single run. The predicted resonant frequency deviated from the experimentally measured one with a maximum error of 11%. Moreover, the predicted acoustic pressure distribution was given for the radiated noise outside the pipe rather than the standing wave inside the duct that interacts with the shear layers along the cavities. Additionally, the radiated acoustic levels were not

validated. The new approach is ambitious but still fails to provide reliable results. Further work should be directed towards analyzing the performance of the coupling between the flow and acoustic solvers. The acoustic losses are also hard to be accurately simulated in the model such as the radiation from the pipe open end.

Another approach of CFD models is using the Lattice Boltzmann Method (LBM). This method is based on modelling the collision processes across different fluid particles. It is not commonly used in aeroacoustics applications. However, the methodology is in principle adequate, as it solves for unsteady compressible flows. Amielh et al. (2014) applied LBM simulations for self-excited acoustic modes in a corrugated pipe. A mismatch was observed, in the relative strength of the different modes in the acoustic power spectra, between the model results and the experimentally measured data. This was explained by differences between the experimental setup and the model geometries. Moreover, the Palabos open source code, used in this study, didn't allow for defining the proper acoustic boundary conditions which mimic corrugated pipes with open ends. This leaves the model unvalidated, yet capable of detecting different acoustic resonant modes.

2.2.2 Experimental Approach

2.2.2.1 Sound Wave Measurements

Coltman (1968) performed one of the early experimental attempts to measure the acoustic impedance of an organ pipe as a representation of a flute. A special experimental setup was established where the input acoustic wave was

determined using a single microphone. The acoustic impedance was then transferred to the organ pipe using electrical circuit analogy assuming harmonic propagation of the acoustic waves. The experiments were done first without flow to evaluate the acoustic losses in order to separate it later from acoustic generation across the flute mouth. This special setup of Coltman is not suitable for more complicated duct acoustics problems. However, it inspired later research work to evaluate the aeroacoustic source based on the analysis of sound waves propagating across the duct.

Graf and Ziada (1992; 2010) developed a three-microphone method to measure the aeroacoustic source of closed side-branches. The three microphones were used to reconstruct the acoustic standing wave along the side-branch and other three microphones were used to reconstruct the wave from the pipe side. The acoustic pressure at the branch mouth was determined twice from both the pipe side and the branch side. The change in the acoustic pressure value across the shear layer was basically attributed to the presence of an aeroacoustic source. The aeroacoustic power can be calculated as the multiplication of the acoustic pressure difference by the acoustic velocity. A schematic of the shear layer excitation model is shown in Figure 2.6. The basic advantage of this experimental method is that it extracts the global value of the source without getting into the details of the complicated flow field. The experimental setup allowed for a full aeroacoustic map covering the source value for a wide range of Strouhal numbers and acoustic velocity ratios.

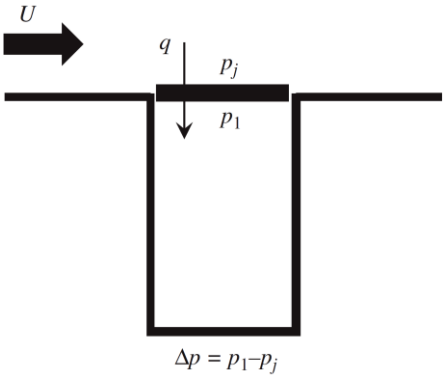

Figure 2.6. Schematic of the shear layer excitation model at the branch mouth (Graf and Ziada, 2010)

The acoustic standing wave in a duct can be described using equation (2.2), where P^+ and P^- represent the amplitude of two different acoustic waves travelling with and against the mean flow in the duct, respectively. The complex wave number (β) accounts for the visco-thermal losses in the duct while the Mach number (*M*) term accounts for the presence of the mean flow. Resolving the standing wave in the duct requires two different acoustic measurements to estimate the two parameters P^+ and P^-. The measurement methodology of Graf and Ziada relied on three-microphone measurements and applied a least square method to resolve the standing wave to enhance the source measurement reliability.

$$P(x,t) = \left\{ P^+ \, e^{\frac{-j\,\beta\,x}{(1+M)}} + \; P^- \, e^{\frac{j\,\beta\,x}{(1-M)}} \right\} e^{j\,(2\pi f)t} \tag{2.2}$$

A Semi-empirical model was further developed by Graf and Ziada and was capable of predicting both the frequency and the pressure amplitude resulting from self-excited oscillations in side-branches based on the measured aeroacoustic source. The prediction process requires searching the source map for a pair of

Strouhal number and acoustic velocity ratio at which the acoustic energy produced by the source balances the modelled system losses. The model was validated using experimental measurements of the amplitude of actual self-excited oscillations.

Mohamed et al. (2018) applied the standing wave method (i.e. three-microphone method) to determine experimentally the aeroacoustic source of a single shallow cavity. Using three microphones upstream of the cavity and another three downstream, the acoustic standing wave parameters were well estimated. The method was successful in determining the aeroacoustic source for a new pattern of flow-sound interaction which is different from the side-branch case investigated by Graf and Ziada as previously depicted in Figure 2.4. In the case of the side-branches, the acoustic waves were trapped within the side-branch with the acoustic velocity perpendicular to the main flow direction. On the other hand, ducted shallow cavities are exposed to longitudinal plane waves along the pipe with the acoustic velocity parallel to the main flow. One of the challenges associated with applying the standing wave method was to ensure that the cavity dimensions are much smaller than the acoustic wavelength to verify the assumption of using a uniform acoustic velocity in the source estimation. This challenge was tackled by using a long piping system which consequently increased the acoustic wavelength. Moreover, the long upstream pipe achieved fully developed turbulent conditions at the cavity mouth that resemble the industrial applications.

Mohamed and Ziada (2015) further applied the standing wave method to study the effect of the cavity volume on the generated aeroacoustic source. The source consistently increased upon increasing the cavity volume for the same investigated length to depth ratios with a corresponding increase in the peak whistling Strouhal number. These findings were validated by similar trends which were observed for the corresponding self-excited resonance cases. The increase in the source was attributed to the change of the acoustic velocity field. The acoustic field was simulated using finite element analysis. Larger cavity volumes were associated with a higher cross-stream component of the acoustic velocity that was responsible for the boost in the acoustic power generation.

Another measurement method was proposed by Golliard et al. (2015) based on resolving the scattering matrix of acoustic travelling waves, with and against the mean flow in a corrugated pipe. The schematic of the used experimental setup is shown in Figure 2.7. The setup requires anechoic terminations at both ends to sustain the travelling wave condition. The wave is resolved upstream and downstream the tested pipe to estimate the transmission and reflection coefficients, with and against the flow, which are the components of the scattering matrix. Consequently, two experiments are conducted per each case study using two speakers at both ends of the duct. The flow velocity was kept constant and the sweep over different Strouhal numbers was accomplished by changing the frequency of the excited acoustic waves. A no flow test was used to estimate the acoustic damping losses in the corrugated pipe to be able afterwards to distinguish the net

acoustic energy produced as a result of the flow-structure interaction. The net acoustic energy produced per corrugation was compared with the one estimated using the same numerical CFD model developed by Golliard et al. (2013). That model was previously reported to perform well for single cavity configurations as discussed in section 2.2.1.2. However, in this case study, the model overestimated the source by 40%. This deserves more investigation towards the cause of the shortcoming whether it is attributed to the CFD model or the measurement methodology.

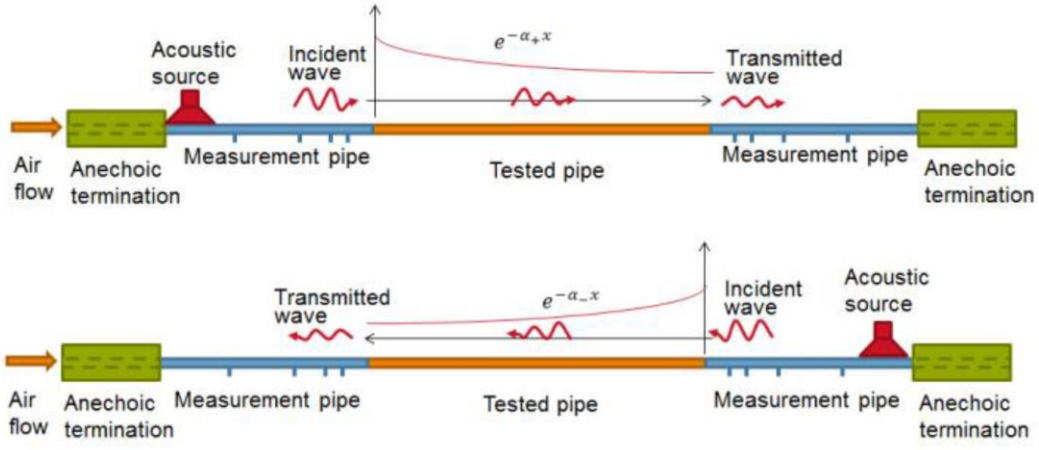

Figure 2.7. Schematic of the experimental setup to measure the source of a corrugated pipe using the scattering matrix method (Golliard et al., 2015)

2.2.2.2 Howe's Analogy Flow Visualization

Another experimental approach is based on the vortex sound theory and the volume integral proposed by Howe (1980) where the acoustic power generation can be estimated based on the knowledge of both the velocity and the acoustic fields. The details of Howe's analogy were described in details in section 2.2.1.1. Flow

visualization using Particle Image Velocimetry (PIV) laser technique, providing the details of the flow field, paved the way for using Howe's analogy to estimate the aeroacoustic source experimentally. Oshkai and Yan (2008) applied this methodology on a co-axial closed side-branch. The acoustic field was simplified as one dimensional and measured by microphones at the end of the side-branches. Phase averaged measurements allow to illustrate the synchronization between the growth of the coherent vortical structure and the acoustic cycle. Moreover, it visualized the effect of the main duct width on the mechanism of the acoustic power generation.

Finnegan et al. (2010) investigated the aeroacoustic power generated by the flow around two tandem cylinders. The acoustic field was estimated based on finite element modelling using ANSYS. The simulations yielded normalized spatial pressure distribution. The amplitude and the frequency of the resonant mode were obtained from the time signal of a microphone. The acoustic particle velocity was computed from the acoustic pressure field using Euler's equation. The PIV measurement schematic is shown in Figure 2.8 (a), while the net acoustic energy obtained through Howe's integral is depicted in Figure 2.8 (b). The spatial distribution of the aeroacoustic source, which is a unique characteristic of this methodology, reveals the locations of the acoustic sources and sinks. This consequently helps in understanding the nature of the flow-sound interaction pattern. Identifying the locations of the generated source is the first step towards applying the proper countermeasures and comprehending the effect of changing

different geometrical parameters. In the investigation by Finnegan et al., two different modes were identified with sources located in the wake after the cylinders. However, for the mode at low flow velocities, shown in Figure 2.8 (b), additional sources with net positive power generation were located in the gap region between the two cylinders.

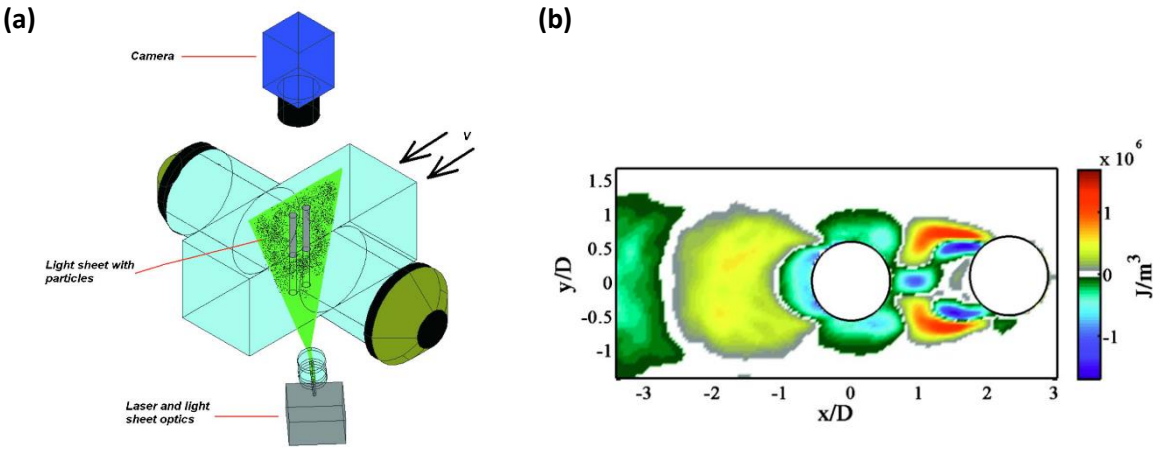

Figure 2.8. (a) Schematic of the PIV experimental setup, (b) Net acoustic energy spatial distribution (Finnegan et al., 2010)

Mohamed and Ziada (2014) visualized the flow field within a single shallow cavity using Particle Image Velocimetry (PIV) technique. The acoustic flow field was simulated using finite element method using ABAQUS. The aeroacoustic source distribution for the investigated shallow cavities showed two sources located near the upstream and downstream edges of the cavity with a sink in the middle. The source distribution, being different from that of the side-branch case, offered an explanation for the different effect of geometrical parameters on the acoustic response, such as rounding the downstream edge. This investigation provided

a comparison between the source value measured by Howe's analogy method and that measured using the standing wave method. A fair agreement in the source values from both approaches was found for the cases with intermediate and high acoustic excitation levels. However, some discrepancy was observed for the cases with low acoustic velocity ratios. This was attributed to the fact that at low excitation levels, the interaction mechanism is more affected by flow turbulence. The turbulence is characterized by its three-dimensional nature, while the measurements were conducted using two-dimensional PIV. Two-dimensional assumption was quite fair for the cases with higher excitation levels given the axisymmetric geometry and the plane acoustic wave along the duct.

2.3 Corrugated Pipes

In this section, research on self-sustained oscillations of corrugated pipes is introduced with the focus dedicated to the recent investigations. Some of the early studies that reported corrugated pipe oscillations was discussed at the beginning of section 2.2. Nakiboglu et al. (2010) studied the self-excited oscillations in corrugated pipes for different geometrical configurations. Lock-in resonance modes are supposed to be excited at the same Strouhal number range given that the appropriate characteristic length is chosen. The cavity length plus the upstream edge radius of curvature proved to be the most suitable characteristic length based on the gathered experimental data for different piping geometries. Moreover, the cavity depth was found to have a negligible effect on the peak whistling Strouhal

number. This agrees with the findings of Mohamed (2015) for single shallow cavities where the cavity depth was changed while keeping the cavity length constant for three different sets of cavity lengths.

Nakiboglu et al. (2011) experimentally investigated the effect of the corrugated pipe length on the maximum attained acoustic pressure amplitude. Initially, the pressure amplitude increased while increasing the pipe length until saturation was observed at the pipe length to diameter ratio (L_{pipe}/D) of 100 as shown in Figure 2.9 (b). Further increases of "L_{pipe}/D" to 800 did not have any noticeable effect on the pressure amplitude. The Strouhal number corresponding to peak oscillations was independent of the pipe length as shown in Figure 2.9 (a). Testing another corrugated pipe with a different geometry led to the same general conclusion regarding the saturation of the pressure amplitude. However, the saturation was observed at a different value of pipe length to diameter ratio of 60. It is worth mentioning that for the two investigated geometries, the saturation dimensionless pressure amplitude was consistent being about 0.1. Moreover, Nakiboglu et al. investigated the effect of the confinement ratio on the oscillations amplitude. The confinement ratio is defined as "D_p-$D_r/L_{characteristic}$" where D_p is the pipe diameter and D_r is the diameter of a rod inserted inside the main pipe. Increasing the confinement ratio was associated with a decrease in the peak whistling Strouhal number. Numerical investigations using CFD have shown that the whistling Strouhal number is basically affected by the grazing velocity profile which differs substantially with the confinement ratio. Different confinement ratios

will lead to the variation of boundary layer momentum thickness relative to the cavity length. Similar observations were previously reported by Ziada and Shine (1999) while studying the effect of changing the side-branch to the main pipe diameter ratio.

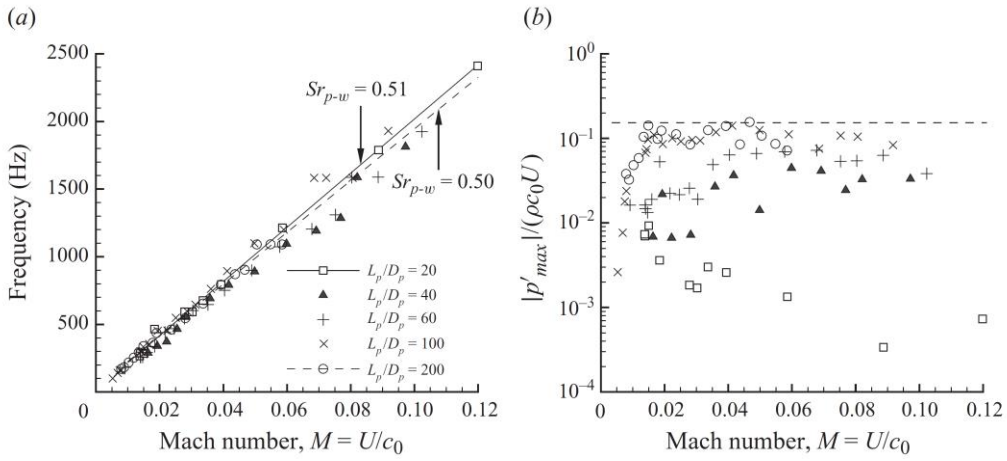

Figure 2.9. Measured self-excited oscillations of corrugated pipes with different lengths; (a) Resonance frequency, (b) Dimensionless pressure amplitude vs. Mach number (Nakiboglu et al., 2011)

Belfroid et al. (2011) investigated aeroacoustic characteristics of a new carcass design of corrugated pipes proposed by a corrugated pipe manufacturer NKT Flexibles. The new design suggested smaller cavity volume as compared to the classic design. This is illustrated in the schematic shown in Figure 2.10. The predicted flow velocity for oscillation onset increased by 5 to 9 times which reduced the probability of resonance occurrence within the normal operating conditions. The dimensionless amplitude was also reduced to about 20 to 50% of the original case. The authors also suggested that the acoustic resonance of the new design would occur at higher frequencies, for which the acoustic losses are higher and

thereby the self-sustained oscillations may be avoided. These findings were based on an established empirical model which was tested experimentally on the classical design only.

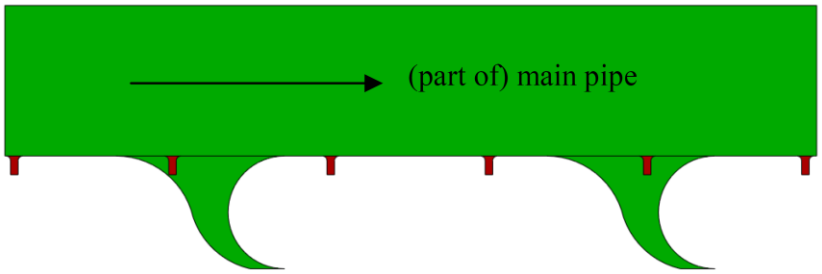

Figure 2.10. Schematic of the new carcass design of corrugated pipes showing the corrugations in red compared to the classical design in green (Belfroid et al., 2011)

This motivated a recent study by Golliard et al. (2013) to experimentally test small-scale models of this new design. Self-sustained oscillations were not observed for the new design over the whole testing range backing up the high onset velocity value predicted by the model. The predicted high value was beyond the capability of the test setup which was limited to about 50 m/s at an absolute pressure of 4 bars. The new design seems to be successful from the acoustics point of view which may be attributed to the substantial decrease in the cavity volumes. However, the decreased cavity volume may have an adverse effect on the flexibility of the corrugated pipe, which is one of its unique characteristics. The mechanical behaviour of the new design was not addressed in either of the two investigations.

Amielh et al. (2014) experimentally investigated the corrugated pipe oscillations using a two-dimensional rectangular model. The setup was capable of exciting different acoustic modes of self-excited oscillations. PIV flow

visualization was done on the 35th cavity in the piping configuration. The study didn't attempt to evaluate the aeroacoustic source generated by the cavity. Only the mean flow field is analyzed without performing a phase locked PIV to trace the vortical structures with the acoustic cycle. However, the mean flow image indicated the existence of a vortical structure in the center of the cavity. A countermeasure for the oscillations was suggested by applying a low frequency modulation. A low frequency acoustic wave is excited using an external speaker to over-ride the self-excited acoustic mode. The countermeasure managed to eliminate the whistling mode. On the other hand, the low frequency pressure peak was higher than the original one. Although, the low frequency applied of 10 Hz is outside the audible range, the acoustic oscillations would still affect the structure and even the human bodies. Additionally, the countermeasure may neither be practically nor economically feasible to apply for a corrugated pipe that extends for kilometers.

2.4 Multiple Cavities

All the previously presented research on corrugated pipes did not attempt to link the global oscillations to the individual contributions of the cavities relying on a multiple-cavity approach. Limited research effort has addressed the flow over multiple cavities. Nakiboglu and Hirschberg (2012) experimentally investigated the self-excited oscillations of multiple cavities as a model for corrugated pipes. In the case of multiple cavities located at separate acoustic pressure nodes, the combined effect was almost the summation of their respective contributions indicating the

absence of any hydrodynamic interaction. This is not surprising given that the cavities were far apart which does not allow hydrodynamic interference. Measured dimensionless acoustic pressure amplitude corresponding to different configurations of multiple cavities is presented in Figure 2.11. Hydrodynamic interference between two neighbouring cavities (Configurations D and E) may be constructive and thereby exceeds the two hydrodynamically separated cavities (Configuration C).

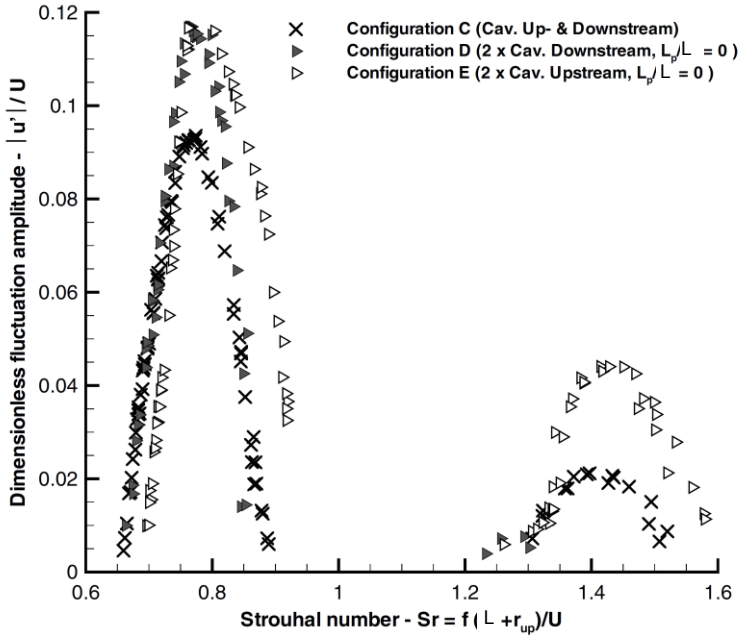

Figure 2.11. Dimensionless acoustic amplitude vs Strouhal number for different multiple-cavity configurations (Nakiboglu and Hirschberg, 2012)

The plateau length (L_p) is defined as the flat length between each two consecutive cavities. The ratio of L_p to the cavity length (L) was found to be very important in determining whether the interference was constructive or destructive for the investigated two-cavity configuration. The spacing ratio "L_p /L" close to

zero and 1.375 yielded the highest pressure pulsation levels in the self-excited experiments. However, the pressure amplitude decreased as the ratio varied away from these two values. The minimum pulsations amplitude was observed at an intermediate "L_p/L" of 0.75 with almost half of the maximum attained value. In a subsequent study, Nakiboglu et al. (2013) simulated multiple cavity configurations using CFD for up to a four-cavity configuration. Constructive hydrodynamic interference was still observed in the simulation results.

2.5 Summary and Proposed Research

The literature review introduced in this chapter shows that most of the recent research focused on understanding the flow over a single cavity or the global oscillations of corrugated pipes. However, limited research has been concerned with investigating the flow over multiple cavities as a model for corrugated pipes. The ultimate goal of the current research is to predict the amplitude of self-excited oscillations in a corrugated pipe based on a multiple cavity model.

The estimation of the generated acoustic power has been intensively approached numerically and experimentally. The standing wave method (SWM) stands out as an accurate methodology of experimentally measuring the aeroacoustic source. The method is efficient in accounting for the three-dimensional effects of the problem without getting into the complicated details of the flow structure interaction or simplifying the geometry of the problem. Consequently, the current work represents the first attempt to adapt the SWM to

measure the source of multiple cavity configurations. Moreover, the work aims at developing a semi-empirical model relying on the measured source data to predict the self-excited oscillations amplitude of piping systems housing multiple shallow cavities.

The separation distance is a new parameter distinctive to multiple cavities. The limited research in this area only covered self-excited oscillations measurements for a two-cavity configuration. The effect of the separation distance on experimentally measured aeroacoustic source is extensively investigated in the current study for both two and three-cavity configurations. The physics of the hydrodynamic interaction is further illustrated with the aid of flow visualization.

The development of the source upon increasing the number of cavities has not been addressed in the literature. The source of downstream cavities is expected to reach a constant level after a certain number of entrance cavities defining a building unit cavity source. Fully developed conditions are sought using the SWM for multiple cavity configuration encompassing up to six cavities. The building unit source is validated by comparison with the source of a general downstream cavity in a long multiple cavity section extracted using PIV. Moreover, the building unit source is used in a model to estimate the oscillation amplitude of a long multiple cavity section. The latter is a substantial progress towards estimating the oscillation amplitude in a corrugated pipe based on a multiple cavity model.

CHAPTER 3

Acoustic Response of Multiple Shallow Cavities and Prediction of Self-Excited Acoustic Oscillations

Complete Citation:

Shaaban, A. and Ziada, S., 2018. Acoustic response of multiple shallow cavities and prediction of self-excited acoustic oscillations, Journal of Fluids Engineering, ASME, 140 (9), 91203.

Copyright:

Relative Contributions:

Shaaban, A.: Performed all the experimental measurements, data analysis, interpretation and model development, wrote the first draft of the manuscript including all figures and text.

Ziada, S.: Supervisor of Shaaban, A. during the course of work, revised and edited the manuscript draft.

Abstract

Self-sustaining oscillations of flow over ducted cavities and in corrugated pipes are a known source of tonal noise and excessive vibration in industrial applications. Corrugated pipes can be modelled as a series of axisymmetric cavities. In the current study, the aeroacoustic sources generated by one, two and three-cavity configurations have been experimentally investigated by means of the Standing Wave Method (SWM) for a wide range of Strouhal numbers and acoustic excitation levels. The source strength is found to increase in a non-linear manner with increasing the number of cavities. Moreover, the self-excited acoustic resonances of the same cavity combinations are investigated. The source characteristics are compared with the observed lock-in range from the self-excited experiments. A prediction model is also developed to utilize the measured source characteristics for estimating the amplitude of the cavities self-sustained oscillations. The self-excited experimental data are used to assess the effect of acoustic absorption at the cavity edges. This absorption is found to be substantial and must be accounted for in the prediction model. When the model is supplemented with appropriate loss coefficients, it predicts fairly well the pulsation amplitude within the resonance lock-in range of the studied multiple cavity configurations.

Keywords: *multiple cavities, aeroacoustic source, fluid structure interaction, flow-sound interaction*

3.1 Introduction

Self-sustaining oscillations of pipe flows can pose potential danger and lead to system failure. Corrugated pipes are commonly used in offshore gas fields because of their flexibility while offering high stiffness as a result of the corrugations. Belfroid et al. (2007) stated that acoustic pressure pulsations in corrugated pipes used in high pressure gas installations may attain a value in the order of bars. This is clearly a serious issue regarding the system integrity in addition to the high noise level. Moreover, the energy consumed in sustaining the resonance adds to the running cost of pumping the fluid through such a pipeline. The latter is already addressed in some recent investigations (Stel et al., 2010; Popiel et al., 2013). The present work investigates the aeroacoustic source generated by flow over multiple shallow cavities, as a first step towards modeling corrugated pipes as a series of consecutive cavities.

The self-excited oscillations associated with flow over cavities are caused by the free shear layer instability which must be sustained by means of a feedback mechanism. Rockwell and Naudascher (1978) classified cavity oscillations into three main categories: fluid dynamic, fluid resonant and fluid elastic oscillations. In the case of fluid resonant oscillations, which represents the current research case, the shear layer oscillations interact with an acoustic standing wave along the pipe. The acoustic standing wave acts as a band-pass filter. The lock-in will only occur when the free shear layer oscillations are in phase with the acoustic particle velocity

at the cavity mouth, i.e. at specific combinations of flow velocities and acoustic resonance frequencies.

Recent research work improved our understanding of the flow-excited acoustic response of single shallow cavities. The challenge is to predict whether resonance will take place or not, and to quantify the acoustic pulsation amplitude if it occurs. First, different numerical approaches together with their achievements and limitations are briefly discussed. Line Vortex models such as that developed by Bruggeman et al. (1989) represent early attempts to simplify the vorticity field, yet the acoustic pulsations were overestimated. More recently, numerous papers developed improved methodologies (Kriesels et al., 1995; Radavich et al., 2001; Dequand et al., 2003), but the majority of them dealt with the cases of closed side-branch and deep cavity resonances.

Nakiboglu et al. (2012) proposed a computational fluid dynamics (CFD) model to compute the aeroacoustic power of a single shallow cavity coupled with a longitudinal acoustic mode. Laminar incompressible flow was simulated with the acoustic fluctuating component added to the velocity profile. Despite its simplicity, the model performed very well in predicting the Strouhal number at which the maximum resonance amplitude occurs, but the aeroacoustic power was overestimated. Golliard et al. (2013) improved the model by using URANS K-ω turbulence solver. Using Large Eddy Simulation (LES) turbulence modeling provided good flow field data for open cavity flows as recently reported by Nair

and Sarkar (2016). Rajavel and Parasad (2014) simulated corrugated pipes by combining LES with the acoustics based on Ffowcs Williams and Hawkings (FW-H) analogy (1969). The predicted frequency deviated by 11% from the experimental measurements.

On the other hand, there are many experimental investigations to measure the aeroacoustic sources generated by flow over confined cavities (Graf and Ziada, 1992; 2010; Oshkai et al., 2008; Mohamed et al., 2011; Mohamed and Ziada, 2014). The most common approach is based on the analogy proposed by Howe (1980) where the acoustic power is computed from the measured flow field and the simulated acoustic velocity distribution (Oshkai et al., 2008; Mohamed and Ziada, 2014). This approach however requires complete knowledge of the time dependent components of the flow and acoustic fields and is therefore time consuming, especially when dealing with multiple cavities. To resolve this difficulty, Graf and Ziada (1992; 2010) and Mohamed et al. (2011) developed an alternative approach, the Standing Wave Method (SWM), which is based on the fact that the source generated by the flow-sound interaction process is compact because its size is much smaller than the acoustic wavelength. The source is therefore modelled as a pressure discontinuity and the three-microphone method is used to measure the acoustic pressure discontinuity at the cavity. This approach has been demonstrated to be very efficient (Graf and Ziada, 1992; 2010; Mohamed et al., 2011), because it extracts the global value of the source, even when three-dimensional effects are present, without getting into the details of the complex flow field at the cavity. This

is the methodology which will be used in the present study of multiple shallow cavities in a pipeline.

Limited research effort addressed hydrodynamic coupling between consecutive shallow cavities. For the case of self-excited resonance of multiple cavities, Nakiboglu and Hirschberg (2012) investigated experimentally the effect of hydrodynamic interference between two consecutive cavities. This study indicated that, depending on the distance between the cavities, the effect of this interference on the self-excited oscillation amplitude can be either constructive or destructive. In a successive study (Nakiboglu et al., 2013), CFD simulations were done for up to four-cavity configuration showing that constructive interference could still be observed.

The aim of the current study is to investigate the case of flow over multiple shallow cavities and the accompanied fluid resonant oscillations as an essential step towards understanding corrugated pipe acoustic oscillations. The Standing Wave Method (SWM) is adopted due to its high efficiency and accuracy in measuring aeroacoustic sources (Graf and Ziada, 1992; 2010; Mohamed et al., 2011). The aeroacoustic source is measured for one, two and three-cavity configurations in an attempt to understand the hydrodynamic interaction between neighboring cavities. Corresponding self-excited measurements are then performed to compare the lock-in trends with the source findings. A prediction model is eventually developed to estimate the amplitude of the self-excited oscillation based on the

measured source. The model is also validated against the self-excited oscillation amplitude which is obtained from a different test arrangement.

3.2 Experimental Setup

The first experimental facility used in this investigation allows for measuring the aeroacoustic source of multiple cavities using the Standing Wave Method. A schematic of the setup is shown in Figure 3.1. The entrance pipe is longer than 40 times the nominal pipe diameter (*D*) to achieve fully developed turbulent flow conditions ahead of the test section. The system includes standard 4" PVC schedule 80 pipes. A speaker is installed at the end of a downstream side branch to generate an acoustic standing wave whose frequency and amplitude are controlled via a function generator. A power amplifier is used to excite the speaker and generate waves of high amplitudes where the acoustic velocity values reached 20% of the mean flow velocity. A Pitot tube is used to measure the flow velocity (*U*) located 11 diameters from the pipe entrance. The differential pressure from the Pitot tube is measured using Validyne (DP103) pressure transducer. The pitot tube measures the velocity at the pipe centerline in the entrance region which is correlated to the center line velocity in the fully developed region as given by Doherty et al. (2007). The mean flow velocity is estimated as a function of the center line velocity as indicated by White (2001). A circular bell-mouth entrance is used to avoid flow separation followed by a honeycomb flow straightener. The cavities are located at the acoustic velocity antinode to maximize the excitation of

the cavities shear layers. Three microphones are installed upstream of the cavities with another set of three microphones are located in the downstream pipe. The acoustic standing wave equation requires two pressure measurements to estimate its two unknown parameters. However, three microphones are installed in order to apply a least square method to enhance the accuracy of the measurements. Preliminary accuracy tests are made as will be discussed later. The acoustic power generated by the multiple cavities can be directly computed by multiplying the acoustic pressure difference across the cavities (ΔP) by the acoustic particle velocity (v). The aeroacoustic source is then calculated, as given by equation (3.1), which is a normalized representation of the source impedance. National Instruments data acquisition card (NI DAQPad-6015) is used to read and record the signals of the Pitot tube, the six microphones and the function generator. For each test case, all signals are recorded for a duration of 60 seconds and the data is then processed to obtain the acoustic pressure at the excitation frequency.

$$S = \frac{\Delta P/(0.5 * \rho_0 U^2)}{v/U} \tag{3.1}$$

The facility allows for altering both the approach flow velocity (U), via the variable speed blower, as well as the acoustic particle velocity (v) amplitude, by adjusting the speaker amplifier. Therefore, the aeroacoustic source can be measured for a wide range of Strouhal number ($St = fL/U$) and acoustic velocity ratios (v/U), i.e. aeroacoustic map.

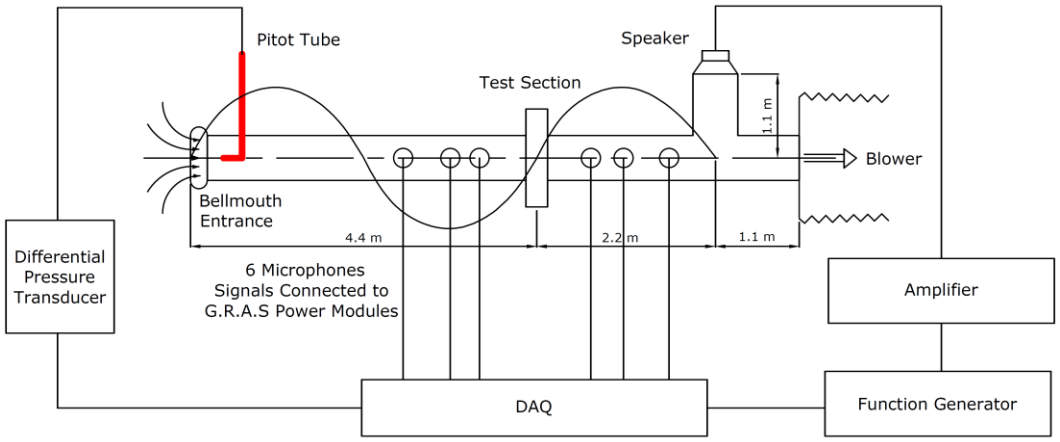

Figure 3.1. Schematic of the externally excited experimental setup

The microphones calibration is done on two stages; a relative and an absolute calibration. The relative calibration entails placing the six microphones in a calibration chamber and at equal distances from the speaker diaphragm. The speaker is excited using a white noise signal and the transfer functions of all microphones are obtained with respect to the reference microphone. This calibration procedure is similar to that illustrated in details by Mohamed (2015). The absolute calibration then involves calibrating the reference microphone using G.R.A.S 42AB pistonphone. The three microphones, either upstream or downstream of the test section, are strategically placed to enhance the measurement accuracy. The middle microphone is close to the maximum acoustic pressure location with the other two microphones being located at unequal distances from the antinode to avoid redundancy. The calibration of the Validyne pressure transducer, that is used to read the differential pressure signal from the Pitot tube, is accomplished using Fluke 922 pressure reader with a resolution of 1 Pa.

The resonance frequency at which the tests are performed is near 78 Hz with a corresponding wavelength of 4.4 m. This long wavelength is chosen during the design stage of the setup to ensure a virtually constant acoustic velocity along the three cavities to properly apply the SWM. For the longest test section case, the three cavities are centered at the acoustic velocity antinode with a maximum variation in the acoustic velocity of 2% along the test section.

Another test setup is used in the current study for measuring self-excited oscillations by multiple cavities. The schematic of the self-excited test setup is shown in Figure 3.2. It consists of two symmetric PVC pipes with the multiple cavity section located in the middle. Two different sets of pipe lengths are used. The long set is 60 cm while the short one is 30 cm. These lengths are carefully chosen to facilitate the occurrence of self-sustained oscillations, during which the aeroacoustic source of the cavities will be counterbalanced by the system losses. The two pipe lengths are tested to vary the wave frequencies and associated radiation and visco-thermal losses. This is essential to assess the developed prediction model that will be presented in the modeling section.

A Pitot tube is used to measure the flow velocity as in the long pipe facility. Two microphones are situated at the locations of the acoustic pressure antinodes of the odd and even harmonic modes, as illustrated in Figure 3.2. The sweep of different flow velocities is accomplished by gradually changing the blower motor speed using a variable frequency drive. The initiation of resonant acoustic

oscillations defines the onset Strouhal number of different hydrodynamic modes. The whole lock-in range is determined by measuring the acoustic pressure amplitude and frequency as functions of the varying flow velocity.

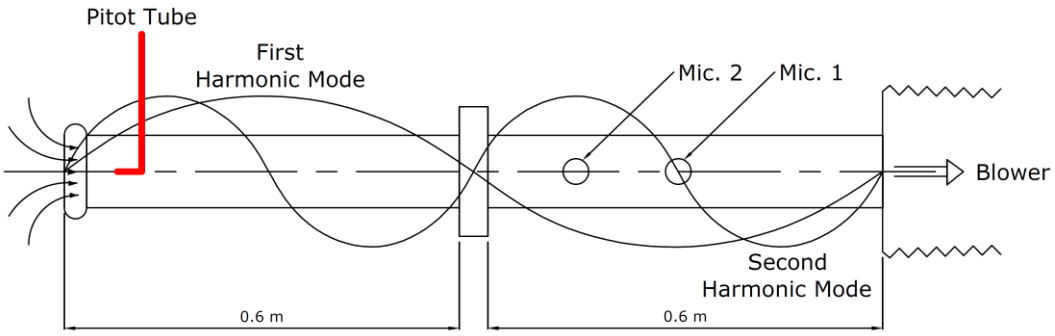

Figure 3.2. Schematic of the self-excited experimental setup

The schematic of the tested sharp edged multiple cavities is shown in Figure 3.3 with the experimental matrix of the source investigation summarized in Table 3.1. The tested cavities are 2″ long (L) and 1″ deep (H), and the separation plateau distance (L_p) is kept equal to the cavity length (L). The number of cavities is varied being one, two or three cavities. These geometrical parameters are maintained the same for the self-excited experiments for the sake of comparison. The tested Strouhal number range, from 0.35 to 1.2, covers the flow conditions corresponding to the first two hydrodynamic modes of the shear layer oscillation. For each Strouhal number, the acoustic velocity ratio is varied from 0.002 to 0.2.

3.3 Modeling

A semi-empirical model is developed to predict the acoustic response of multiple cavities. During resonance, the acoustic power generated by the multiple

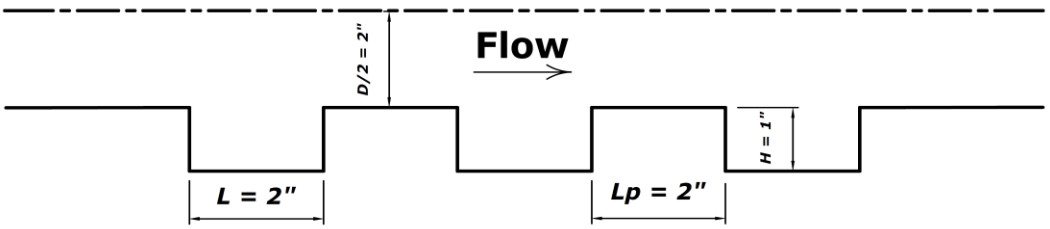

Figure 3.3. Sketch of the multiple cavities configuration in the current Study

Table 3.1. Experimental matrix for the aeroacoustic source investigation

Length to Depth Ratio (*L/H*)	2:1		
Spacing Ratio (L_p/L)	unity		
Strouhal Number (*St*)	0.35 – 1.2		
Excitation level (v/U)	0.002 – 0.2		
Number of Cavities	1	2	3

cavities counterbalances the piping system acoustic losses. In the empirical part of the model, the dimensionless aeroacoustic source, measured by the SWM in the experimental investigation, is used to estimate the acoustic power generated. The piping system acoustic losses, including radiation and visco-thermal losses, are calculated from basic principles. The equilibrium state, between the source and sink terms, represents the system conditions at which the resonance could be self-sustained and the corresponding amplitude of pressure oscillations. The model is validated against the data obtained from the self-excited experiments. The developed model, in conjunction with the measured source term, can be used to

predict self-excited resonances in various industrial systems that include multiple cavities with different boundary conditions.

A sweep test is performed over different flow velocities that covers the relevant range of Strouhal numbers. The acoustic velocity ratio (*v/U*), corresponding to steady state oscillation at each flow velocity, is defined from the amplitude at which the residual between the source and loss terms is minimum. For multiple cavity configurations, the source corresponds to the average acoustic velocity amplitude across the cavities section. The loss sink term (S_{loss}) is non-dimensionalized in the same manner as the source term for the sake of comparison.

$$S_{loss} = \frac{2\,\Delta Z}{Y_o\,M} \tag{3.2}$$

where, ΔZ is the acoustic impedance difference ($\Delta Z = \Delta P/(v\,.\,\pi a^2)$), Y_o is the characteristic acoustic impedance ($Y_o = \rho\,C/\pi a^2$) and M is the Mach number ($M = U/C$). The density and the speed of sound is determined based on the measured room parameters using the formulas given by Keefe (1984).

The impedance difference at the midspan of the test section is calculated from the upstream and downstream ends accounting for all different types of acoustic losses. The radiation impedance of an open ended pipe is known analytically and can be computed from the following expression reported by Munjal (1987) based on the fourth-order approximation done by Davies et al. (1980) for Levine and Schwinger model (1948):

$$Z = Y_o \frac{1+R}{1-R}, \tag{3.3}$$

$$R = |R| e^{j(\pi - 2k\delta)}, \tag{3.4}$$

$$|R| = 1 + 0.01336\, ka - 0.59079\, (ka)^2 + 0.33576(ka)^3 - 0.06432(ka)^4, \tag{3.5}$$

$$\frac{\delta}{a} = \begin{cases} 0.6133 - 0.1168\, (ka)^2, & ka < 0.5 \\ 0.6393 - 0.1104\, ka\,, & 0.5 < ka < 2 \end{cases}. \tag{3.6}$$

where, R is the reflection coefficient at the open end, k is the wave number and a is the pipe radius.

The other end of the piping system is a sudden expansion to a flexible hose that connects the system to the suction blower. An empirical reflection coefficient for that end was already measured by Mohamed (2015) for the same experimental setup in the presence of mean flow using the two microphone method and is shown by equation (3.7).

$$|R| = 1 - 0.022\, ka - 0.383\, (ka)^2, \tag{3.7}$$

The end impedances are then transferred along the duct by applying the acoustic standing wave equation, that gives the spatial acoustic pressure distribution, along with Euler's equation which yields the acoustic velocity distribution. The acoustic impedance is then defined as the ratio between the acoustic pressure and acoustic flux. The acoustic standing wave, as defined by equation (3.8), is based on two travelling waves P^+ and P^- that are travelling with and against the flow, respectively, at angular frequency (ω). The visco-thermal losses are included within the complex wave number (β) and the Mach number (M)

accounts for the effect of the mean flow. The complex wave number is estimated using equation (3.9) as shown by Davies (1981; 1988) and Munjal and Doige (1990). The attenuation coefficient (α_{flow}) is based on the no-flow attenuation coefficient given by Davies (1981; 1988) including the flow effect represented by the Mach number (M) as defined by Munjal (1987).

$$P(x,t) = \left\{P^{+}\, e^{\frac{-j\,\beta\,x}{(1+M)}} + \; P^{-}\, e^{\frac{j\,\beta\,x}{(1-M)}}\right\} e^{j\,\omega t}, \tag{3.8}$$

$$\beta = \; k \; + \; \alpha_{flow}\,(\,1 - i). \tag{3.9}$$

The cross-sectional area change at the cavities acts as reactive inductance (I) as given by Kregomard and Garcia (1987). The value of I depends on the diameter ratio (α) as shown by equation (3.10), where $\varepsilon = 1 - \alpha$. This is understood in the context of sound wave reflection upon duct area change.

$$\frac{I\,a}{\rho} = (4/\pi^2)\varepsilon^2(-0.49198\; ln\varepsilon + 0.50349 - 0.376246\;\varepsilon^2 - 0.852222\;\varepsilon^2\; ln\varepsilon). \tag{3.10}$$

The presence of an impedance (Z) in-line with the path of an acoustic wave, as in the case of area change, between two points (1) and (2) will not affect the value of the acoustic flux based on continuity. So, applying the conservation of normal acoustic flux (Q) and then applying the definition of impedance yields:

$$Q_1 = \; Q_2, \tag{3.11}$$

$$P_2 = P_1 - Z\,.\,Q_1\,. \tag{3.12}$$

As will be shown in the results section, the initial formulation of the present model is found to over predict the amplitude of the self-excited oscillations, which

indicates an underestimation of the system losses. This is because the model did not account for any absorption losses at the cavity edges upon area change. This effect has been addressed by Ronneberger (1967), Boij and Nilsson (2006) and Dupere and Dowling (2001). Ronneberger (1967) validated experimentally the absorption losses of acoustic waves upon area change in circular ducts. The absorption was defined as the discrepancy between the intensity of the incident wave as compared to the summation of both the reflected and transmitted waves. Boij and Nilsson (2006) developed a vortex sheet numerical model that showed good agreement with Ronneberger data. Dupere and Dowling (2001) employed an analytical approach by solving the acoustic wave equation using Green's functions. The energy exchange between the flow and the acoustic wave was estimated based on the analogy proposed by Howe (1980). The model indicated that a portion of the incident acoustic energy was dissipated at the varying area interface. Acoustic measurements were also performed to validate the model findings. It should be noted however that the geometrical parameters and flow conditions in the aforementioned investigations do not quite match those encountered in the current study. Therefore, the adopted approach is to tune the absorption impedance for a single cavity in a short piping system to adequately predict the oscillation amplitude. The tuned model is then tested against different pipe lengths and different number of cavities. Moreover, the current absorption coefficient is

compared with the corresponding values in the literature while illustrating the differences in the experimental conditions.[1]

3.4 Results

3.4.1 Assessment of the Measurement Technique Accuracy

Uncertainty analysis is done on the measured aeroacoustic source. The propagation of the basic equipment uncertainties towards the final source value is calculated using Kline McClintock approach (1953) that is based on Taylor series method (Coleman and Steele, 2009). The uncertainty of the source, for the three-cavity configuration at an intermediate excitation level of 3.2% and a Strouhal number of 0.6, is estimated to be 2%, which is fairly acceptable. However, as the source value varies with Strouhal number, this uncertainty percentage is not descriptive of the error involved in the source term when its value becomes very small. For this reason, a series of tests are performed to assess the accuracy of the SWM that is applicable even for small source values.

The standing acoustic wave equation in a duct, shown in equation (3.8), includes two unknowns that need two microphone measurements to be evaluated. Three microphones are used in the current experimental facility, as previously discussed, and the wave equation unknowns are evaluated based on least square method to increase the accuracy of the measurements. In the first accuracy check,

[1] More information about the cavity edge absorption losses is presented in Appendix C.1.1.

the average residual error percentage in both the upstream and downstream microphones is calculated at different Strouhal numbers and acoustic excitation levels for the three-cavity configuration and is shown in Figure 3.4 for the upstream pipe. The residual error percentage is defined as the deviation of the microphone acoustic pressure estimated by the three-microphone method from the actual measurement normalized by the actual measurement. For the whole measurement range, including conditions of small source values, the maximum residual error percentage is below 0.8%. For the downstream pipe, this value has been found to be even smaller (0.3%).

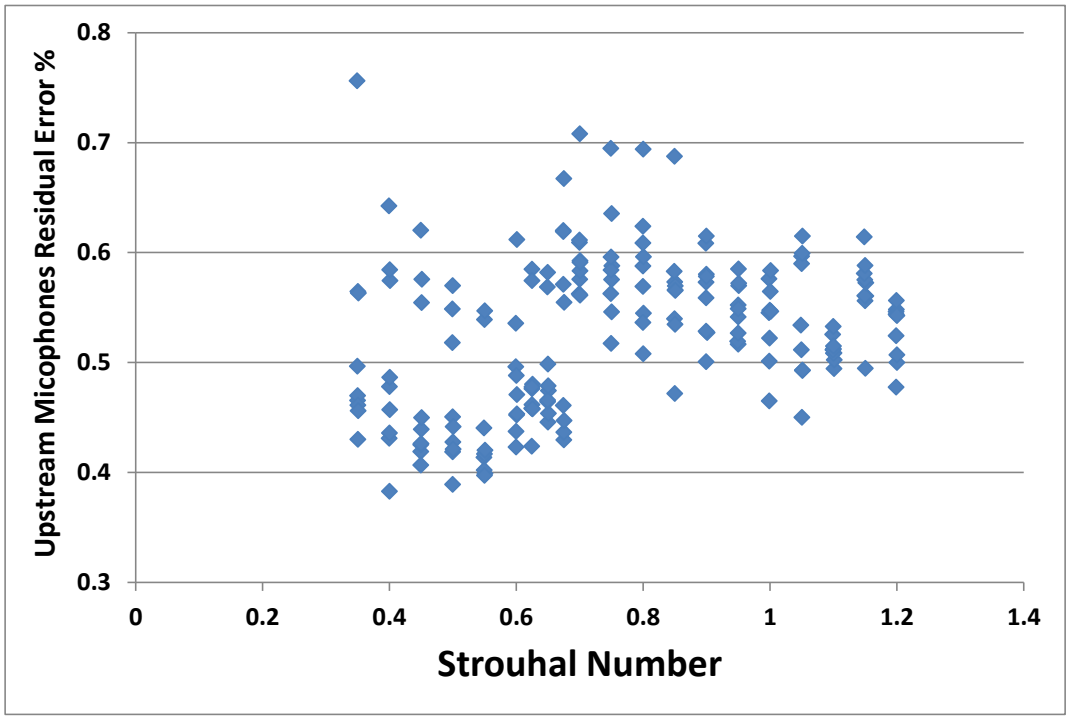

Figure 3.4. The residual error percentage for upstream microphones at different Strouhal numbers for the three-cavity configuration. Data points at the same Strouhal number represent different excitation levels.

The second accuracy test is to verify the conservation of acoustic flux (i.e. continuity equation). The acoustic flux at the middle section of the multiple cavities is calculated from both the upstream and downstream acoustic standing waves. The percentage error in the acoustic flux is defined as the difference between the upstream and downstream fluxes normalized by the mean acoustic flux. The maximum percentage error in the acoustic flux for the three-cavity configuration has been found to be less than 1.8% for all possible combinations of Strouhal numbers and acoustic excitation levels. The results of these preliminary tests confirmed the high accuracy of the method used to measure the aeroacoustic source.

3.4.2 Source characteristics of multiple cavity configurations

The aeroacoustic source results, measured by means of the SWM, will be presented for different cavity configurations. The source is measured as a complex value with the real part representing the active energy exchange between the flow and the sound field. On the other hand, the imaginary part of the source is a measure of the reactive energy which affects the resonance frequency, albeit only slightly. The real part of the source for the two-cavity configuration, non-dimensionalized as shown by equation (3.1), is plotted against the Strouhal number in Figure 3.5 for different acoustic velocity ratios. The regions of positive real source (St = 0.45 - 0.7 and St = 0.9 – 1.1) indicate acoustic energy generation by the first and second hydrodynamic modes of the shear layer oscillations, respectively. The hydrodynamic mode number represents the instantaneous number of vortices travelling streamwise along the cavity span. Stronger aeroacoustic sources are

associated with the first hydrodynamic mode, which is also called the fundamental mode, and industrial problems are usually attributed to this stronger mode. Consequently, the main focus in the current investigation is dedicated to that mode and its corresponding high source value. The onset Strouhal number for both hydrodynamic modes seems to be independent of the acoustic velocity ratio; being 0.7 for the first and 1.1 for the second hydrodynamic modes. The dimensionless source value decreases consistently upon increasing the excitation level. This is a typical trend in aeroacoustic maps based on the source definition being normalized by the acoustic velocity ratio. The source value exhibits a considerable dip at Strouhal numbers below the peak of the fundamental mode. This observation is unique to the two-cavity configuration and was not reported for the single cavity measurements neither in the current nor previous investigations. This may be attributed to a destructive interference as a result of the hydrodynamic coupling between the two neighboring cavities. However, this phenomenon becomes less pronounced with higher excitation levels and eventually disappears for sufficiently high acoustic velocity ratios ($v/U \geq 0.02$). This change in behavior is likely caused by variations in the convection speed of shear layer disturbances which affect the synchronization of vortical structures at the neighboring cavities. The decrease of the Strouhal number corresponding to the peak source at high excitation levels backs up a corresponding decrease in the convection speed. The effect of excitation level on the vortex convection speed was previously reported for the flow over a single cavity by Mohamed and Ziada (2015) via tracing the vortex center over the

acoustic cycle using phase locked Particle Image Velocimetry (PIV) images. The same phenomenon was also observed for the flow over a deep cavity by Ziada (1994) using smoke flow visualization techniques. At high excitation levels, the vortices were trapped inside the cavity near the leading edge for a considerable portion of the acoustic cycle. Similar observation was reported by Bruggeman et al. (1991) and Peters (1993) for closed side-branches fluid resonant oscillations.

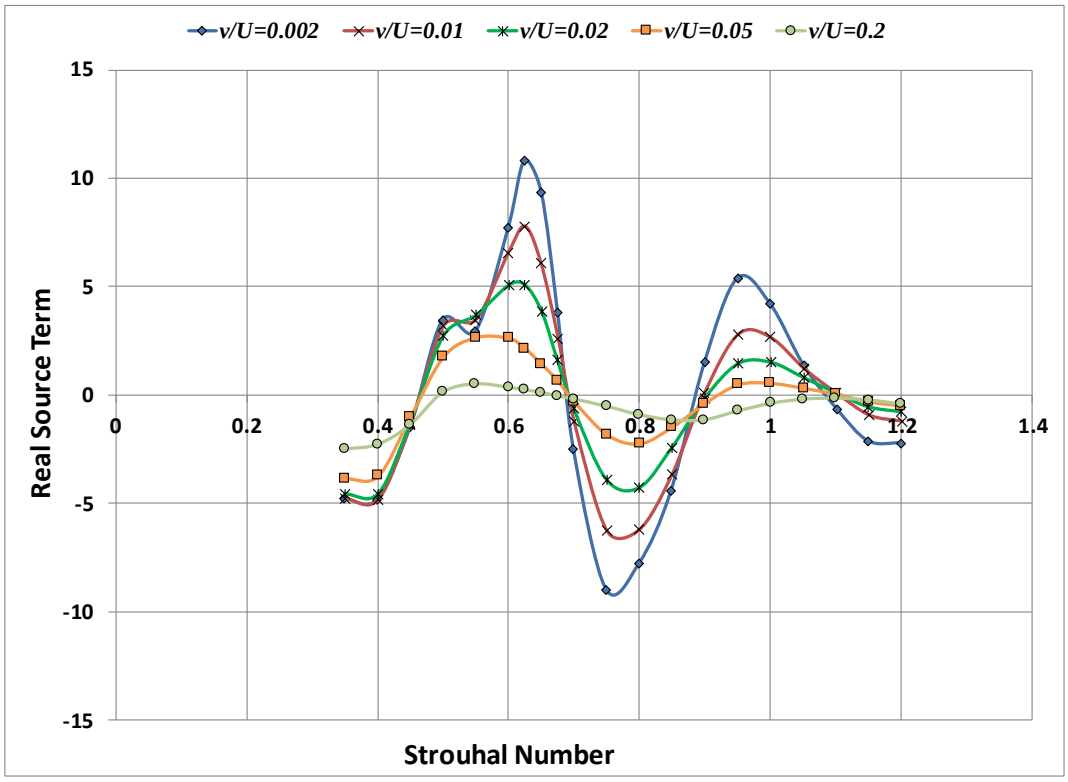

Figure 3.5. Real source term vs. Strouhal number for different acoustic velocity ratios for the two-cavity configuration

The real part of the aeroacoustic source is presented against the acoustic velocity ratio for different Strouhal numbers in Figure 3.6 for the three-cavity configuration. The source value decreases with the increasing acoustic velocity ratio beyond 0.01. The non-linear relationship between the source and the excitation

level is clearly depicted in Figure 3.6 which agrees with the reported trends for the single cavity source. The maximum value of the source, and whether being positive or negative, depends on the Strouhal number and its location with respect to the lock-in regions. Five Strouhal values are chosen to represent the full spectrum. Acoustic power generation, accompanied with positive source, is shown by two values picked near the center of the fundamental and second hydrodynamic modes, St = 0.6 & 0.95, respectively. The other three values correspond to one case in between the two hydrodynamic modes and two cases with extremum values at the higher and lower ends. Consequently, the corresponding source values are negative, i.e. sink term.

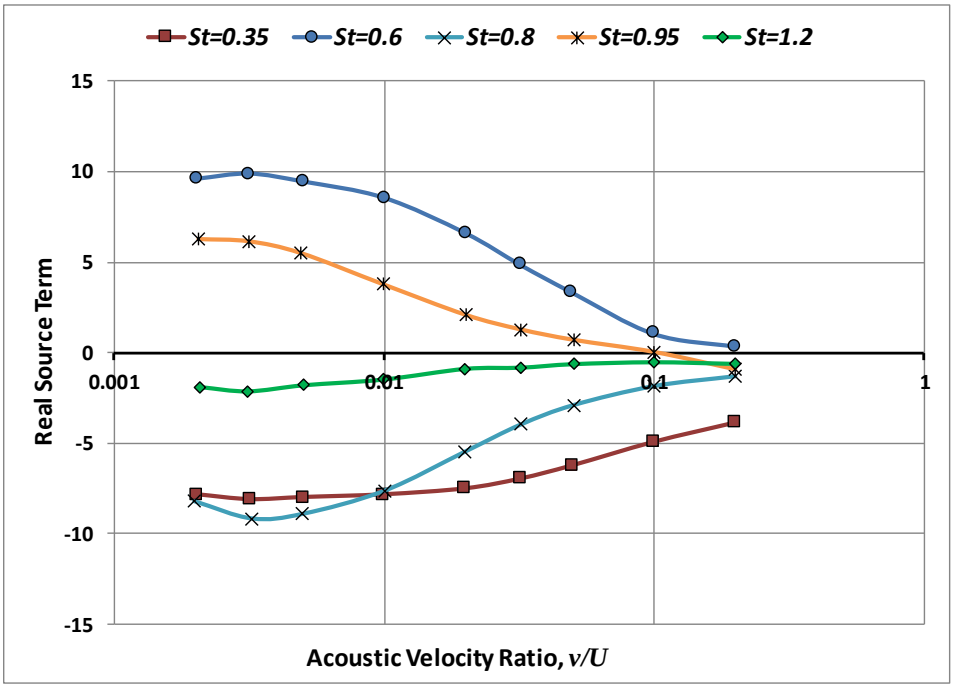

Figure 3.6. Real source term vs. acoustic velocity ratio for different Strouhal numbers for the three-cavity configuration

The imaginary part of the source term, non-dimensionalized as shown by equation (3.1), is plotted against the Strouhal number in Figure 3.7 for different excitation levels for the two-cavity configuration. It is noted that at the Strouhal number where the maximum real source is measured, the imaginary part nearly vanishes showing pure resonance independent of the excitation level. The general characteristics discussed above for the aeroacoustic source are found to be similar for all the three investigated configurations.

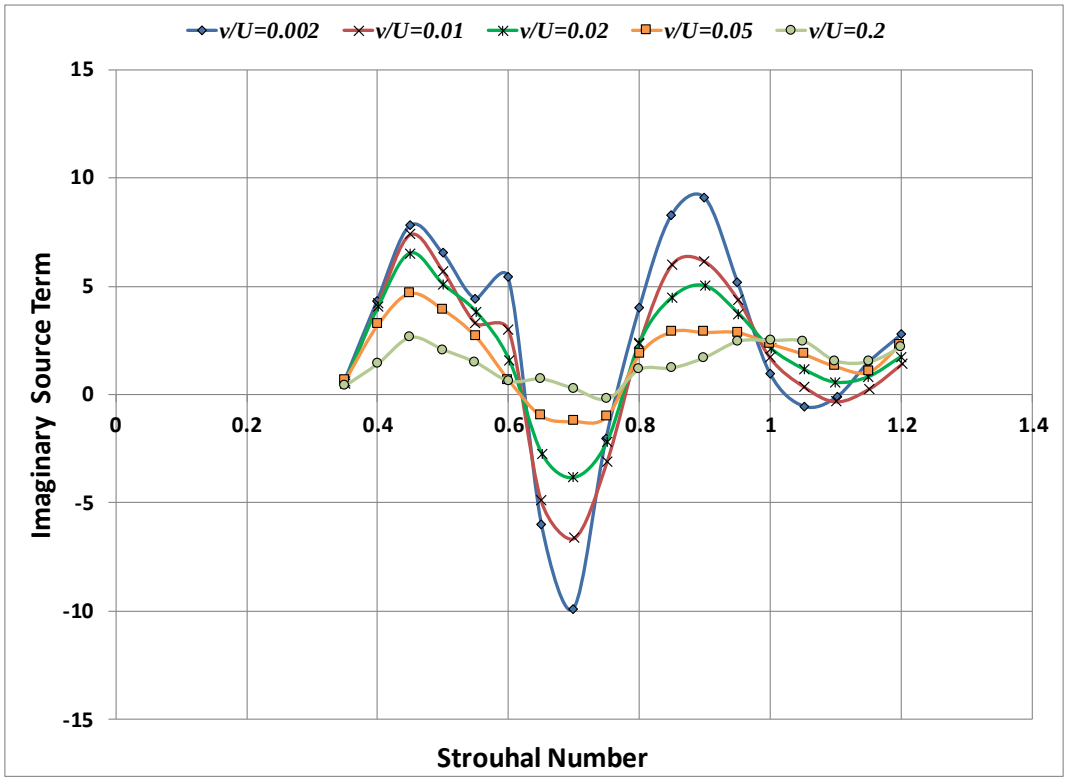

Figure 3.7. Imaginary source term vs. Strouhal number for different acoustic velocity ratios for the two-cavity configuration

The measured source is compared with the recently published data for single shallow cavities (Nakiboglu et al., 2012; Mohamed and Ziada, 2015). The comparison is held for the single cavity case with a length-to-depth ratio of 2:1 and

an acoustic excitation level of 5%. However, the cavity volumes are different in the three studies. Mohamed and Ziada (2015) measured the source experimentally using the SWM and reported a value of 1.96, which is 8% higher than the current value of 1.81. This is quite acceptable taking into consideration that Mohamed and Ziada's cavity is 18% larger in volume and it is experimentally proven that the source non-linearly increases with the increased cavity volume for the same length-to-depth ratio (Mohamed and Ziada, 2015). By means of CFD simulation, Nakiboglu et al. (2012) estimated the source to be 3.08, upon normalization using equation (3.1). It is pointed out in their investigation that the source is over estimated by a factor of two as compared to experiments. However, half of their estimated source is 15% lower than the currently measured one which can be explained by acknowledging that their cavity volume is 68% smaller.

The real source term is plotted against Strouhal number for different cavity combinations in Figure 3.8 for v/U = 0.002, 0.01 and 0.1. The aeroacoustic source non-linearly increases with the increasing number of cavities. This trend is consistent regardless of the value of the acoustic velocity ratio. At the low excitation level in Figure 3.8(a), the dip in the source around a Strouhal number of 0.55, attributed to the destructive coupling, results in almost the same source for the single and double cavity configurations, indicating minimal contribution of the second cavity. It is worth mentioning that for the three-cavity configuration at the same test conditions, the dip in the source is not as pronounced due to the more complicated interaction mechanism. The unsteady vorticity field of the first cavity

is expected to counteract that of the second, as mentioned earlier, which may leave a better chance for the third cavity to freely shed vorticity and thereby produces acoustic power. As discussed earlier, the destructive interference effect is less pronounced for higher excitation levels. The lock-in ranges of the different configurations collapse to the same Strouhal range, which emphasizes the fact that the length of the cavity remains the proper length scale for the case of multiple cavities. The Strouhal numbers at the onset of the lock-in ranges for the first and second shear layer modes are virtually the same for the three cavity combinations and are independent of the excitation level; indicating the initial flow conditions when the cavity is about to generate acoustic energy. On the other hand, the lock-in range becomes wider slightly upon increasing the number of cavities. In order to have a deeper look, the increase in the peak source value upon adding each extra cavity, as compared with the previous configuration, is shown in Figure 3.9 for different excitation levels. The third cavity generally does not have as strong impact as the second one. However, the difference between the contributions of the second and third cavities decreases upon increasing the excitation level and almost vanishes at the 10% excitation case. This may be attributed to the changes in the phase speed at the high excitation levels affecting the hydrodynamic coupling nature as pointed out earlier in the discussion.

3.4.3 Self-excited oscillations

Self-excited oscillations of the multiple cavity configurations have also been investigated. The dimensionless acoustic pressure is shown versus the

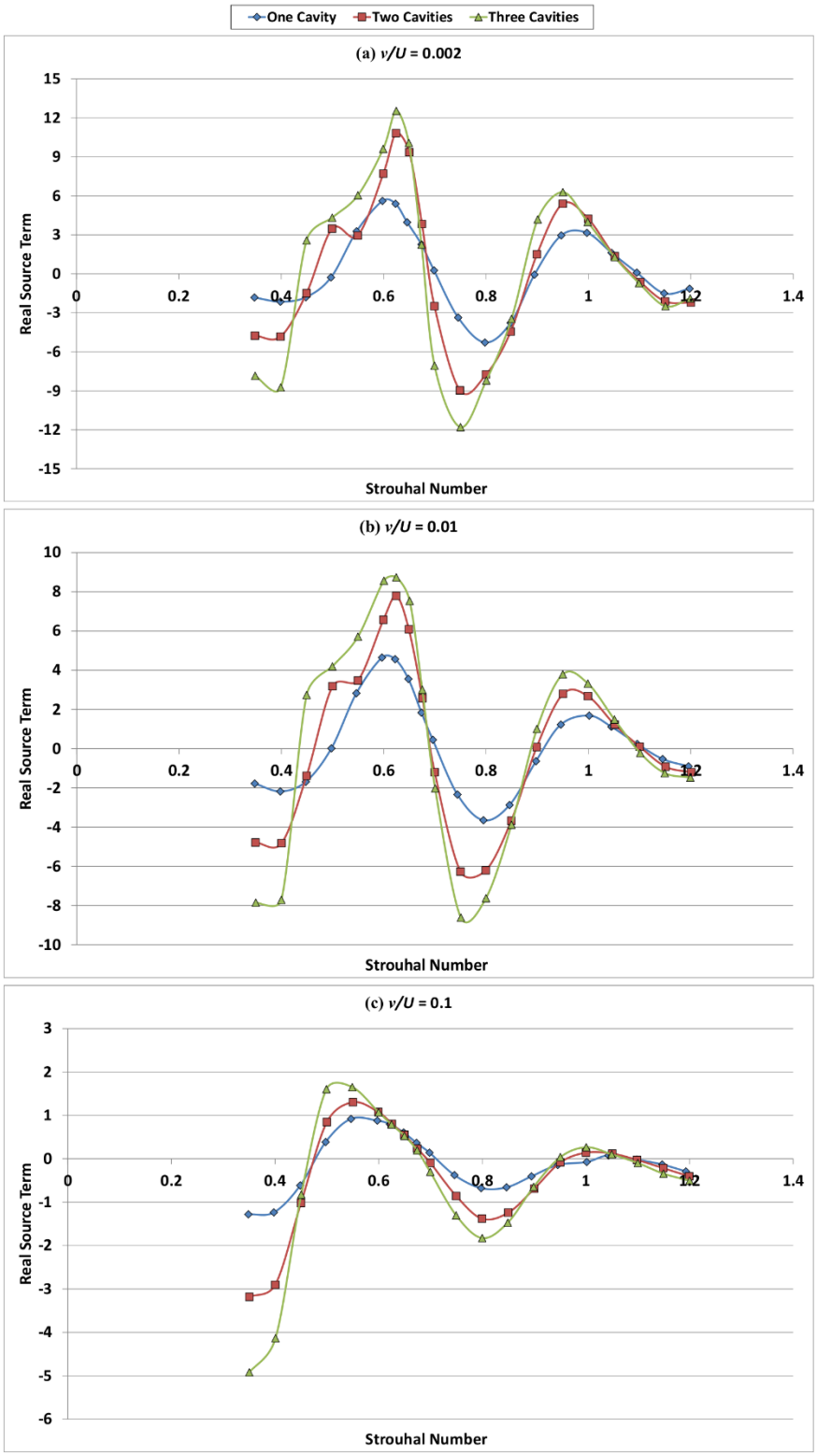

Figure 3.8. Real source term vs. Strouhal number for different number of cavities at *ν/U* = 0.002, 0.01 and 0.1

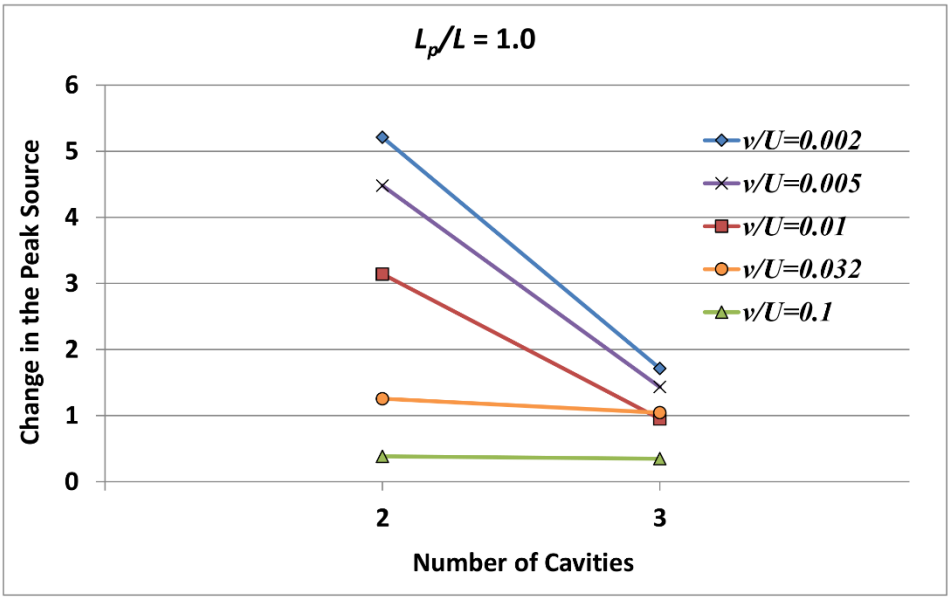

Figure 3.9. The change in the peak source with the increasing number of multiple cavities for different excitation levels

Strouhal number in Figure 3.10 for the one, two and three-cavity configurations. The resonance Strouhal number range is virtually similar in the three cases; providing additional evidence on the validity of using the cavity length for defining the Strouhal number for sharp edged multiple cavities. The pressure amplitude increases non-linearly with the number of multiple cavities. The amplitude of oscillations for the two-cavity configuration is enhanced by 69% above the single cavity amplitude, while the third cavity has a limited impact as it increases the pressure amplitude by only 6% above the two-cavity case. The destructive interference effect is observed again for the two-cavity configuration, around a Strouhal number of 0.67, with a clear drop in the oscillations amplitude. So, it can be concluded that similar features have been observed for the measured aeroacoustic source and the self-excited response.

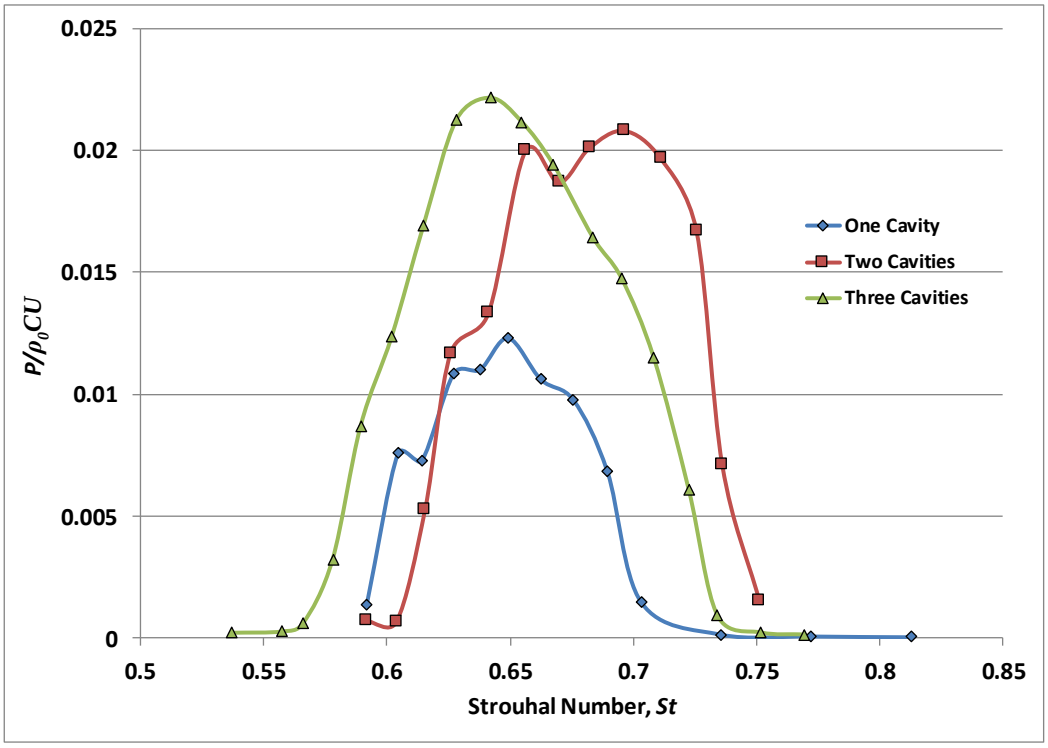

Figure 3.10. Self-excited normalized pressure amplitude vs. Strouhal number for one, two and three cavities

The resonance frequency is expected to remain fairly constant throughout the lock-in range. This phenomenon is observed for each of the three multiple cavity configurations as illustrated in Figure 3.11. The increasing number of multiple cavities increases the physical length of the system and consequently the wavelength also increases, which results in a slight decrease in the resonance frequency. This is never a concern with the fairly long setup used for the externally excited experiments. However, a deviation of the resonance frequency for the self-excited test cases is observed up to a maximum value of about 8%. Another interesting phenomenon, which is consistently observed for each of the tested configurations, is the slight increase of the resonance frequency as the Strouhal

number decreases, i.e. with increasing flow velocity. This is essential to maintain the synchronization between the acoustic and hydrodynamic cycles within the lock-in range. This phenomenon was also previously reported in other fluid resonant cases as in the case of flow over closed side-branches which is recently reviewed by Tonon et al. (2011).

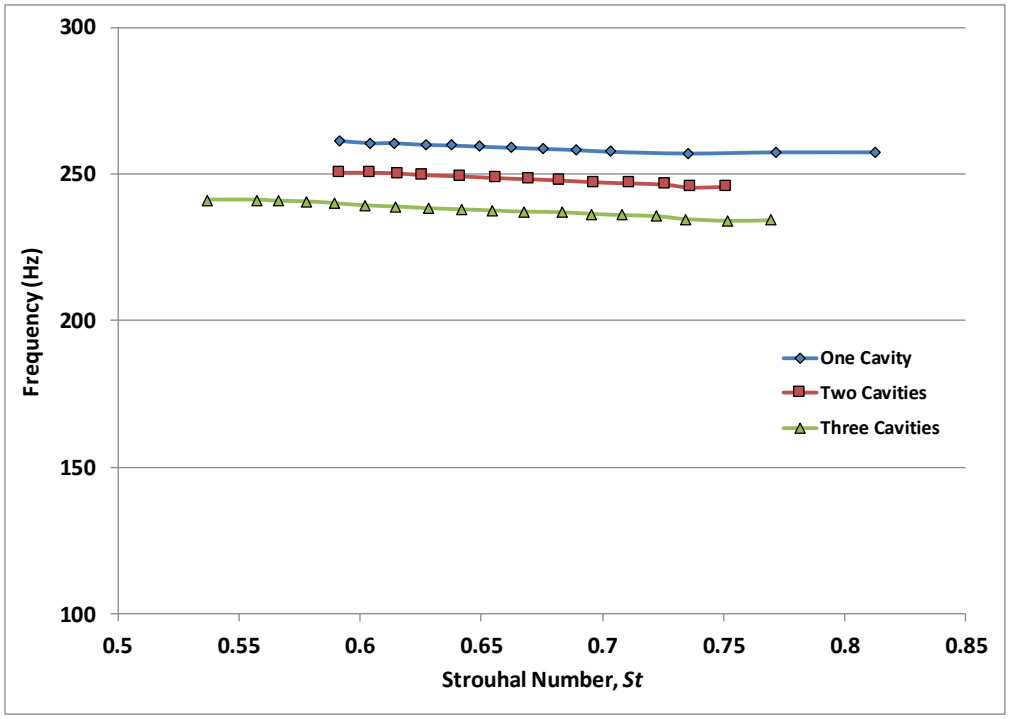

Figure 3.11. Self-excited lock-in frequency vs. Strouhal number for one, two and three cavities

3.4.4 Prediction of the Self-Excited Resonance

A model is developed to estimate the amplitude of pressure pulsations in a piping system housing multiple shallow cavities. The details of the model have already been described in the modelling section. The self-excited measurements will be used to validate the model. As mentioned earlier, accurate prediction requires that the system acoustic losses be properly modelled. Attention is first

dedicated to the single cavity configuration before proceeding to the multiple cavity configurations.

The model results for a single cavity centered between two short pipes 30 cm in length are shown in Figure 3.12. The initial acoustic model seems to over predict the pressure amplitude indicating an underestimation of the piping system losses. As discussed earlier in the modelling section, the absorption losses at the cavity edges are not included in the initial model. Since these losses were proven in the literature experimentally and numerically, a tuned model is developed to take these absorption losses into consideration. The data in the aforementioned literature could not be utilized directly in the current study because of differences in the area ratio and the flow parameters. An absorption impedance is selected such that the model results agree with the experimental amplitude as indicated in Figure 3.12. In order to verify the selected absorption impedance value, which is obtained from the discussed single cavity case, the model prediction is tested against cases with different piping length and different arrangements of multiple cavities. Moreover, a comparison between the selected absorption coefficient and those reported in the literature will be discussed. Absorption loss upon area change, as reported in the literature, is typically a function of the Strouhal number (St_a) defined based on the smaller pipe radius (a). The selected model absorption impedance is given by equation (3.13), where (k) is the wave number and (M) is the Mach number. The absorption impedance is defined in this manner to account for any slight variation in the Strouhal (St_a) value among the different studied cases.

$$Z_{abs} = 570 \frac{k\,a}{M} \tag{3.13}$$

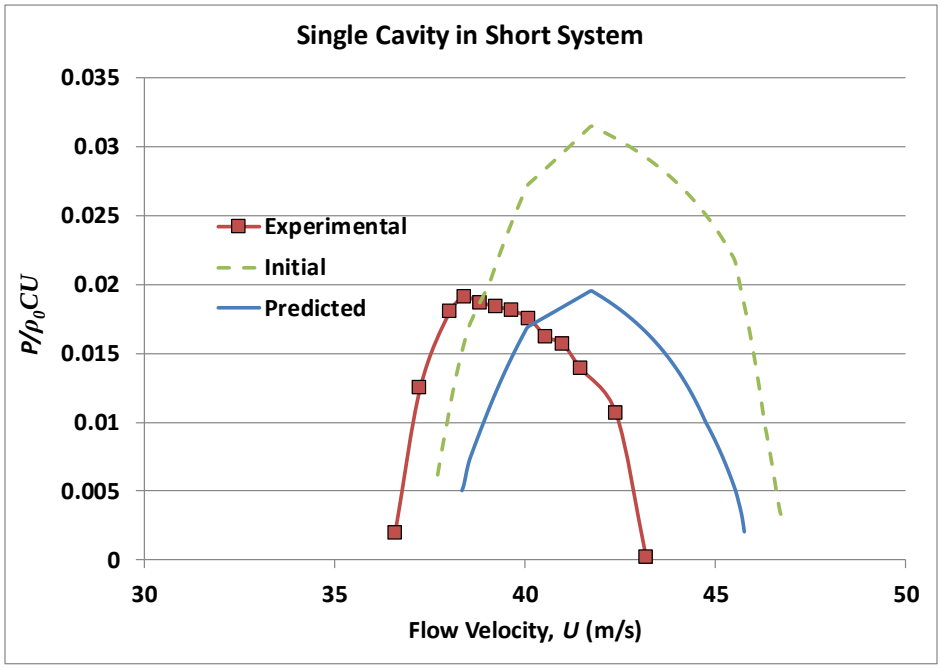

Figure 3.12. Experimental vs. predicted dimensionless amplitude for the single cavity in the short piping system

The tuned model is then used to estimate the single cavity response with longer pipes of 60 cm as shown in Figure 3.13. The lock-in resonance range is predicted, and the peak amplitude matches the experimental value satisfactorily. Before proceeding to the multiple cavities, the selected loss coefficient is compared with the values given in the literature. The area ratio considered in the study by Dupere and Dowling (2001) is the closest to the geometry of current investigation. The comparison is summarized in Table 3.2. Considering the differences between the two studies, fair agreement is observed between the current absorption coefficient (20%) and that reported by Dupere and Dowling (11%). The slightly higher absorption coefficient may be attributed to the higher Mach number and

smaller area ratio encountered in the current study. Both differences are expected to increase the absorption losses. The model is then used to predict the oscillations of two and three-cavity configurations as shown in Figure 3.14 and Figure 3.15, respectively. The long piping system is used for both configurations. The model successfully predicts the oscillation amplitude for the multiple cavity cases. The maximum deviation in the dimensionless peak amplitude for all the encountered cases is about 17% for the case with the minimum amplitude.

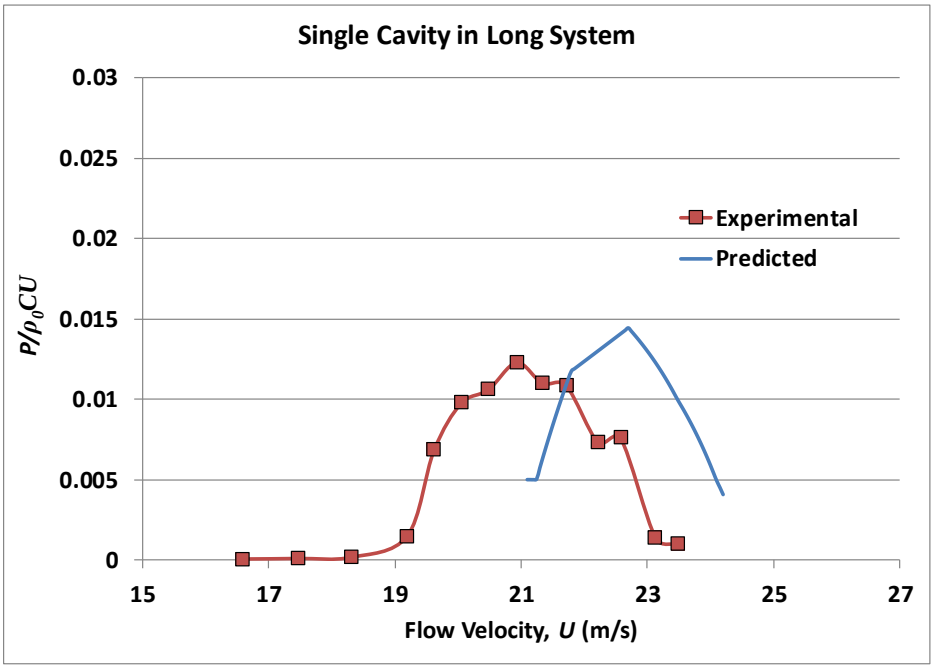

Figure 3.13. Experimental vs. predicted dimensionless amplitude for the single cavity in the long piping system

The lock-in ranges predicted by the semi-empirical model are slightly shifted towards higher flow velocities as compared to the self-excited experimental measurements. This can be explained by the difference in the boundary layer

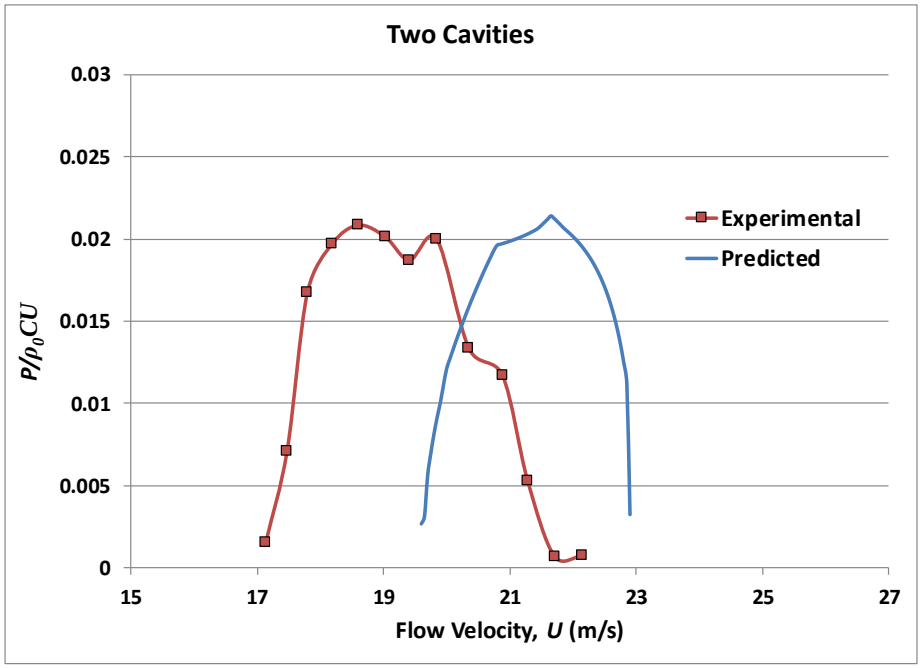

Figure 3.14. Experimental vs. predicted dimensionless amplitude for the two-cavity configuration

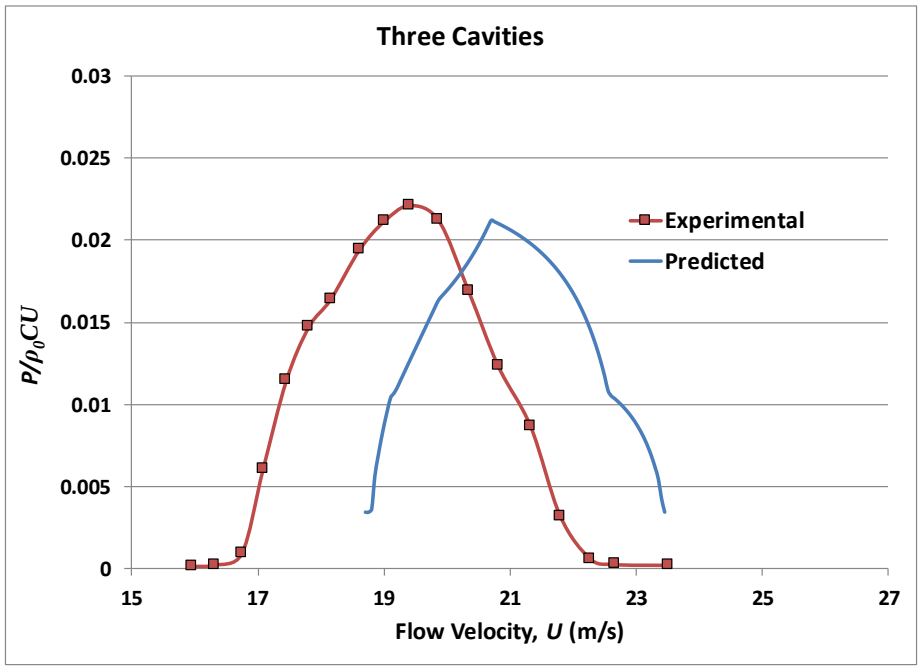

Figure 3.15. Experimental vs. predicted dimensionless amplitude for the three-cavity configuration

Table 3.2. Comparison between the absorption coefficient of the current study and that reported by Dupere and Dowling (2001)

	Prediction Model	Dupere & Dowling (2001)
Strouhal Number (St_a)	0.6	0.6
Area Ratio (λ)	0.65	0.73
Mach Number (M)	0.06	0.05
Absorption Coefficient	**20%**	**11%**

thickness between the SWM setup, from which the source term is measured, and setup of the self-excited oscillations. The SWM setup is fairly long to achieve fully developed flow conditions but the self-excited oscillation in the short setup is excited by developing flow with a thinner boundary layer. In the case of fully developed flows with thicker boundary layer, a higher mean flow is required for the local velocity at the shear layer to reach the value at the onset of the lock-in range. A similar phenomenon was reported by Nakiboglu et al. (2012). This difference of flow conditions would not be an issue while utilizing the present model and the measured source term for industrial applications where fully developed flows are prominent.

3.5 Conclusions

This study investigated the acoustic response for the flow over multiple shallow cavities. Single, double and triple-cavity configurations were tested with fixed geometrical parameters. The aeroacoustic source increases in a non-linear

manner with increasing the number of cavities which indicates a hydrodynamic interaction mechanism between neighboring cavities. At certain flow conditions, a dip in the source strength is observed such that the source of the two-cavity configuration becomes comparable to that of the single cavity as a result of destructive hydrodynamic interference between the cavities. The contribution of the third cavity source is generally less than that of the second at low and intermediate excitation levels. This becomes less significant at high acoustic excitation levels. The collapse of the lock-in ranges of different configurations substantiates using the cavity length as the appropriate physical length scale to describe the acoustic response of multiple cavities. The width of the lock-in range increases with the increasing number of cavities. Self-sustained acoustic pressure pulsations of the same cavity configurations are tested showing features similar to the aeroacoustic source characteristics.

The source measured by means of the SWM was then used to predict the self-excited oscillation amplitude with the aid of a developed semi-empirical model. This is an essential step towards applying the laboratory measured source to an industrial system with different geometrical parameters and boundary conditions. The system radiation and visco-thermal losses are modelled from basic principles. Acoustic absorption upon area change at the cavity edges is shown to be crucial in properly estimating the system losses. The model is capable of successfully predicting the oscillation amplitude of a single cavity in two different

piping configurations, as well as the self-excited acoustic response for the two and three-cavity configurations.

Nomenclature

a	Pipe radius (m)
C	Speed of sound (m/s)
D	Pipe diameter (m)
f	Resonance frequency (Hz)
H	Cavity depth (m)
I	Inductance upon area change (Pa s/m^3)
K	Wave number (m^{-1})
L	Cavity length (m)
L_p	Separation plateau distance between cavities (m)
M	Mach number
P	Acoustic pressure (Pa)
ΔP	Acoustic pressure difference across the cavity section (Pa)
Q	Acoustic flux (m^3/s)
R	Acoustic wave reflection coefficient
S	Normalized aeroacoustic source
S_{loss}	Normalized aeroacoustic loss or sink term
St	Strouhal number based on the cavity length

St_a	Strouhal number based on the pipe radius
U	Flow velocity (m/s)
v	Acoustic particle velocity (m/s)
Y_0	Characteristic acoustic impedance (Pa s/m^3)
ΔZ	Acoustic impedance difference across the cavity section (Pa s/m^3)
Z_{abs}	Absorption impedance loss at the cavity edges (Pa s/m^3)
ρ_0	Air density (kg/m^3)
A	Pipe diameter ratio
λ	Area change ratio
β	Complex wave number (m^{-1})
ω	Angular frequency (rad/s)

References

Belfroid, S., Shatto, D., and Peters, M., 2007. Flow induced pulsations caused by corrugated tubes. *In*: *Pressure Vessels and Piping Conference*. ASME, 439–447.

Boij, S. and Nilsson, B., 2006. Scattering and absorption of sound at flow duct expansions. *Journal of Sound and Vibration*, 289 (3), 577–594.

Bruggeman, J., Hirschberg, A., van Dongen, M., Wijnands, A., and Gorter, J., 1989. Flow Induced Pulsations in Gas Transport Systems: Analysis of the Influence of Closed Side Branches. *Journal of Fluids Engineering*, 111 (4), 484–491.

Bruggeman, J., Hirschberg, A., Van Dongen, M., Wijnands, A., and Gorter, J., 1991. Self-sustained aero-acoustic pulsations in gas transport systems: experimental study of the influence of closed side branches. *Journal of Sound and Vibration*, 150 (3), 371–393.

Coleman, H. and Steele, W., 2009. *Experimentation, validation, and uncertainty analysis for engineers*. Third edition. John Wiley & Sons.

Davies, P., 1981. Flow-acoustic coupling in ducts. *Journal of Sound and Vibration*,

77 (2), 191–209.

Davies, P., 1988. Practical flow duct acoustics. *Journal of Sound and Vibration*, 124 (1), 91–115.

Davies, P., Coelho, J., and Bhattacharya, M., 1980. Reflection coefficients for an unflanged pipe with flow. *Journal of Sound and Vibration*, 72 (4), 543–546.

Dequand, S., Hulshoff, S., and Hirschberg, A., 2003. Self-sustained oscillations in a closed side branch system. *Journal of Sound and Vibration*, 265 (2), 359–386.

Doherty, J., Ngan, P., Monty, J., and Chong, M., 2007. The development of turbulent pipe flow. *In*: *16th Australasian Fluid Mechanics Conference*. 266–270.

Dupere, I.D.J. and Dowling, A.P., 2001. The absorption of sound near abrupt axisymmetric area expansions. *Journal of Sound and Vibration*, 239 (4), 709–730.

Golliard, J., González-Díez, N., Belfroid, S., Nakiboğlu, G., and Hirschberg, A., 2013. U-RANS model for the prediction of the acoustic sound power generated in a whistling corrugated pipe. *In*: *Pressure Vessels and Piping Conference*. ASME, PVP2013-97385.

Graf, H. and Ziada, S., 1992. Flow induced acoustic resonance in closed side branches: an experimental determination of the excitation source. *In*: *International Symposium on Flow-Induced Vibration and Noise*. ASME, 63.

Graf, H. and Ziada, S., 2010. Excitation source of a side-branch shear layer. *Journal of Sound and Vibration*, 329 (14), 2825–2842.

Howe, M., 1980. The dissipation of sound at an edge. *Journal of Sound and Vibration*, 70 (3), 407–411.

Keefe, D., 1984. Acoustical wave propagation in cylindrical ducts: Transmission line parameter approximations for isothermal and nonisothermal boundary conditions. *The Journal of the Acoustical Society of America*, 75 (1), 58–62.

Kergomard, J. and Garcia, A., 1987. Simple discontinuities in acoustic waveguides at low frequencies: critical analysis and formulae. *Journal of Sound and Vibration*, 114 (3), 465–479.

Kline, S. and McClintock, F., 1953. Describing uncertainties in single-sample

experiments. *Mechanical Engineering*, 75, 3–8.

Kriesels, P., Peters, M., Hirschberg, A., Wijnands, A., Iafrati, A., Riccardi, G., Piva, R., and Bruggeman, J., 1995. High amplitude vortex-induced pulsations in a gas transport system. *Journal of Sound and Vibration*, 184 (2), 343–368.

Levine, H. and Schwinger, J., 1948. On the Radiation of Sound from an Unflanged Circular Pipe. *Physical Review*, 73 (4), 383–406.

Mohamed, S., 2015. Sound waves excitation by flow in a pipe housing a shallow cavity. PhD Thesis, McMaster University.

Mohamed, S., Graf, H., and Ziada, S., 2011. Aeroacoustic source of a shallow cavity in a pipeline. *In*: *Pressure Vessels and Piping Conference*. ASME, 269–276.

Mohamed, S. and Ziada, S., 2014. PIV Measurements of Aeroacoustic Sources of a Shallow Cavity in a Pipeline. *In*: *Pressure Vessels and Piping Conference*. ASME, PVP2014-28508.

Mohamed, S. and Ziada, S., 2015. Effect of Cavity Volume on the Flow-Excited Acoustic Resonance of a Shallow Cavity in a Pipe-Line. *In*: *Pressure Vessels and Piping Conference*. ASME, PVP2015-45205.

Munjal, M., 1987. *Acoustics of ducts and mufflers with application to exhaust and ventilation system design*. First edition. John Wiley & Sons.

Munjal, M. and Doige, A., 1990. The two-microphone method incorporating the effects of mean flow and acoustic damping. *Journal of Sound and Vibration*, 137 (1), 135–138.

Nair, K. and Sarkar, S., 2016. Large Eddy Simulation of Self-Sustained Cavity Oscillation for Subsonic and Supersonic Flows. *Journal of Fluids Engineering*, 139 (1), 11102.

Nakiboglu, G. and Hirschberg, A., 2012. Aeroacoustic power generated by multiple compact axisymmetric cavities: Effect of hydrodynamic interference on the sound production. *Physics of Fluids*, 24 (6), 67101.

Nakiboglu, G., Rudenko, O., and Hirschberg, A., 2013. Hydrodynamic interference in corrugated pipes. *In*: *ICSV 20*. 865–872.

Nakiboglu, G., Manders, H., and Hirschberg, A., 2012. Aeroacoustic power generated by a compact axisymmetric cavity: prediction of self-sustained oscillation and influence of the depth. *Journal of Fluid Mechanics*, 703, 163–

191.

Oshkai, P., Yan, T., Velikorodny, A., and VanCaeseele, S., 2008. Acoustic Power Calculation in Deep Cavity Flows: A Semiempirical Approach. *Journal of Fluids Engineering*, 130 (5), 51203.

Peters, M., 1993. Aeroacoustic sources in internal flows. PhD Thesis, Eindhoven University of Technology.

Popiel, C., Kozak, M., Małecka, J., and Michalak, A., 2013. Friction Factor for Transient Flow in Transverse Corrugated Pipes. *Journal of Fluids Engineering*, 135 (7), 74501.

Radavich, P., Selamet, A., and Novak, J., 2001. A computational approach for flow–acoustic coupling in closed side branches. *The Journal of the Acoustical Society of America*, 109 (4), 1343–1353.

Rajavel, B. and Prasad, M., 2014. Parametric studies on acoustics of corrugated tubes using large eddy simulation (LES). *Noise Control Engineering Journal*, 62 (4), 218–231.

Rockwell, D. and Naudascher, E., 1978. Review—self-sustaining oscillations of flow past cavities. *Journal of Fluids Engineering*, 100 (2), 152–165.

Ronneberger, D., 1967. Experimentelle Untersuchungen zum akustischen Reflexionsfaktor von unstetigen Querschnittsänderungen in einem luftdurchströmten Rohr. *Acustica*, 19 (4), 222–235.

Stel, H., Morales, R., Franco, A., Junqueira, S., Erthal, R., and Gonçalves, M., 2010. Numerical and Experimental Analysis of Turbulent Flow in Corrugated Pipes. *Journal of Fluids Engineering*, 132 (7), 71203.

Tonon, D., Hirschberg, A., Golliard, J., and Ziada, S., 2011. Aeroacoustics of pipe systems with closed branches. *International Journal of Aeroacoustics*, 10 (2–3), 201–275.

White, F., 2001. *Fluid Mechanics*. Fourth edition. McGraw Hill.

Williams, J. and Hawkings, D., 1969. Sound generation by turbulence and surfaces in arbitrary motion. *Philosophical Transactions of the Royal Society of London A: Mathematical, Physical and Engineering Sciences*, 264 (1151), 321–342.

Ziada, S., 1994. A flow visualization study of flow-acoustic coupling at the mouth of a resonant side-branch. *Journal of Fluids and Structures*, 8 (4), 391–416.

CHAPTER 4

Effect of the Separation Distance on the Aeroacoustic Source of Multiple Shallow Cavities

Complete Citation:

Shaaban, A. and Ziada, S., 2019. Effect of the separation distance on the aeroacoustic source of multiple shallow cavities, Journal of Fluids Engineering, ASME, 141 (1), 011102.

Copyright:

Relative Contributions:

Shaaban, A.: Performed all the experimental measurements, data analysis and analytical interpretation, wrote the first draft of the manuscript including all figures and text.

Ziada, S.: Supervisor of Shaaban, A. during the course of work, revised and edited the manuscript draft.

Abstract

Flow over ducted shallow cavities can excite fluid resonant oscillations. A common industrial application is the flow in corrugated pipes that can be modelled as a series of consecutive shallow cavities. In the current study, the effect of the separation distance on the aeroacoustic source of multiple shallow cavities is investigated. The Standing Wave Method (SWM) is used to measure the source, where multiple microphones reconstruct the acoustic standing wave upstream and downstream of the cavities. The effect of the ratio between the separation distance to cavity length is investigated for a practical range from 0.5 to 1.375 for two and three-cavity configurations. At low and intermediate sound levels, constructive hydrodynamic interference, resulting in a strong source, is observed for the extremum spacing ratios of 0.5 and 1.375. However, at high excitation levels, 10% and higher, the source, slightly but consistently, decreases upon increasing the separation ratio. These trends persist for both the double and triple-cavity configurations. On the other hand, the separation distance of destructive interference is found to depend on the number of cavities of the tested configuration. Particle Image Velocimetry (PIV) measurements of the constructive interference cases show strong synchronized vorticity shedding in all cavities. Each cavity contribution to the total aeroacoustic source is then examined by means of Howe's analogy and the percentage contribution of each cavity is found to depend on the excitation level.

Keywords: *multiple cavities, aeroacoustic source, separation distance, flow-sound interaction, fluid structure interaction*

4.1 Introduction

Corrugated pipes are widely used in offshore gas and oil fields as they offer global flexibility while maintaining local rigidity owing to the stiffening effect provided by the pipe corrugations. However, the associated free shear layer flow over the corrugations can excite acoustic resonances (or fluid resonant oscillations) at low gas speeds. This problem is also known as whistling of flexible risers in offshore gas transport. Acoustic pressure pulsations can reach the order of bars as reported by Belfroid et al. (2007). Such high pulsation amplitudes can endanger the safety of the plant. Moreover, the substantial hydrodynamic losses in corrugated pipes (Stel et al., 2010; Popiel et al., 2013) can be increased due to the energy consumed in sustaining the acoustic pulsation. Corrugated pipes can be modelled as a series of consecutive shallow cavities. Thus, the flow over multiple consecutive cavities will be the focus of the current study investigating the effect of the spacing between the cavities on the acoustic power generated.

Free shear layer hydrodynamic instability has first been observed by Rayleigh (1879). This instability is verified analytically by Michalke (1965). The non-linear stages of disturbance growth has been captured experimentally by Miksad (1972). However, for a shear layer over a cavity mouth to produce self-sustained oscillations, the production of initial disturbances at the cavity upstream

edge and their amplification by means of the hydrodynamic instability process must be provided by a feedback mechanism. Different feedback categories were reviewed by Rockwell and Naudascher (1978). The category of interest here is the fluid resonant oscillations where the feedback is provided by means of an acoustic standing wave. The acoustic wave can be either within the cavity walls, i.e. a trapped mode, or along the length of the duct housing the cavity section, i.e. a longitudinal mode. The latter is the case for self-sustained oscillations generated by flow over corrugated pipes, which is characterized by a wavelength much larger than the cavity length.

Interest in recent investigations focused on the flow over a single cavity as a first step towards understanding corrugated pipe oscillations. Evaluation of the aeroacoustic source of a cavity shear layer has been the focus of several numerical and experimental investigations. Earlier numerical attempts (Bruggeman et al., 1989; Kriesels et al., 1995; Radavich et al., 2001; Dequand et al., 2003) involved simplification of the flow field that hindered accurate estimation of the acoustic power generated. Moreover, these studies were concerned with deep cavity oscillations. More recently, Nakiboglu et al. (2012) proposed a simplified CFD model simulating the flow over a single cavity. The model captured the lock-in range of oscillations. However, the amplitude prediction was later enhanced in a further study (Golliard et al., 2013) which employed k-omega turbulence modelling instead of the earlier laminar simulations. Using more advanced turbulence models as Large Eddy Simulation (LES), as in the study by Nair and

Sarkar (2016), successfully simulated the flow field over an open cavity. Rajavel and Parasad (2014) proposed one CFD model that combined the flow modelling based on LES and acoustics based on Ffowcs Williams and Hawkings (FW-H) analogy (Williams and Hawkings, 1969).

Experimental measurement of the aeroacoustic source based on the analysis of propagating sound waves is inspired by the early work done by Coltman (1968) investigating the organ pipe. Graf and Ziada (1992;2010) developed the Standing Wave Method (SWM) to measure the source of closed side-branches. This method was further developed and applied to the case of flow over a single shallow cavity by Mohamed et al. (2018). The standing wave method employs multiple microphones located at both upstream and downstream of the source to measure the acoustic pressure discontinuity at the cavity. This method however is valid for "simple sources" which are substantially smaller than the acoustic wavelength. Shaaban and Ziada (2018) adapted this method for the flow over multiple cavities. The measured source is found to be successful in prediction of the *amplitude* of self-excited oscillations. The SWM will be adopted in the current study because it has been proven to be an efficient and accurate method to extract the global characteristics of three-dimensional sources without simplifying the geometry of the investigated configuration. Another experimental approach has been proposed by Golliard et al. (2015) based on measuring the scattering matrix of the piping system including a corrugated pipe section. Travelling waves are excited, with and

against the flow, and the matrix components of transmitted and reflected coefficients are resolved.

Another experimental technique involves flow visualization of the flow field using Particle Image Velocimetry (PIV) and combining that with a simulated acoustic field to be able to compute the acoustic power based on Howe's analogy (Howe, 1980). This methodology is applied for the flow over closed side branches (Oshkai et al., 2008) and around two tandem cylinders (Finnegan et al., 2010). Mohamed and Ziada (2014) investigated the source distribution for a single shallow cavity case using this approach. It helps in better understanding the physics of the flow and will be employed in the current study to investigate the hydrodynamic interference between neighbouring cavities.

Most studies which investigated corrugated pipe oscillations tested a long corrugated pipe section and measured the lock-in resonance characteristics (Belfroid et al., 2007; Nakiboglu et al., 2010;2011). However, limited research has been concerned with understanding of the phenomenon using a multiple-cavity model. This is an essential bridge to link the corrugated pipe response to that of single cavities that are thoroughly investigated in the literature. The only attempt, to the far of the authors knowledge, was done by Nakiboglu and Hirschberg (2012) to study self-excited oscillations of two-cavity combination complemented by some CFD simulations. The study showed a substantial effect of the separation distance between the cavities on the self-sustained oscillations amplitude. However, the

source was not experimentally measured in the aforementioned study. The present work includes an extensive study for two as well as three-cavity configurations under controllable excitation level which was not investigated on (Nakiboglu and Hirschberg, 2012).

The aim of the current study is to investigate the effect of the separation distance, as a critical geometrical parameter, on the aeroacoustic source generated by multiple cavities exposed to grazing flow. The SWM will be used as an efficient experimental method to measure the aeroacoustic source (Graf and Ziada, 1992;2010; Mohamed et al., 2018; Shaaban and Ziada, 2018). The spacing ratios are investigated over a practical range from 0.5 to 1.375 for both two and three-cavity configurations. The effect of the excitation levels (i.e. the ratio of acoustic velocity to mean flow velocity) is also studied for the range of 0.2% up to 20%, will also be studied. Furthermore, the cases of constructive hydrodynamic interference, which increases source levels, will be visualized using PIV to better understand the interaction mechanism. The sources of the multiple cavities are estimated based on Howe's analogy and a comparison is finally held with the sources obtained using SWM.

4.2 SWM Experimental Setup

The experimental setup is designed to measure the aeroacoustic source of the multiple cavities using the Standing Wave Method (SWM). The upstream pipe length is more than 40 times the pipe nominal diameter to ensure fully developed

turbulent conditions that are prominent in industrial applications. The setup encompasses 4" PVC schedule 80 pipes. The schematic of the test setup is shown in Figure 4.1(a) with a schematic of the multiple cavities depicted in Figure 4.1(b). The multiple cavity section is located at an acoustic pressure node associated with maximum acoustic particle velocity in order to excite the cavity shear layer. Since the piping system is designed to have a standing wave of relatively long wavelength of 4.4 m (i.e. frequency approximately 78 Hz), the variation of the acoustic particle velocity over the three cavities is limited to a maximum of 3% in all the investigated test cases. Therefore, the total acoustic power generated by the multiple cavities can be estimated as the product of the induced acoustic pressure difference, generated by the flow over the cavities, multiplied by the virtually constant acoustic velocity. The acoustic pressure difference across the cavities is determined form measuring the acoustic wave by installing a set of three microphones both upstream and downstream of the cavities section. The aeroacoustic source strength (*S*) is obtained by normalizing acoustic power and is given by equation (4.1):

$$S = \frac{\Delta P/(0.5 * \rho\, U^2)}{v/U} \tag{4.1}$$

The acoustic standing wave along the duct is described by equation (4.2), where P^+ and P^- represent the amplitudes of two acoustic waves with and against the flow, respectively. The complex wave number (β) accounts for the visco-thermal losses while the Mach number (M) terms accounts for the presence of a mean flow. Two microphone measurements are required in each of the upstream and downstream ducts to resolve P^+ and P^-. However, three microphones are used

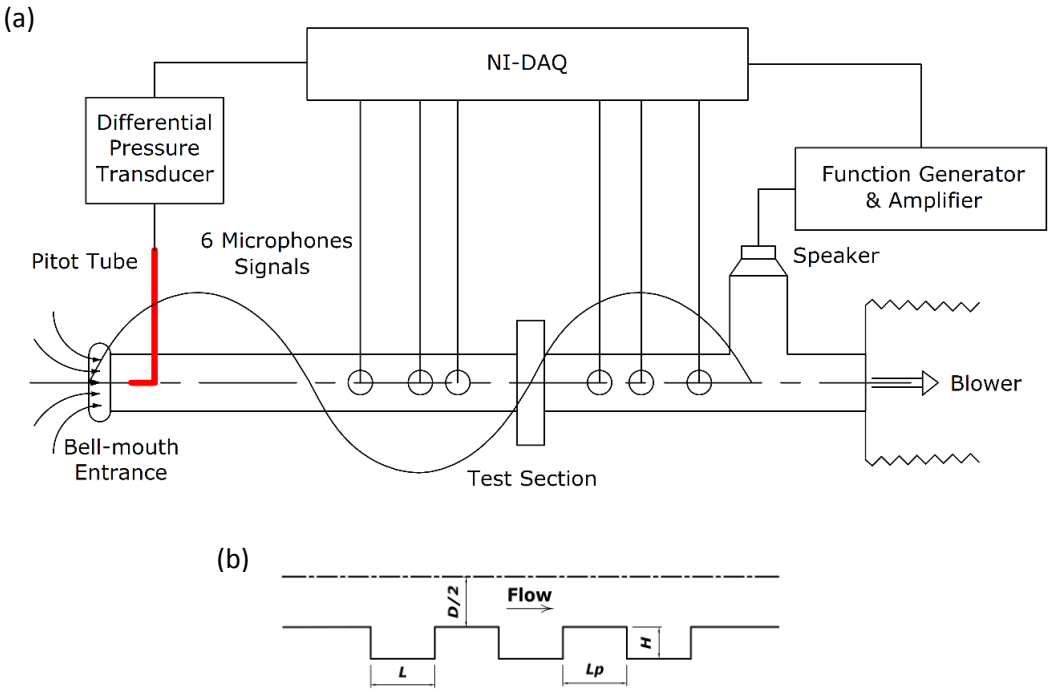

Figure 4.1. (a) Schematic of the SWM setup, (b) Sketch of the multiple cavities configuration showing the relevant geometrical parameters

in the current study, while applying a least square method, to enhance the measurement accuracy.

$$P(x,t) = \left\{P^{+}\, e^{\frac{-j\,\beta\,x}{(1+M)}} + P^{-}\, e^{\frac{j\,\beta\,x}{(1-M)}}\right\} e^{j\,(2\pi f)t}, \tag{4.2}$$

A standing sound wave is excited along the duct at its resonance frequency via a loud speaker. This allows for measuring the aeroacoustic map, i.e. the cavities source for a wide range of Strouhal numbers ($St = fL/U$) and excitation levels (v/U). Different flow velocities (U) can be achieved via a variable speed blower, and the excitation level of the speaker (v) is controlled by a function generator and an amplifier. The current system is capable of exciting waves having acoustic velocity amplitude as high as 20% of the mean flow velocity.

The mean flow velocity is measured using a Pitot tube and a Validyne pressure transducer. The acoustic pressure is measured by means of $1/4"$ condenser microphones type G.R.A.S. 40 BP. The transfer functions of all the microphones are determined with respect to one reference microphone over a wide frequency spectrum. The microphones are installed closer to the acoustic pressure antinode to enhance the measurement accuracy and at different distances from the antinode to avoid redundancy.

The uncertainty in the measured aeroacoustic source is estimated based on the propagation of uncertainties in the flow velocity and acoustic pressure measurement sensors. The acoustic pressure measured by microphones is associated with 0.7% uncertainty, while the Validyne transducer, which measures the Pitot tube differential pressure, is characterized with 0.25% uncertainty. Uncertainty propagation is computed using Kline McClintock approach. For the three-cavity configuration, with a spacing ratio of unity, at an intermediate excitation level of 3.2% and a Strouhal number of 0.6, the uncertainty in the source is estimated to be 2%. However, since the source value varies with Strouhal number, this uncertainty percentage is not descriptive of the error involved in the source term when its value becomes very small. Therefore, another set of tests is performed to assess the accuracy of the measured source even when its value is very small. In the SWM, three microphones are used to evaluate the acoustic standing wave parameters using a least square method, instead of only using two microphones, to enhance the accuracy. The deviation of the acoustic pressure

calculated by the SWM from the actual microphone measurement is used to define a residual error, which can then be used to check the SWM accuracy. The maximum residual error percentage for the whole aeroacoustic map, including points with small source values, is below 0.8%. More details about the uncertainty analysis and the accuracy checks are found in the previous work (Shaaban and Ziada, 2018).

In the current study, four separation distance to cavity length ratios (L_p/L) are investigated in a practical range of from 0.5 to 1.375. The tested cavities are 2″ long (L) and 1″ deep (H). The aeroacoustic maps for the two and three-cavity configurations are measured. For every arrangement, the source is measured for a wide range of Strouhal numbers (0.35 – 1.2) covering both the first and second shear layer modes where one and two vortices, respectively, forms along the cavity span at resonance. The Strouhal number is varied by changing the flow velocity up to 12 m/s, which corresponds to a Reynolds number of about 7×10^4 and a Mach number of about 0.03. Acoustic velocity ratios corresponding to each Strouhal number varies from low excitation level of 0.2% up to a high level of 20% to capture the non-linearity behaviour of the source.

4.3 PIV Experimental Setup

Particle Image Velocimetry (PIV) measurements are employed to measure the aeroacoustic source of each cavity. Transparent acrylic cavity is used to allow optical access. After measuring the instantaneous velocity and vorticity fields, the instantaneous aeroacoustic power (Π) is estimated using Howe's integrand (Howe,

1980), as shown by equation (4.3), based on the measured flow field vorticity (ω) and velocity (U) and the acoustic particle velocity (v) that is simulated using finite element analysis. The flow oscillation at the resonance frequency is assumed to be two-dimensional using the axisymmetric assumption. (Howe's integrand assumes the flow to be incompressible which is justified by the low Mach number of the encountered flow)

$$\Pi = -\rho \int \omega . (U \times v) \, \mathrm{dV} \tag{4.3}$$

The Nd:YAG laser is situated in a horizontal plane shooting a laser beam of 532 nm wavelength across the mid plane of the acrylic cavity. The laser can produce maximum energy output of 120 mJ per pulse. Nikon Camera, with a resolution of 4MP, is situated above the cavity to capture the flow in that 2D illuminated plane using AF Nikkor lens of 50 mm focal length. The camera is equipped with 12 bit CCD chip to allow for a digital output to the computer. The schematic of the test setup is shown in Figure 4.2 along with the visualized area of the cavity. The flow is seeded with tracer bis(2-ethylhexyl) sebacate particles using aerosol generator. The seeding particles have a mean diameter of 1 μm. The small size of the seeding particles ensured Stokes number $\ll 0.1$ amd that the tracing error is less than 1% (Melling (1997) and Tropea et al. (2007)). The field of view for a cavity 2″ length by 1″ depth in a 4″ piping system is typically 80 mm × 80 mm. Thus, to ensure a good resolution, only one cavity is visualized at a time. The attained resolution in any of the images is typically in the range of 23 pixels for every visualized 1 mm. The interrogation region starts with a coarse one of 32 × 32 pixels and then goes

down to a fine region of 16 × 16 pixels. The time difference between both image frames is chosen to ensure that the particles do not translate by more than quarter the side length of the interrogation region (i.e. 4 pixels).

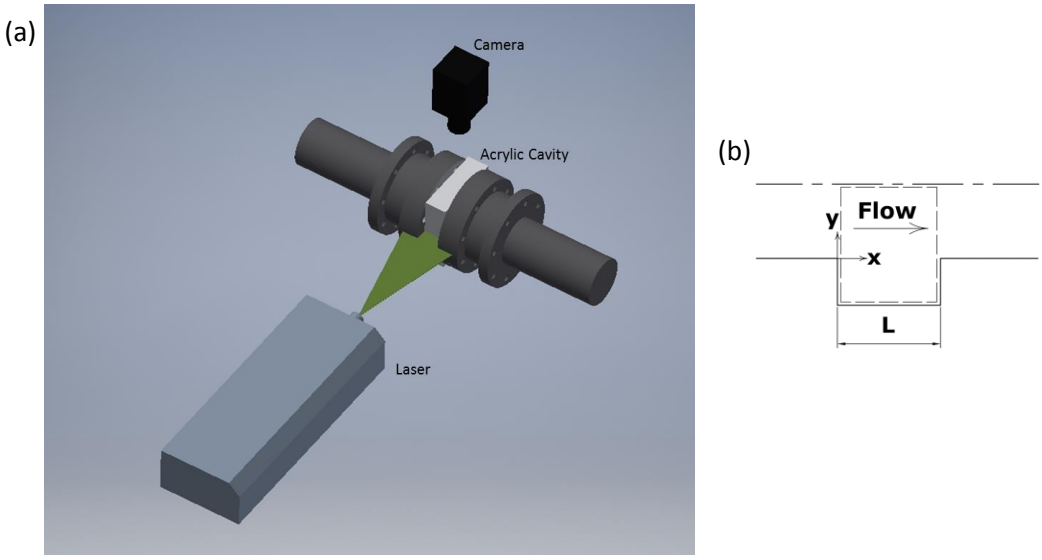

Figure 4.2. (a) Schematic of the PIV setup, (b) The cavity field of view

The laser pulses are triggered by the speaker signal that externally excites the acoustic wave along the duct, therefore allowing for freezing the flow at a certain phase of the acoustic cycle, i.e. phase locked PIV measurements. TSI LaserPulse Model 610035 synchronizer receives the trigger signal and controls the timing of both the laser and the camera. Insight 4G software is used for capturing and processing the raw images. The validation rate, in all the cases, is maintained to a benchmark of at least 99% good vectors.

Vector fields have been processed using a first order deformation grid employing gaussian sub-pixel interpolation. A typical flow field for the investigated

cavities involved maximum streamwise velocity gradient $(\partial u/\partial y)_{max}$ of about 0.041 pixel/pixel at the shear layer near the cavity upstream edge. The maximum cross-stream velocity gradient $(\partial v/\partial x)_{max}$ is about 0.007 pixel/pixel. The uncertainty associated in the processed velocity field is determined from the investigation by Scarano and Riethmuller (2000) who adopted similar vector processing scheme. Corresponding to the aforementioned velocity gradients, the uncertainties in the particle displacement for streamwise (ε_u) and cross-stream (ε_v) directions are estimated to be 0.015 and 0.005 pixels, respectively. Thus, the maximum relative uncertainty percentage in the velocity gradients, computed using central difference technique, is less than 4% and 6% for the streamwise and cross-stream directions, respectively.

Three consecutive cavities have been tested as a first attempt to visualize the flow. The main interest here is to understand the constructive hydrodynamic interference observed in the SWM measurements. A spacing ratio of 1.375 is selected to replicate constructive interference favourable conditions. Three different test cases are investigated at a Strouhal number of 0.6 which corresponds to the peak aeroacoustic source value. The acoustic excitation level covered a low value of 0.002, an intermediate value of 0.02 and eventually a high value of 0.1. For every case, the acoustic cycle is split into eight phases with 200 images averaged for each phase. Consequently, the three-cavity configuration involved capturing and processing 4800 images per case.

4.3.1 Finite Element Model

In addition to resolving the flow field parameters using PIV, the acoustic particle velocity field is needed in order to compute the aeroacoustic power applying Howe's integrand. Finite element analysis is performed using ABAQUS to determine the acoustic pressure distribution corresponding to the resonance mode along the duct. Axisymmetric model is built simulating the piping system and the three-cavity configuration with the spacing ratio of 1.375. Large settling chamber, six times the piping diameter, is included at the boundaries of the piping system to act as acoustic pressure nodes. The meshing consists of triangular elements of size 0.003 m along the pipe while using a finer mesh size of 0.0005 m around the three-cavity configuration. The total number of elements in the model is about 400,000. Mesh sensitivity analysis is done by changing the element size by an order of magnitude which resulted in only 0.2 % frequency shift of the resonance mode. The model is depicted in Figure 4.3 with the contours of the pressure distribution along the pipe. The estimated resonance frequency of 77.68 Hz matches the experimentally measured one with about 0.2% deviation. The acoustic pressure node is located at the mid-section of the three-cavity configuration as planned in the setup design to be able to excite the three cavities at a virtually constant amplitude.

The output acoustic pressure field from ABAQUS is normalized, i.e. it ranges from -1 to 1. The pressure amplitude is scaled to match that obtained from

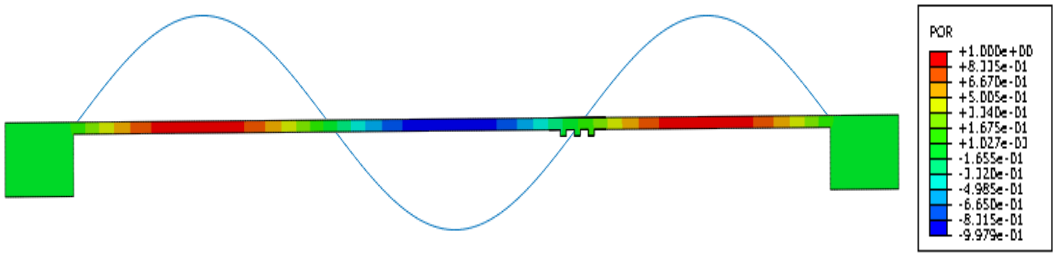

Figure 4.3. The resonant acoustic standing wave along the pipe computed using finite element analysis (length to diameter ratio of main pipe is not to scale in the figure)

the three-microphone measurement of the acoustic standing wave for the different excitation levels investigated. Euler's equation is then used to estimate the acoustic particle velocity field along the multiple cavity section based on the acoustic pressure gradient for the different phases of the acoustic cycle. A Matlab code is developed for this task using central differencing technique. Typical results of the acoustic field stream lines along the third cavity is shown in Figure 4.4. The simulated field is capable of reflecting the smoothness of the longitudinal acoustic streamlines entering and exiting from the cavity and the corresponding path into the cavity's depth.

4.4 Results

4.4.1 Separation Distance Analysis for the Two-Cavity Configuration using SWM

The effect of separation distance is presented as a comparison between the aeroacoustic sources for different spacing ratios between the two-cavity configuration and at a fixed acoustic excitation level. The discussion also focuses on the fundamental mode that is excited around the Strouhal number range from

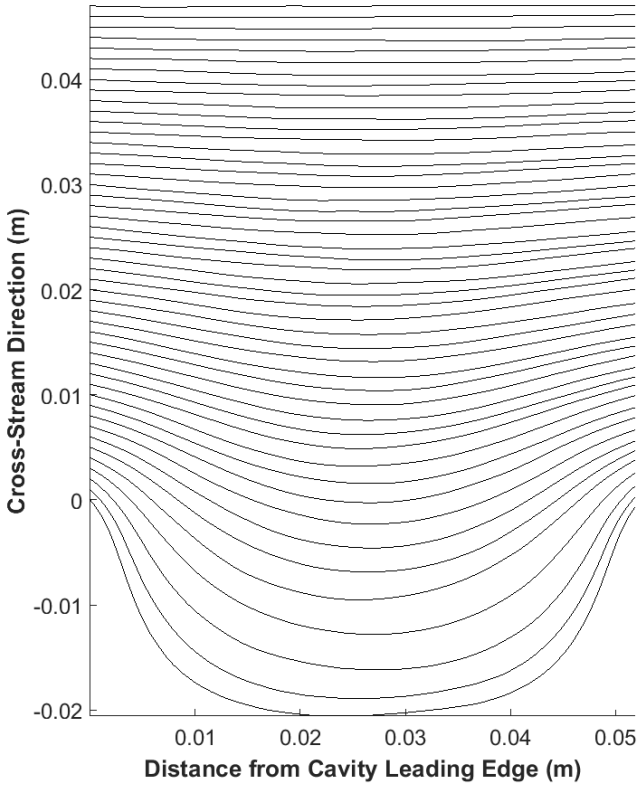

Figure 4.4. Acoustic velocity streamlines along the third cavity using Euler's equation at v/U = 0.02, θ = 0

0.45 – 0.7. The fundamental mode is associated with stronger source and typically has higher potential to cause industrial problems. At low acoustic excitation level of 0.002, the source values for different spacing ratios are shown in Figure 4.5. The aeroacoustic dimensionless source is estimated based on equation (4.1). The real part of the source represents the active energy exchange between the acoustic and flow fields. On the other hand, the imaginary part of the source represents the reactive energy, which can be used to explain slight variations of resonance frequency during self-excited oscillations (Graf and Ziada, 2010). Thus, the real

part of the source is the main concern in the current study. The two extremum spacing ratios (L_p/L) of 0.5 and 1.375 have the highest value of the peak source. The high source value may be attributed to constructive hydrodynamic interference between the neighbouring cavities at these specific separation distances. As the spacing ratio increases beyond 0.5 (i.e. L_p/L = 0.75), the peak source starts decreasing and another secondary peak starts to be noticed at a relatively higher Strouhal number. Further increase of the spacing ratio (i.e. L_p/L = 1.0) leads to more deterioration of the primary peak, but on the other hand, enhancing the secondary peak. At a spacing ratio of 1.375, the primary peak fades out and only one peak dominates yielding the highest peak source value while resonance occurring more acutely with a narrow spectral peak. The peak source value is minimum at the spacing ratio of 0.75, i.e. destructive interference spacing ratio. All the current results of the aeroacoustic source behaviour so far agrees with those reported by Nakiboglu and Hirschberg (2012) who investigated the *self-excited* acoustic pressure amplitude for various spacing ratios for a two-cavity configuration.

The current experimental facility allows for maintaining the acoustic excitation level constant while varying the spacing ratio. Consequently, it is possible to investigate the effect of the excitation level on the previous findings for the two-cavity configuration. Increasing the acoustic excitation level from 0.002 to 0.01 does not have much impact on the previous observations, regarding the constructive vs. destructive interference pattern, as shown in Figure 4.6. Excitation level of 0.05 is found to be a transitional excitation level where no correlation

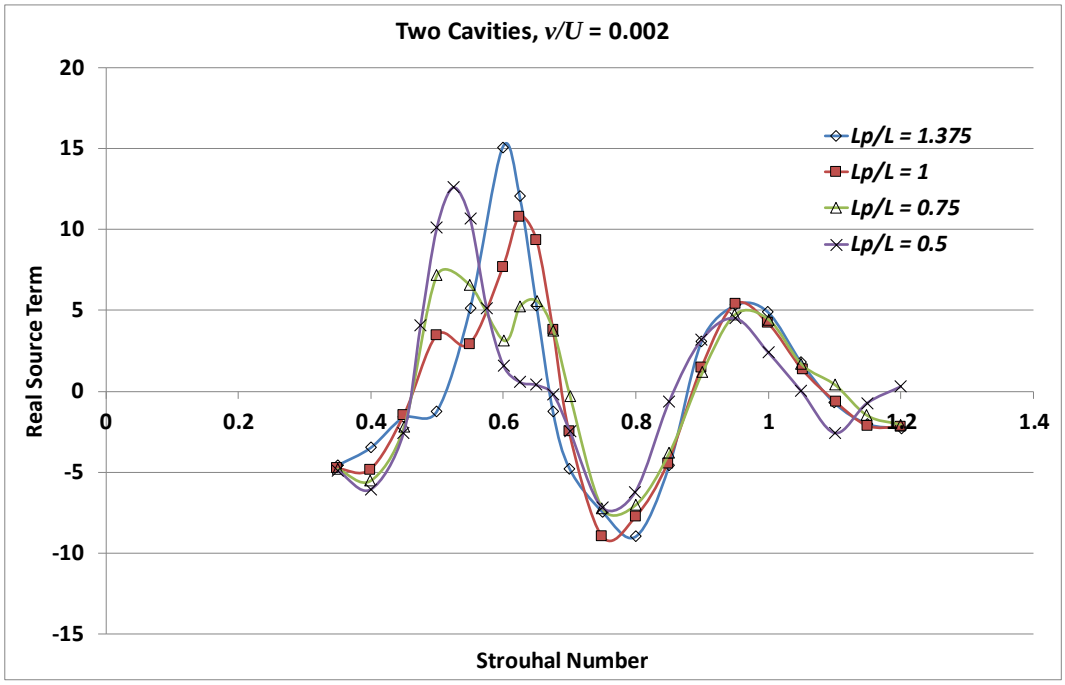

Figure 4.5. Real source vs. Strouhal number for different spacing ratios for the two-cavity configuration with v/U = 0.002

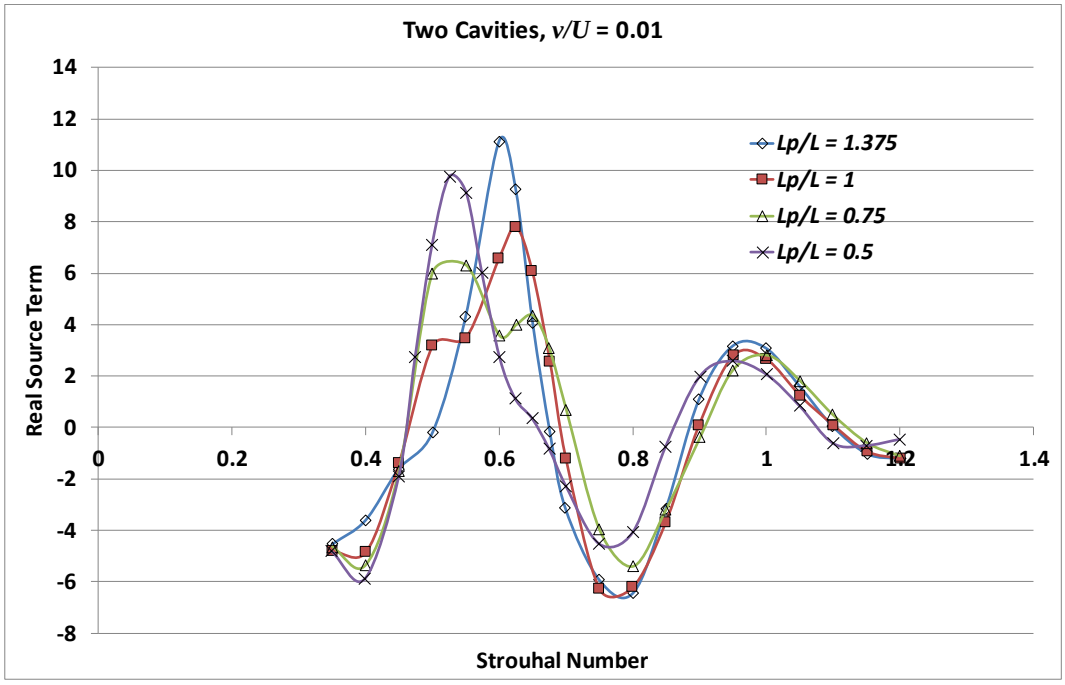

Figure 4.6. Real source vs. Strouhal number for different spacing ratios for the two-cavity configuration with v/U = 0.01

between the spacing ratio and peak source can be deduced as presented in Figure 4.7. For relatively high acoustic velocity ratios, 0.1 and beyond, the source values corresponding to different spacing ratios exhibits a different trend where the peak source value consistently decreases upon increasing the spacing ratio as depicted in Figure 4.8. This can be explained by the non-linearity of the aeroacoustic source behaviour and the fact that the convection speed of vortices is strongly influenced by the excitation level. The convection speed of coherent structures, over large portion of the acoustic cycle, is shown to decrease at high acoustic velocity ratios as previously reported by Ziada (1994) for deep cavity flows. Furthermore, Mohamed and Ziada (2015) reported a similar phenomenon upon visualizing the flow field over a single shallow cavity using PIV.

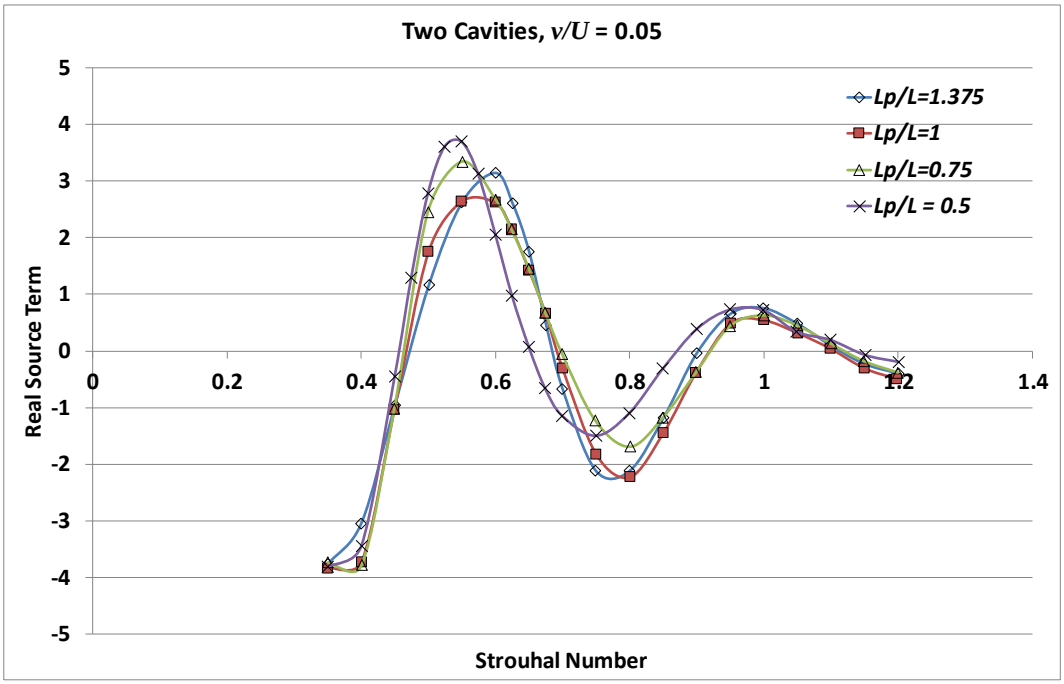

Figure 4.7. Real source vs. Strouhal number for different spacing ratios for the two-cavity configuration with *v/U* = 0.05

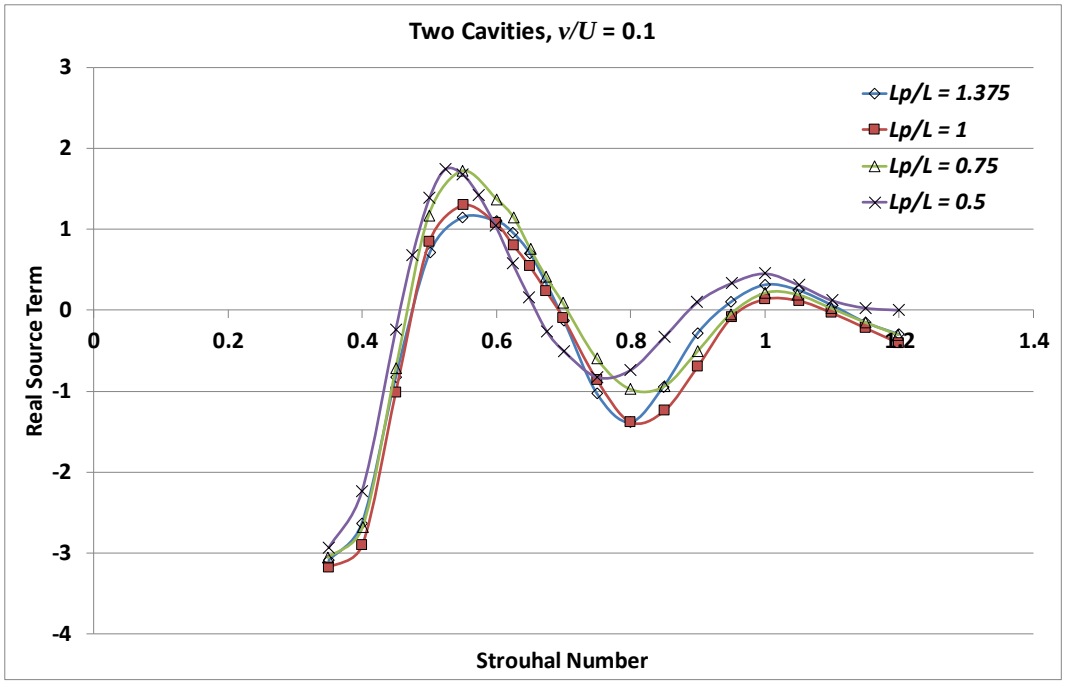

Figure 4.8. Real source vs. Strouhal number for different spacing ratios for the two-cavity configuration with v/U = 0.1

4.4.2 Separation Distance Analysis for the Three-Cavity Configuration using SWM

The effect of separation distance on the source of the three-cavity configuration is shown in Figure 4.9 for a low excitation level case of 0.2%. The main features observed for the two-cavity case are still present. Again, the two extremum spacing ratios produce the highest peak source values indicating constructive hydrodynamic interference. A consistent constructive interference spacing ratio can be explained by considering it as the ratio where the first cavity vorticity field positively enhances that of the second. The strong vorticity of the second cavity is therefore expected to enhance that of the third cavity located downstream at the same spacing ratio. It is therefore reasonable to assume the constructive interference spacing ratio to remain constant regardless the number of

cavities. The constructive interference is so strong that the source of the two cavities is higher than double the source of a single one and that of the three cavities higher than the triple. The spacing ratio with the minimum peak source, i.e. destructive interference, interestingly shifted to 1.0 for the three-cavity case as compared to 0.75 for the two-cavity case. The destructive interference for the two-cavity may be attributed to an adverse effect of the coherent structures of the first cavity diminishing those of the second. It is then expected that the second cavity would not possess sufficiently strong vortical structures that can negatively affect a cavity downstream at the same spacing ratio. This explains why the spacing ratio yielding overall destructive interference for the three-cavity case is different. Moreover, it is worth mentioning that for the three-cavity configuration with the longest separation distance, the variation in the acoustic particle velocity over the three cavities is limited to 3%. Therefore, the current setup is adequate in maintaining the acoustic velocity constant along the multiple cavities section.

The effect of acoustic excitation level on the three-cavity configuration is found to be similar to that observed for the two-cavity case. Excitation level of 0.05 is again found to be a transitional level, whereas for high excitation levels, i.e. 0.1 and beyond, a new correlation between the spacing ratio and the source is established. This is depicted in Figure 4.10 which shows the source results for the three-cavity configuration for different spacing ratios at 10% acoustic excitation level. The peak aeroacoustic source decreases slightly upon increasing the plateau distance between the cavities. This consistent relationship at high excitation levels

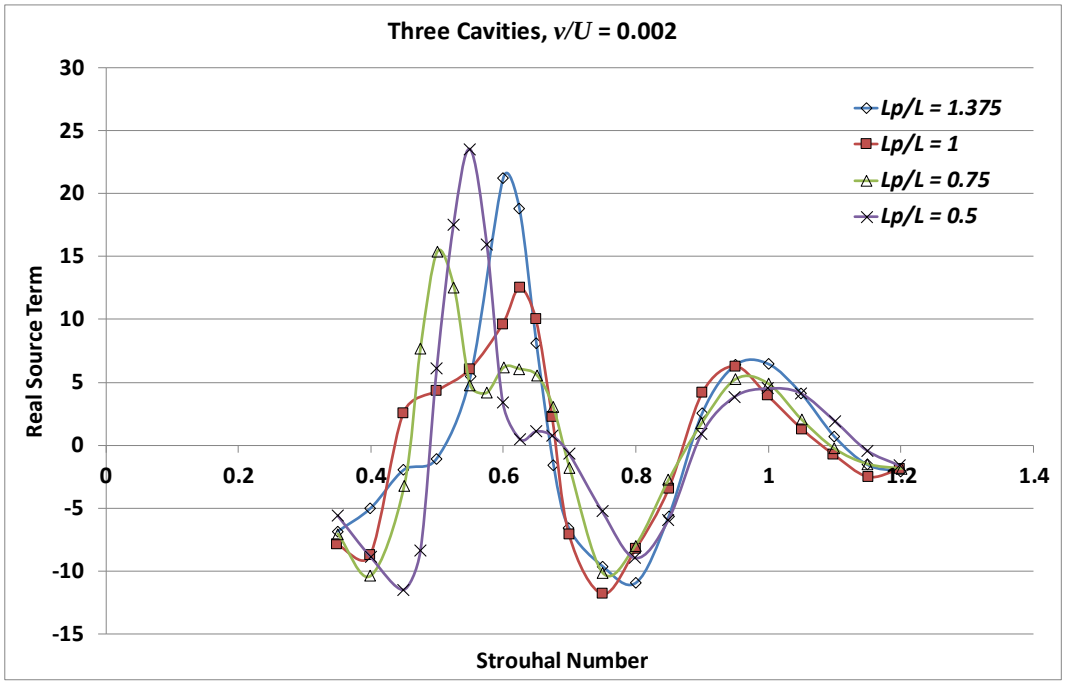

Figure 4.9. Real source vs. Strouhal number for different spacing ratios for the three-cavity configuration with v/U = 0.002

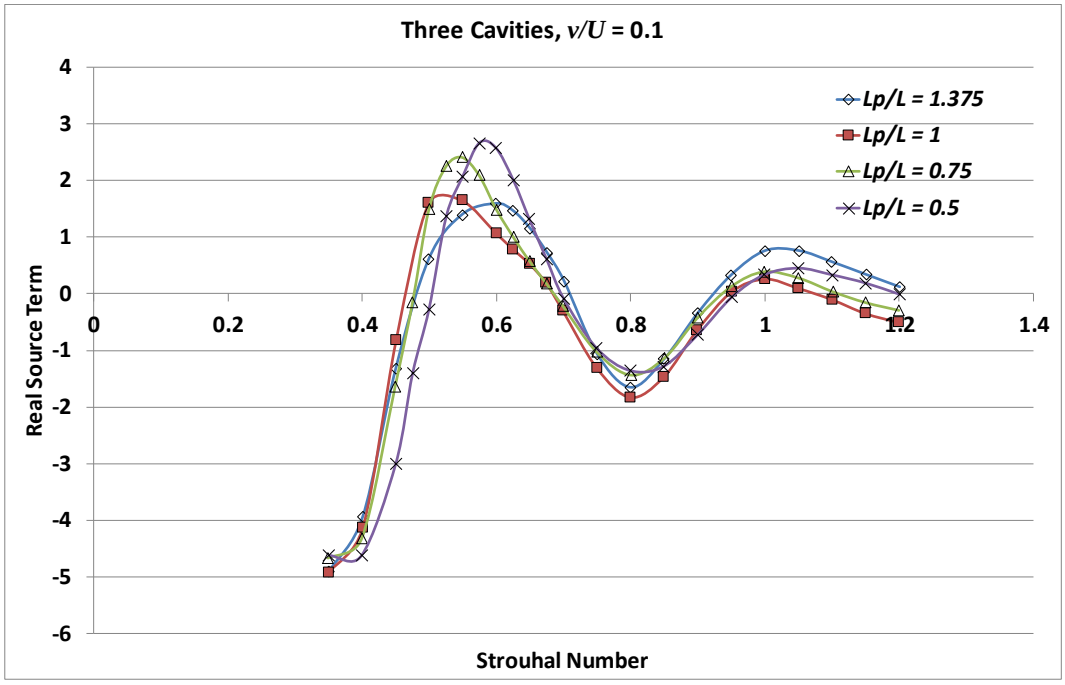

Figure 4.10. Real source vs. Strouhal number for different spacing ratios for the three-cavity configuration with v/U = 0.1

is better presented by plotting the peak source versus the spacing ratio in Figure 4.11 for both double and triple-cavity configurations with excitation level of 10%. As the spacing ratio is increased from 0.5 to 1.375, the peak source decreases by 34% and 40% for the two and three-cavity configurations, respectively. This may be attributed to the aforementioned variation of the convection speed of vortical structures at elevated excitation levels. Such convection speed is critical in the synchronization between the hydrodynamic disturbance and the acoustic standing wave at the cavity mouth.

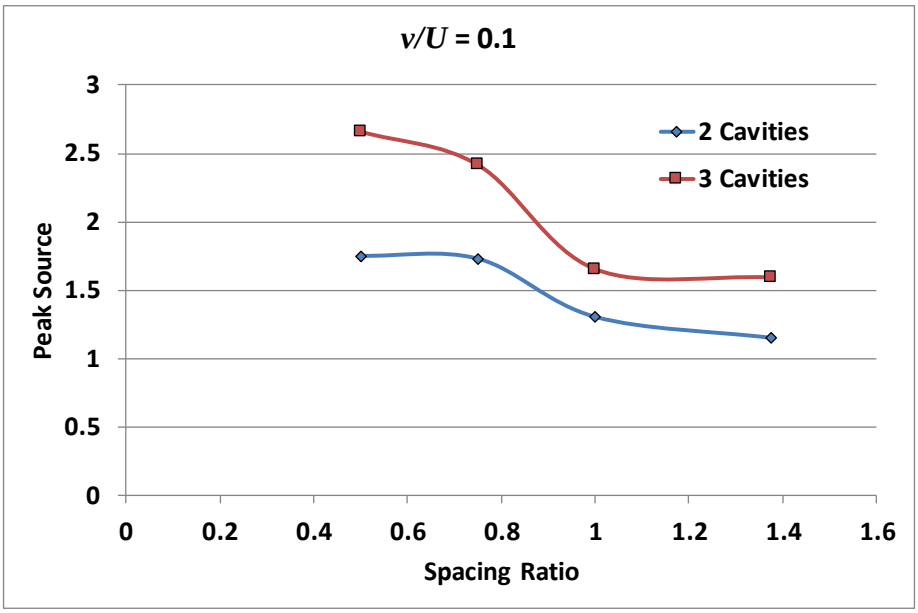

Figure 4.11. Peak source vs. spacing ratio for both two and three-cavity configuration with *v/U* = 0.1

4.4.3 PIV Visualization for Constructive Interference

A typical image of velocity magnitude contours for the flow over a cavity is shown in Figure 4.12(a). The velocity magnitude increases towards the pipe centreline and low velocity region is observed within the cavity. The shear layer is

formed along the cavity mouth where a large velocity gradient is present. The typical vorticity distribution is shown in Figure 4.12(b) depicts vortical structures forming in the shear layer. A high excitation level case is chosen to facilitate observing large vortices. The black line contours define the vortex boundaries using the discriminant parameter that detect the coherent structures as its sign changes to negative. This parameter was developed by Vollmers (2001) to distinguish coherent vortices in shear layers and other forms of flow circulation.

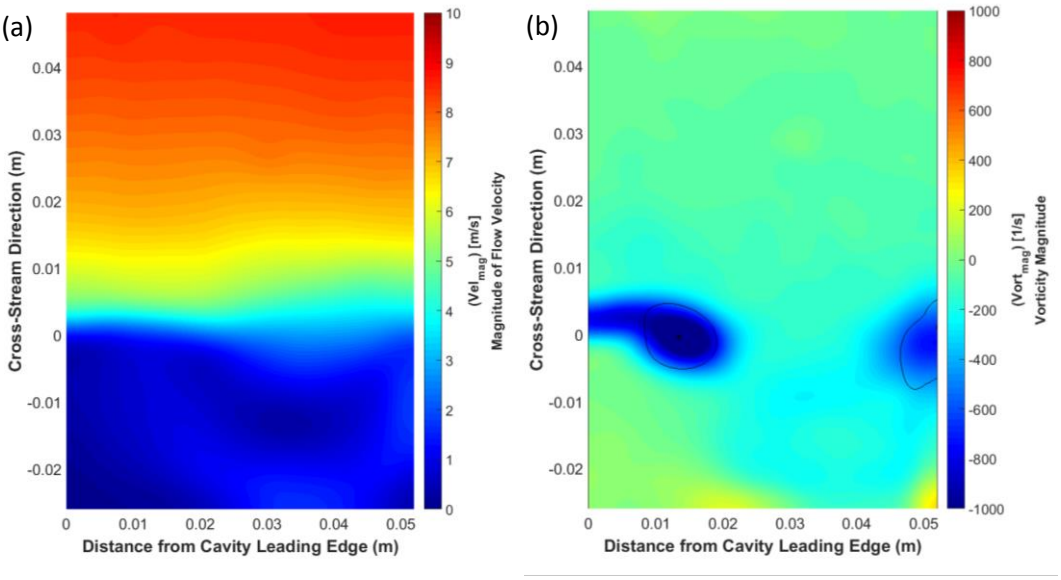

Figure 4.12. (a) Velocity magnitude contours for the flow over the third cavity, *v/U* = 0.02, $\theta = 3\pi/4$, (b) Vorticity distribution contours for the flow over the second cavity, *v/U* = 0.1, $\theta = \pi/2$. Black contours define the borders of coherent vortical structures using the discriminant parameter.

Phase locked PIV measurements have been performed splitting the acoustic cycle into eight phases. The zero phase corresponds to zero acoustic pressure on the rising signal at the upstream cavity. The acoustic pressure node is situated at the mid span of the intermediate cavity. The vorticity distribution over each of the three cavities over the eight phases of the acoustic cycle is shown in Figure 4.13 for

excitation levels 2% and 10%. Strong vortical structures are present in each of the three cavities, including the last one. This clearly points towards constructive hydrodynamic interference that is previously detected using the Standing Wave Method. The convection speed of vortical structures generally deteriorates for the highest excitation case. This can be illustrated by considering any of the acoustic phases in Figure 4.13, especially those for small phases after vortex formation, which show the vortex to be closer to the upstream edge for the higher acoustic excitation case. For the lowest excitation case of 0.2%, coherent vortical structures are not detectable. Only a vortex cloud is present over the shear layer, which is similar to that reported by Mohamed and Ziada (2014). Therefore, showing the different phases of the acoustic cycle is not beneficial and thus vorticity data for only one of the phases is shown in Figure 4.14. Again, strong vorticity cloud covering large portion of the cavity span is observed in any of the three cavities. Consequently, it can be concluded that the vorticity field of the upstream cavity enhances that of the downstream one at this spacing ratio, i.e. constructive hydrodynamic interference.

The synchronization of the hydrodynamic disturbance between neighbouring cavities can be shown by the respective location of the coherent structures at a certain phase. The two cases of intermediate and high excitation levels are used to show this synchronization as they are characterized by clear coherent structures. The vortex center location normalized by the cavity length for each of the three cavities over the acoustic cycle is presented in Figure 4.15 for the

excitation level of 2%. The locations of the vortex centres in the three cavities are strongly correlated. A similar correlation, yet stronger, is observed for the higher excitation level where the center locations almost coincide.

The velocity profiles across the axisymmetric pipe at the upstream corners of the three cavities are found to be very similar and overlap over the top of each other. The dimensionless momentum thickness (θ/R_{pipe}) is estimated to be approximately the same value of 0.11 for each of the three profiles. This matches the momentum thickness of a theoretical one-sixth power law velocity profile corresponding to a fully developed turbulent flow. The Strouhal number based on the momentum thickness (St_θ) is therefore the same for each of the three cavities. Thus, the three shear layers are most vulnerable to hydrodynamic instabilities at the same flow velocity range. This backs up the observed constructive hydrodynamic interference at this spacing ratio. Moreover, the Strouhal number corresponding to the peak source for the investigated three-cavity configuration, being 0.6 based on cavity length, matches that of a single cavity exposed to a similar approaching fully developed velocity profile that has been previously studied by Shaaban and Ziada (2018). This Strouhal number also matches that of the two-cavity configuration with the same spacing ratio.

4.4.4 Source Estimation using Howe's Analogy

The average power can be computed over the whole acoustic cycle based on Howe's analogy that is described by equation (4.3). The spatial distribution of

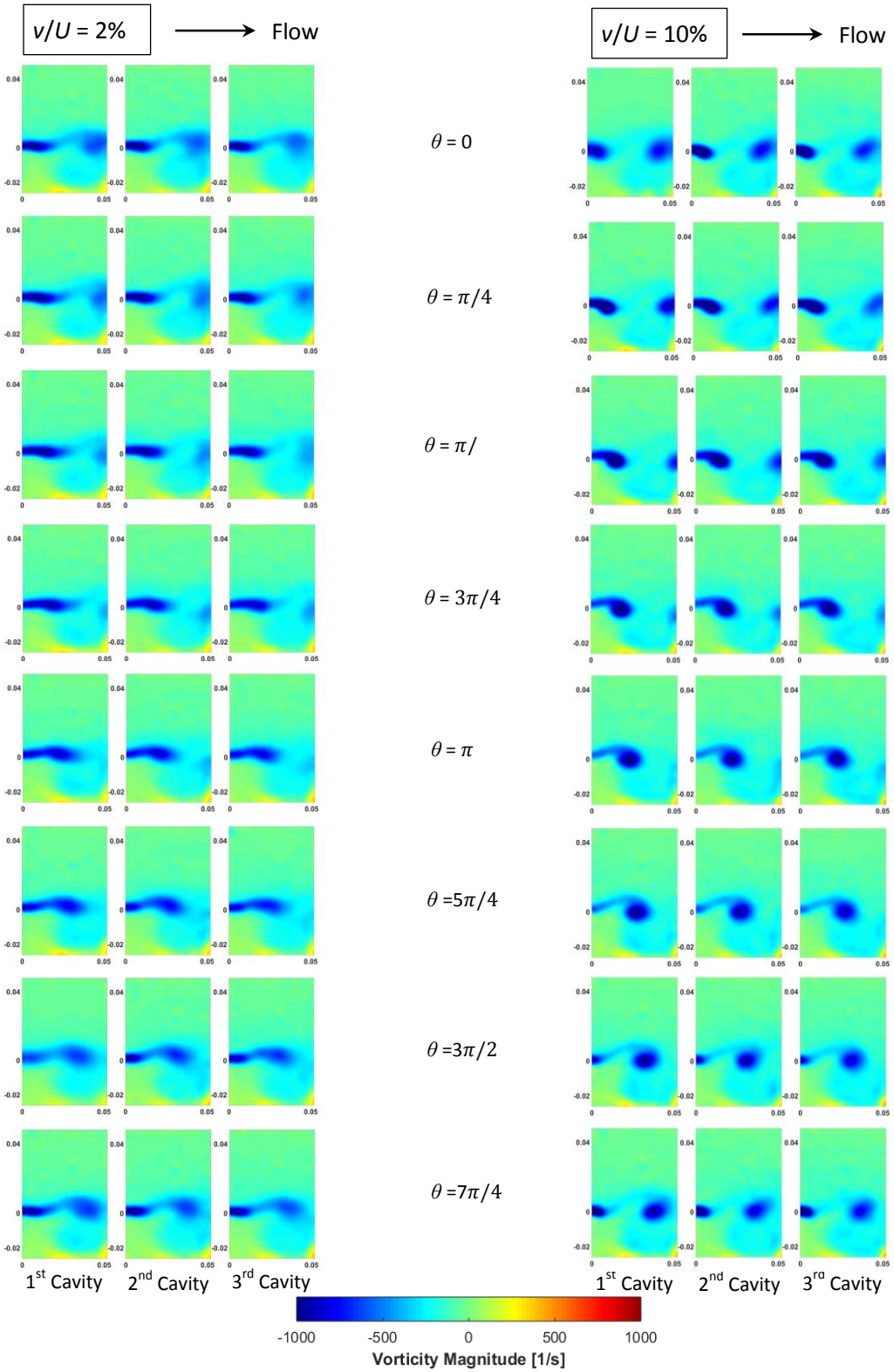

Figure 4.13. Vorticity distribution for the flow over the three cavities for *v*/U = 0.02 and 0.1 over the eight points of the acoustic cycle

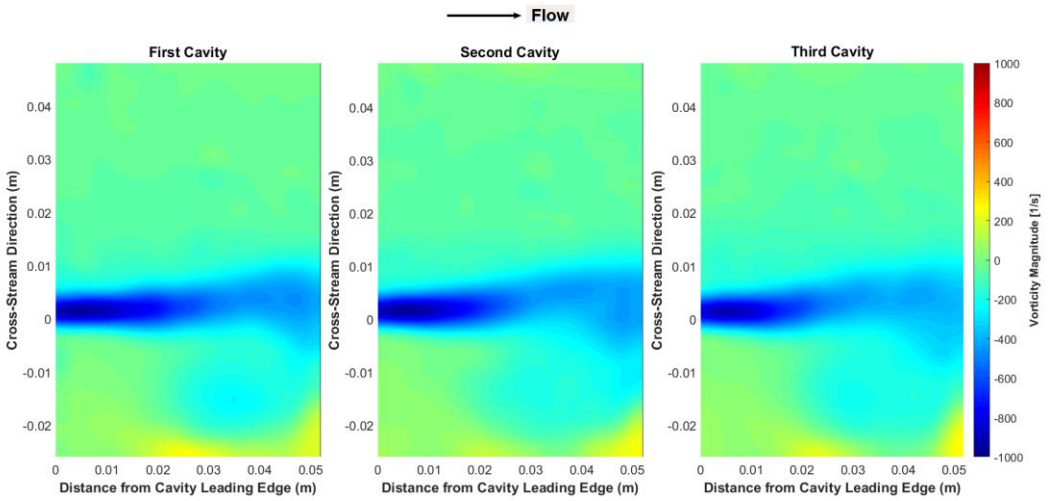

Figure 4.14. Vorticity distribution for the flow over the three cavities for v/U = 0.002 at $\theta = \pi/2$

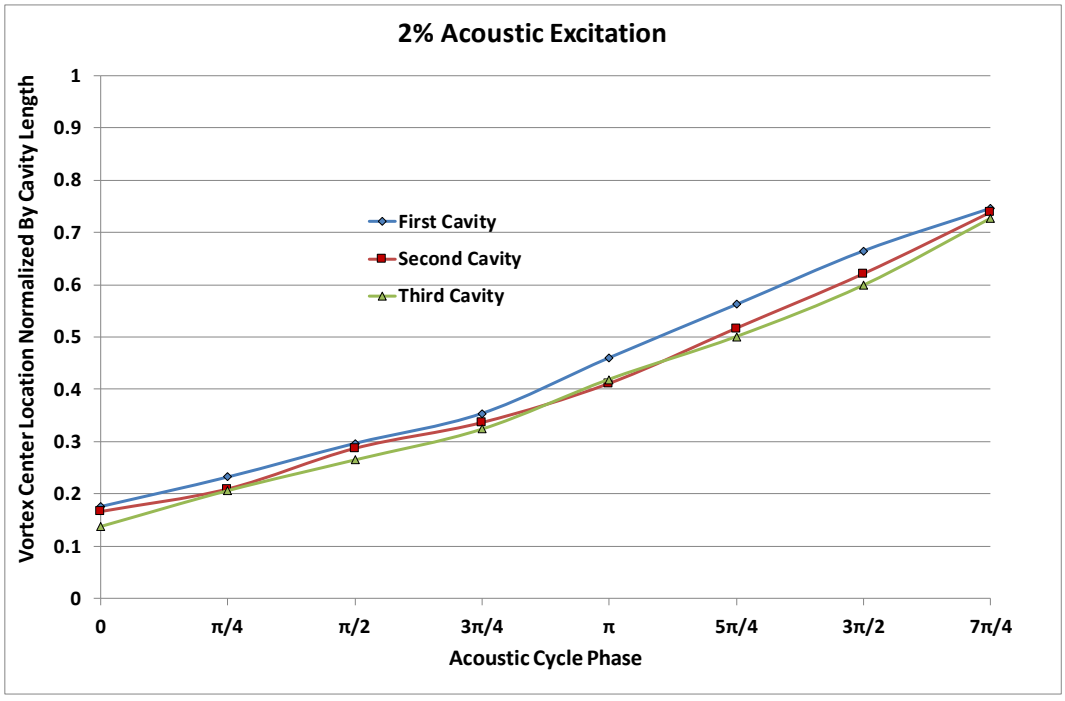

Figure 4.15. Vortex center location normalized by cavity length for each of the three cavities over the eight points of the acoustic cycle at v/U = 0.02

the average acoustic power for each of the three cavities is shown in Figure 4.16, Figure 4.17 and Figure 4.18 for the excitation levels 10%, 2% and 0.2%, respectively. Each cavity in the three cases is characterized by two main sources at the upstream and downstream edges with a sink in the middle. A small sink is observed at the bottom of the shear layer near the upstream edge. The source distribution trend generally agrees with that of a single cavity studied by Mohamed and Ziada (2014). The absolute power generated is directly proportional to the acoustic velocity ratio. This can be observed in the contour limits of each plot. Each cavity share of the total acoustic power generated is an essential issue to be taken into consideration. At the high excitation level presented in Figure 4.16, the first cavity red sources are obviously more intense than that of the second and the third. This is totally reversed for the lowest excitation case shown in Figure 4.18 where the third cavity acoustic sources are the strongest. This is better illustrated in Figure 4.19 which shows the percentage share of each cavity of the total power for different excitation levels. The first cavity clearly generates the largest portion of the acoustic power generation at the high excitation level of 0.1. The second cavity contributes a smaller share of the power as compared to the first one and eventually the third cavity provides the smallest portion. This order is reversed at the low excitation level case of 0.002. The intermediate excitation level case shows a transitional phase, where the first and the third cavities have almost equal shares and the contribution of the second cavity is slightly higher. This backs up the results in the previous task where the relationship between the source and spacing ratio

changes for high excitation levels of 10% and beyond pointing towards different physics of the hydrodynamic interaction between neighbouring cavities at such high excitation levels. The hydrodynamic instabilities travelling from the upstream cavities enhances that at the downstream ones at the constructive interference spacing ratio except at sufficiently high excitation level that are expected to alter the instability convection speed. This will be investigated in more depth in the next section.

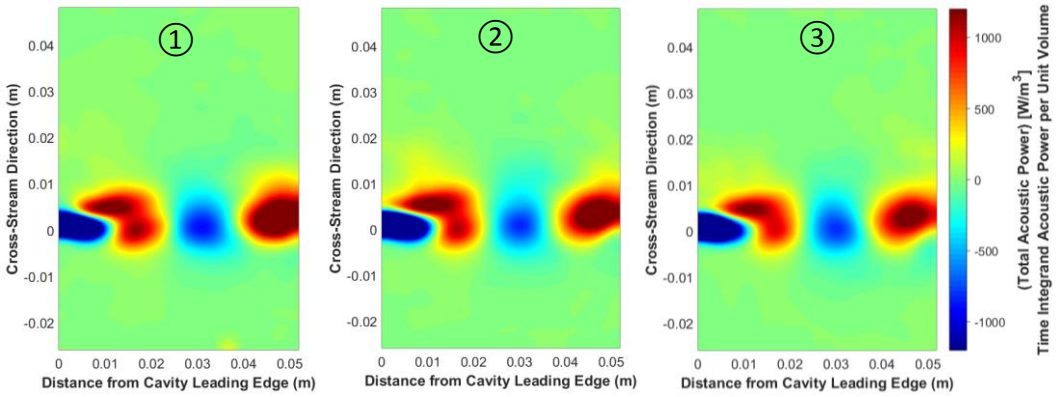

Figure 4.16. Spatial distribution of the average acoustic power over the acoustic cycle for each of the three cavities at *v/U* = 0.1. Labels on contours show the cavity location with ① being the upstream one.

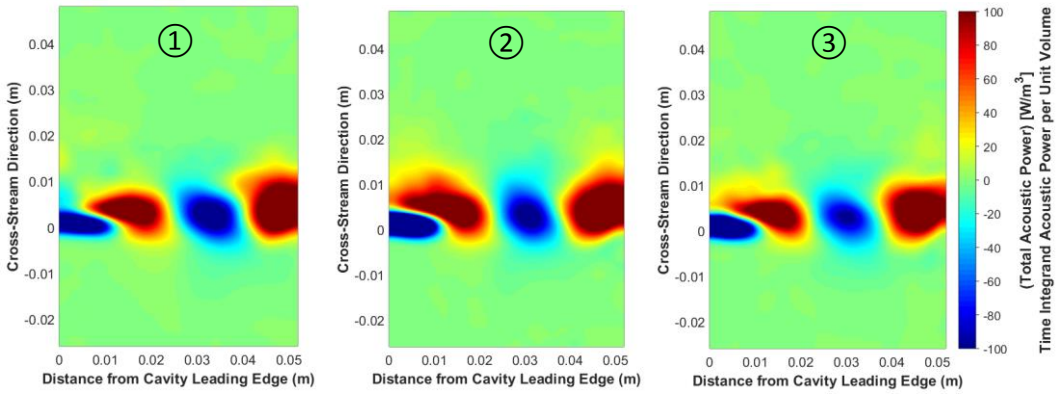

Figure 4.17. Spatial distribution of the average acoustic power over the acoustic cycle for each of the three cavities at *v/U* = 0.02. Labels on contours show the cavity location with ① being the upstream one.

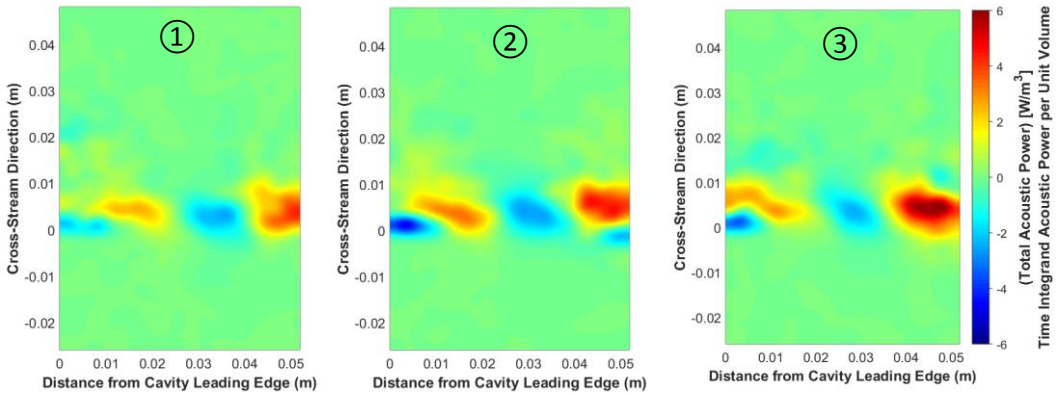

Figure 4.18. Spatial distribution of the average acoustic power over the acoustic cycle for each of the three cavities at *v/U* = 0.002. Labels on contours show the cavity location with ① being the upstream one.

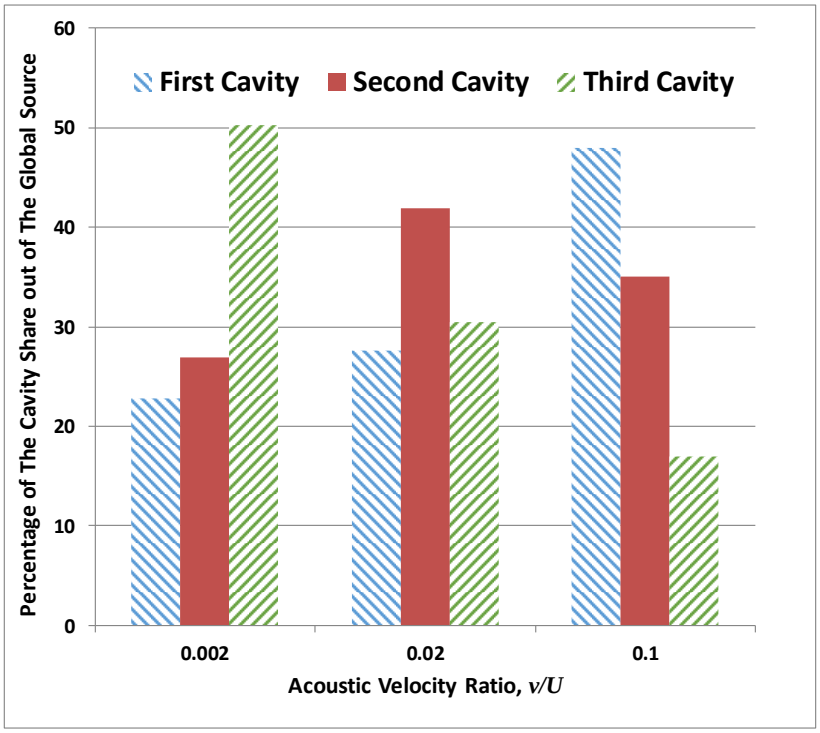

Figure 4.19. Percentage of each cavity share out of the global source at *v/U* = 0.002, 0.02 and 0.1

After applying Howe's analogy and evaluating the acoustic power generated by each cavity, the total power of the three cavities is normalized in the form of dimensionless aeroacoustic source as given by equation (4.1). The

summation of the source of each cavity can be compared with the global source value previously measured using the standing wave method as shown in Figure 4.20. Fair agreement between both methods is observed regarding the trend and the absolute values. The maximum deviation is 22% at the intermediate excitation level case. These findings increase the reliability of the measured data and prove the applicability of either method to measure multiple cavities aeroacoustic source. PIV measurements are superior in giving the spatial distribution of the power generated in each cavity and help in understanding the physics of the phenomenon. On the other hand, the standing wave method is very efficient, timewise and resource-wise, in getting a global accurate value of the source.

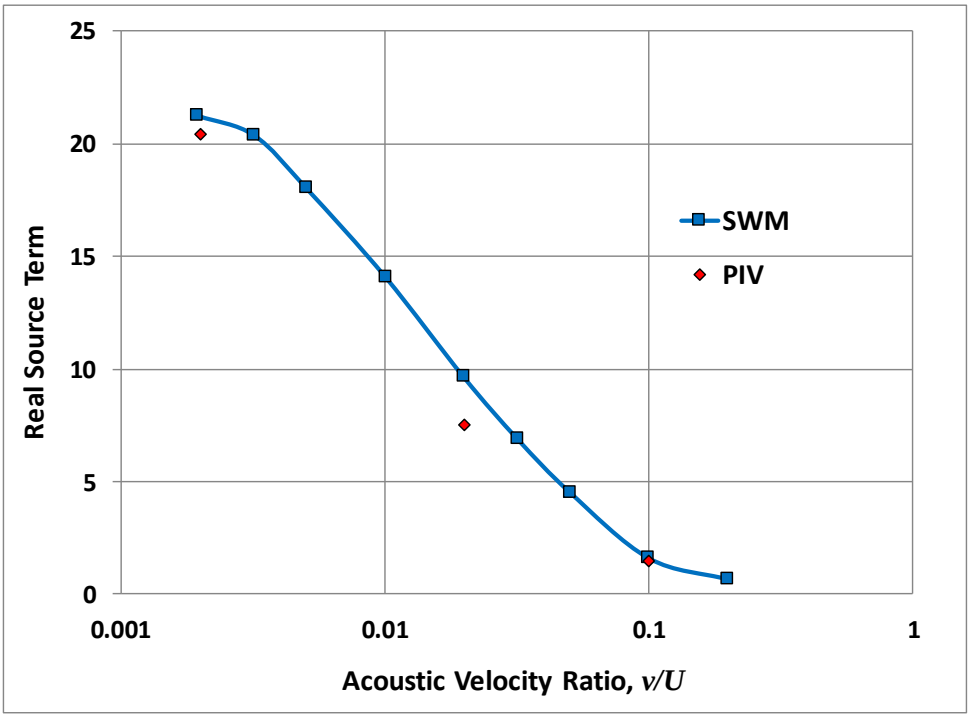

Figure 4.20. Comparison of the source value measured using the Standing Wave Method (SWM) vs. Howe's analogy based on the PIV data

4.4.5 Analytical Interpretation of Hydrodynamic Interaction Patterns

Hydrodynamic interaction between two consecutive cavities enhances aeroacoustic power generation at small and relatively large spacing ratios of 0.5 and 1.375, respectively, for low and intermediate excitation levels. At an intermediate spacing ratio of 0.75, the acoustic power generation substantially deteriorates. This phenomenon may be attributed to the phasing of the interaction between the hydrodynamic disturbance travelling between the cavities and the shear layer instability which is initiated at the upstream corner of the following cavity. Both events appear to be in phase at very low spacing ratios (L_p/L), allowing for almost direct communication between neighbouring cavities. Same sequence may be expected at a relatively large spacing ratio that allows the disturbances leaving the downstream edge of the first cavity to arrive at the upstream of the second cavity at the start of the next acoustic cycle. This supposition is supported by the fact that the destructive interference spacing ratio is almost half that of the constructive interference. Thus, interest in this section will be focused on evaluating the disturbance convection speed in pipes to further substantiate the aforementioned hypothesis.

Instability propagation inside pipes has been a topic of interest to early fluid dynamics researchers to explain the well-known phenomenon of transition from laminar to turbulence at a certain critical Reynolds number (*Re*). Sexl (1927) derived a fourth-order differential equation for a small disturbance travelling along an axisymmetric pipe. Gill (1965) performed an order of magnitude analysis to

simplify the equation and resolve the convection speed of the disturbance along the pipe center line (Center Mode). He found the convection speed to be of the same order as the flow velocity at relatively high *Re*. Salwen and Grosch (1972) attempted to solve the disturbance equation numerically computing the convection velocity to be 0.98 of the flow velocity at *Re* of 5×10^4. O'Sullivan and Breuer (1994) readdressed the problem by replacing the Poiseuille parabolic mean profile by a general Chebyshev polynomial. The Navier-Stokes equations were numerically solved yielding the least damped centre modes having a convection speed of 0.97 of the flow velocity as *Re* approaches 10^4.

Now, based on the above brief review and recalling that the Reynolds number in the present experiments is about 5×10^4, the hydrodynamic interaction between multiple cavities is further discussed with the assumption that the convection speed of hydrodynamic disturbances in the pipe spacing is the same as the mean pipe velocity. The convection speed of the coherent structures along the cavity mouth is about 0.6 of the mean flow velocity based on the peak whistling Strouhal number of the investigated fundamental mode. Based on the hypothesis early mentioned, the constructive hydrodynamic interference occurs when the hydrodynamic cycle in the cavity is well synchronized with the corresponding cycle in the pipe spacing between the cavities, i.e. both cycles have the same period. Consequently, the spacing ratio expected to witness constructive interference is about 1.67 based on the theoretical approach as compared to 1.375 from the current experimental investigation. It is worth mentioning that the theoretical analysis in

the discussed literature did not include the effect of turbulence as well as the effect of the standing acoustic wave on the pipe disturbance convection speed.

The interesting behaviour observed at high excitation levels of 10% and beyond, where the source strength consistently decreases upon increasing the spacing ratio, may be attributed to the domination of acoustic waves on the convection speeds along the pipe spacing and the cavity shear layer. As mentioned earlier, the literature does not consider the effect of a standing acoustic wave in the pipe. Such effect will be substantial as the amplitude of the wave increases at high excitation levels affecting the disturbance convection speed in the pipe spacing. Moreover, the convection speed of vortices travelling along the shear layer is strongly influenced by the excitation level (Ziada, 1994; Mohamed and Ziada, 2015). This is reflected in the current experimental study by the decrease in the peak whistling Strouhal number at high excitation levels. This is expected to shift the constructive interference spacing ratio to a higher value raising the possibility that the current spacing ratio of 1.375 is being trapped in an extended destructive interference range for high excitation levels.

4.5 Conclusions

The current study attempts to understand corrugated pipe oscillations based on a multiple-cavity model. The spacing ratio is a new geometrical parameter distinctive to multiple cavity configurations that was fundamentally absent in the single cavity rich literature. The effect of the separation distance on the aeroacoustic

source of multiple cavities have been investigated. The source of two and three-cavity configurations has been measured over a wide range of spacing ratios using the SWM. The spacing ratio is found to have a significant effect on the total source of multiple cavities. At low and intermediate excitation levels, extremum spacing ratios of 0.5 and 1.375 yields constructive interference conditions that is accompanied by high source values. However, the observed trend changes for high excitation levels, 10% and higher, where the source, slightly but consistently, decreases upon increasing the separation distance ratio. This is explained by the effect of the excitation level on the vortices convection speed. These findings are observed for both the two and the three-cavity configurations. A consistent constructive interference spacing ratio, regardless the number of cavities, may be considered as a favourable spacing where each cavity vorticity field positively enhances that of the downstream one. On the other hand, the destructive interference spacing ratio is found to be affected by the number of tested cavities, reflecting a more complicated hydrodynamic interaction mechanism.

The flow fields for the constructive interference cases of the three-cavity configuration have been visualized using PIV. Strong synchronized vorticity fields are observed in each cavity. Furthermore, the source of each cavity is estimated based on Howe's analogy. The spatial distribution of the source for each individual cavity in the group is found to be similar to that of the single cavity. Each cavity share of the overall source is found to be a function of the excitation level. At high levels, the upstream cavity contributed the most with this relationship reversed for

low excitation levels. This indicates a change in the hydrodynamic interaction nature at high acoustic velocity ratios which backs up the previously observed variation in the source trends in the SWM measurements at high excitation levels. The source results of multiple cavities measured by SWM and Howe's analogy are in a good agreement. The SWM is more efficient in getting the global source value while Howe's analogy provides more information regarding the source distribution.

Nomenclature

f	Resonance frequency (Hz)
H	Cavity depth (m)
L	Cavity length (m)
L_p	Separation plateau distance between cavities (m)
M	Mach number
P	Acoustic pressure (Pa)
ΔP	Acoustic pressure difference across the cavity section (Pa)
R_{pipe}	Pipe radius (m)
S	Normalized aeroacoustic source
St	Strouhal number based on the cavity length
St_θ	Strouhal number based on the momentum thickness
U	Flow velocity (m/s)
v	Acoustic particle velocity (m/s)

ρ	Air density (kg/m^3)
β	Complex wave number (m^{-1})
ω	Flow vorticity (1/s)
θ	Momentum boundary layer thickness (m)
Π	Acoustic power (W)

References

Belfroid, S., Shatto, D., and Peters, M., 2007. Flow induced pulsations caused by corrugated tubes. *In*: *Pressure Vessels and Piping Conference*. ASME, 439–447.

Bruggeman, J., Hirschberg, A., van Dongen, M., Wijnands, A., and Gorter, J., 1989. Flow Induced Pulsations in Gas Transport Systems: Analysis of the Influence of Closed Side Branches. *Journal of Fluids Engineering*, 111 (4), 484–491.

Coltman, J., 1968. Sounding mechanism of the flute and organ pipe. *The Journal of the Acoustical Society of America*, 44 (4), 983–992.

Dequand, S., Hulshoff, S., and Hirschberg, A., 2003. Self-sustained oscillations in a closed side branch system. *Journal of Sound and Vibration*, 265 (2), 359–386.

Finnegan, S., Meskell, C., and Ziada, S., 2010. Experimental investigation of the acoustic power around two tandem cylinders. *Journal of Pressure Vessel Technology*, 132 (4), 41306.

Gill, A., 1965. On the behaviour of small disturbances to Poiseuille flow in a circular pipe. *Journal of Fluid Mechanics*, 21 (1), 145–172.

Golliard, J., Belfroid, S., Vijlbrief, O., and Lunde, K., 2015. Direct measurements of acoustic damping and sound amplification in corrugated pipes with flow. *In*: *Pressure Vessels and Piping Conference*. ASME, PVP2015-45494.

Golliard, J., González-Díez, N., Belfroid, S., Nakiboğlu, G., and Hirschberg, A., 2013. U-RANS model for the prediction of the acoustic sound power generated in a whistling corrugated pipe. *In*: *Pressure Vessels and Piping Conference*. ASME, PVP2013-97385.

Graf, H. and Ziada, S., 1992. Flow induced acoustic resonance in closed side

branches: an experimental determination of the excitation source. *In*: *International Symposium on Flow-Induced Vibration and Noise*. ASME, 63.

Graf, H. and Ziada, S., 2010. Excitation source of a side-branch shear layer. *Journal of Sound and Vibration*, 329 (14), 2825–2842.

Howe, M., 1980. The dissipation of sound at an edge. *Journal of Sound and Vibration*, 70 (3), 407–411.

Kriesels, P., Peters, M., Hirschberg, A., Wijnands, A., Iafrati, A., Riccardi, G., Piva, R., and Bruggeman, J., 1995. High amplitude vortex-induced pulsations in a gas transport system. *Journal of Sound and Vibration*, 184 (2), 343–368.

Melling, A., 1997. Tracer particles and seeding for particle image velocimetry. *Measurement Science and Technology*, 8 (12), 1406–1416.

Michalke, A., 1965. On spatially growing disturbances in an inviscid shear layer. *Journal of Fluid Mechanics*, 23 (3), 521–544.

Miksad, R., 1972. Experiments on the nonlinear stages of free-shear-layer transition. *Journal of Fluid Mechanics*, 56 (4), 695–719.

Mohamed, S., Graf, H., and Ziada, S., 2018. Measurement of the Excitation Source of an Axisymmetric Shallow Cavity Shear Layer. *Journal of Pressure Vessel Technology*.

Mohamed, S. and Ziada, S., 2014. PIV Measurements of Aeroacoustic Sources of a Shallow Cavity in a Pipeline. *In*: *Pressure Vessels and Piping Conference*. ASME, PVP2014-28508.

Mohamed, S. and Ziada, S., 2015. Effect of Cavity Volume on the Flow-Excited Acoustic Resonance of a Shallow Cavity in a Pipe-Line. *In*: *Pressure Vessels and Piping Conference*. ASME, PVP2015-45205.

Nair, K. and Sarkar, S., 2016. Large Eddy Simulation of Self-Sustained Cavity Oscillation for Subsonic and Supersonic Flows. *Journal of Fluids Engineering*, 139 (1), 11102.

Nakiboglu, G., Belfroid, S., Golliard, J., and Hirschberg, A., 2011. On the whistling of corrugated pipes: effect of pipe length and flow profile. *Journal of Fluid Mechanics*, 672, 78–108.

Nakiboglu, G., Belfroid, S., Willems, J., and Hirschberg, A., 2010. Whistling behavior of periodic systems: Corrugated pipes and multiple side branch system. *International Journal of Mechanical Sciences*, 52 (11), 1458–1470.

Nakiboglu, G. and Hirschberg, A., 2012. Aeroacoustic power generated by multiple compact axisymmetric cavities: Effect of hydrodynamic interference on the sound production. *Physics of Fluids*, 24 (6), 67101.

Nakiboglu, G., Manders, H., and Hirschberg, A., 2012. Aeroacoustic power generated by a compact axisymmetric cavity: prediction of self-sustained oscillation and influence of the depth. *Journal of Fluid Mechanics*, 703, 163–191.

O'Sullivan, P. and Breuer, K., 1994. Transient growth in circular pipe flow. I. Linear disturbances. *Physics of Fluids*, 6 (11), 3643–3651.

Oshkai, P., Yan, T., Velikorodny, A., and VanCaeseele, S., 2008. Acoustic Power Calculation in Deep Cavity Flows: A Semiempirical Approach. *Journal of Fluids Engineering*, 130 (5), 51203.

Popiel, C., Kozak, M., Małecka, J., and Michalak, A., 2013. Friction Factor for Transient Flow in Transverse Corrugated Pipes. *Journal of Fluids Engineering*, 135 (7), 74501.

Radavich, P., Selamet, A., and Novak, J., 2001. A computational approach for flow–acoustic coupling in closed side branches. *The Journal of the Acoustical Society of America*, 109 (4), 1343–1353.

Rajavel, B. and Prasad, M., 2014. Parametric studies on acoustics of corrugated tubes using large eddy simulation (LES). *Noise Control Engineering Journal*, 62 (4), 218–231.

Rayleigh, Lord, 1879. On the instability of jets. *In*: *Proc. London Math. Soc 10*. 4–13.

Rockwell, D. and Naudascher, E., 1978. Review—self-sustaining oscillations of flow past cavities. *Journal of Fluids Engineering*, 100 (2), 152–165.

Salwen, H. and Grosch, C., 1972. The stability of Poiseuille flow in a pipe of circular cross-section. *Journal of Fluid Mechanics*, 54 (1), 93–112.

Scarano, F. and Riethmuller, M., 2000. Advances in iterative multigrid PIV image processing. *Experiments in Fluids*, 29, S051–S060.

Sexl, T., 1927. Zur Stabilitätsfrage der Poiseuilleschen und Couetteschen Strömung. *Annalen der Physik*, 388 (14), 835–848.

Shaaban, A. and Ziada, S., 2018. Acoustic Response of Multiple Shallow Cavities and Prediction of Self-Excited Acoustic Oscillations. *Journal of Fluids*

Engineering, 140 (9), 91203.

Stel, H., Morales, R., Franco, A., Junqueira, S., Erthal, R., and Gonçalves, M., 2010. Numerical and Experimental Analysis of Turbulent Flow in Corrugated Pipes. *Journal of Fluids Engineering*, 132 (7), 71203.

Tropea, C., Yarin, A., and Foss, J., eds., 2007. *Springer Handbook of Experimental Fluid Mechanics*. First edition. Berlin, Heidelberg: Springer.

Vollmers, H., 2001. Detection of vortices and quantitative evaluation of their main parameters from experimental velocity data. *Measurement Science and Technology*, 12 (8), 1199–1207.

Williams, J. and Hawkings, D., 1969. Sound generation by turbulence and surfaces in arbitrary motion. *Philosophical Transactions of the Royal Society of London A: Mathematical, Physical and Engineering Sciences*, 264 (1151), 321–342.

Ziada, S., 1994. A flow visualization study of flow-acoustic coupling at the mouth of a resonant side-branch. *Journal of Fluids and Structures*, 8 (4), 391–416.

CHAPTER 5

Fully Developed Building Unit Cavity Source for Long Multiple Shallow Cavity Configurations

Complete Citation:

Shaaban, A. and Ziada, S., 2018. Fully developed building unit cavity source for long multiple shallow cavity configurations, Physics of Fluids, AIP, Under Review.

Copyright:

Relative Contributions:

Shaaban, A.: Performed all the experimental measurements, data analysis, interpretation and model development, wrote the first draft of the manuscript including all figures and text.

Ziada, S.: Supervisor of Shaaban, A. during the course of work, revised and edited the manuscript draft.

Abstract

Fluid resonant oscillations have been reported for corrugated pipes installed in offshore gas and oil fields. Corrugated pipes can be modelled as a series of consecutive shallow cavities. The current study investigates the development of the individual cavity source along multiple-cavity arrangements and whether this source eventually reaches a fully developed form with a persistent source contribution. Such a contribution defines a proposed building unit cavity source. To achieve this objective, the aeroacoustic source of a test section with gradually increasing number of cavities is measured by means of the Standing Wave Method (SWM). The individual cavity source is found to asymptotically reach a constant value starting from the fourth cavity. This source value is a function of the excitation level and eventually decays at high excitation level of 10%. The measured building unit source is validated by two different approaches. First, a prediction model is developed for a twelve-cavity configuration based on the building unit source. Fair agreement is found between the predicted and the experimentally measured pressure amplitudes. The second validation approach involves extracting the source of the ninth cavity in a twelve-cavity configuration using Howe's analogy based on Particle Image Velocimetry (PIV) measurements. The ninth cavity source fairly matches the building unit source for excitation levels higher than 1%. For lower excitation levels, three-dimensional flow effects are found to become more dominant and lead to larger discrepancies with the unit source.

Keywords: *multiple cavities, aeroacoustic source, corrugated pipes, fluid structure interaction*

5.1 Introduction

Corrugated pipes are commonly used in offshore gas and oil piping systems. The flexibility offered by the corrugations while maintaining global rigidity is a fundamental advantage for these applications. However, Belfroid et al. (2007) reported high acoustic pressure pulsations, in the order of bars, in pressurized corrugated pipes used for gas transport. Such high level of pulsations often leads to noise and vibration problems and may cause shut-down of the plant. Moreover, the pressure pulsations increase the hydrodynamic losses of the pumping process, which are already considerable (Stel et al., 2010; Popiel et al., 2013).

Corrugated pipes can be modelled as a series of multiple cavities. The flow over each cavity is considered as a free shear layer flow that is vulnerable to hydrodynamic instabilities as earlier reported by Rayleigh (1879). For the case of cavity flows, a feedback loop is required to sustain the initial instability at the upstream edge of the cavity as indicated by Rockwell and Naudascher (1978). Oscillations in corrugated pipes fall in the category of fluid resonant oscillations where an acoustic standing wave serves as the feedback event which initiates and sustains the hydrodynamic instabilities over the corrugations.

The flow over a single shallow cavity has been the concern of many recent studies numerically and experimentally. The CFD model proposed by Nakiboglu et al. (2012) was quite successful in capturing the main features of the lock-in oscillations. The flow was simplified as a laminar flow and the acoustic velocity was superimposed with the inlet flow velocity. However, the cavity source was overestimated. Golliard et al. (2013) readdressed the model and introduced k-omega turbulence model, which relatively improved the estimation of the source. Using more sophisticated turbulence models, such as Large Eddy Simulations (LES), has shown some success in replicating the flow field parameters over an open cavity in a recent study by Nair and Sarkar (2016). Rajavel and Parasad (2014) proposed a CFD model based on LES, including acoustic effects using Ffowcs Williams and Hawkings (FW-H) analogy (Williams and Hawkings, 1969).

An experimental method based on the analysis of the acoustic wave parameters has been suggested by Coltman (1968) to evaluate the aeroacoustic source at the mouth of a flute. More recently, Graf and Ziada (1992;2010) have used a similar approach and developed the Standing Wave Method (SWM) to measure the aeroacoustic source at the mouth of a closed side-branch. Similar approach has also been used for flow over a single shallow cavity, Mohamed et al. (2018), and over multiple-cavity configurations, Shaaban and Ziada (2018). The model based on the SWM source fairly predicted the amplitude of self-excited oscillations (Graf and Ziada, 2010; Mohamed et al., 2018; Shaaban and Ziada, 2018). Golliard et al. (2015) have proposed another experimental approach that

analyze the scattering matrix of travelling waves, with and against the flow direction. This approach requires anechoic terminations on both ends of the test section.

Another approach based on Howe's analogy involves combining the flow field data measured using Particle Image Velocimetry (PIV) with the simulated acoustic field to estimate the acoustic energy generated. This methodology has been used by Oshkai and Yan (2008) to measure the source of closed-side branches. Mohamed and Ziada (2014) analyzed the source of a single cavity using PIV measurements. This method in general is complicated, time consuming and assumes the flow field being two-dimensional. However, it is the only experimental methodology that can be adapted to extract the source of a specific cavity in a long multiple-cavity section which will be needed during the current investigation.

Most of the studies that investigated corrugated pipe oscillations, e.g. Belfroid et al. (2007) and Nakiboglu et al. (2010), measured the self-excited oscillations of different corrugation geometries. Another study by Nakiboglu et al. (2011) focused on the effect of the pipe length and the approaching velocity profile. However, no attempt was made to link the overall oscillations of the corrugated pipe to the individual contributions of the cavities using a multiple-cavity model.

In the current study, the aeroacoustic source of gradually increasing number of cavities will be measured. The contribution of each added cavity is assessed until it asymptotically reaches a consistent value indicating fully developed conditions.

This consistent contribution can be defined as the building unit cavity source that is associated with a general cavity in a long corrugated pipe. The SWM will be used because it is an efficient and accurate experimental approach (Graf and Ziada, 1992; 2010; Mohamed et al., 2018; Shaaban and Ziada, 2018). This building unit source will then be used as a basis for a semi-empirical model to predict the oscillations of a twelve-cavity configuration. The model results are compared with self-excited measurements for the sake of validation. Another validation for the building unit source is accomplished through measuring the source of the ninth cavity in a twelve-cavity configuration using PIV flow visualization technique.

5.2 SWM Experimental Setup

The source of the multiple-cavity section is measured using the Standing Wave Method (SWM). A schematic of the experimental setup is shown in Figure 5.1. A long entrance pipe upstream of the cavities is installed to ensure fully developed turbulence conditions that resembles practical industrial applications. The system includes standard 4" PVC schedule 80 pipes. The mean flow velocity is measured using a pitot tube. The total source of the test section with multiple cavities is computed by analyzing the acoustic standing waves upstream and downstream of the test section, by means of three microphones in each pipe, and computing the acoustic pressure discontinuity over the cavities. The multiplication of this pressure difference and the acoustic particle velocity, that is maintained almost constant over the test section, yields the acoustic power generated by the

cavities. The dimensionless aeroacoustic source is then estimated from the power as given by equation (5.1). The wavelength of the standing wave scales with the physical length of the piping system and has an approximate value of 4.4 m. Consequently, the variation of the acoustic velocity over a six-cavity configuration is less than 5%.

$$S = \frac{\Delta P/(0.5 * \rho\, U^2)}{v/U} \tag{5.1}$$

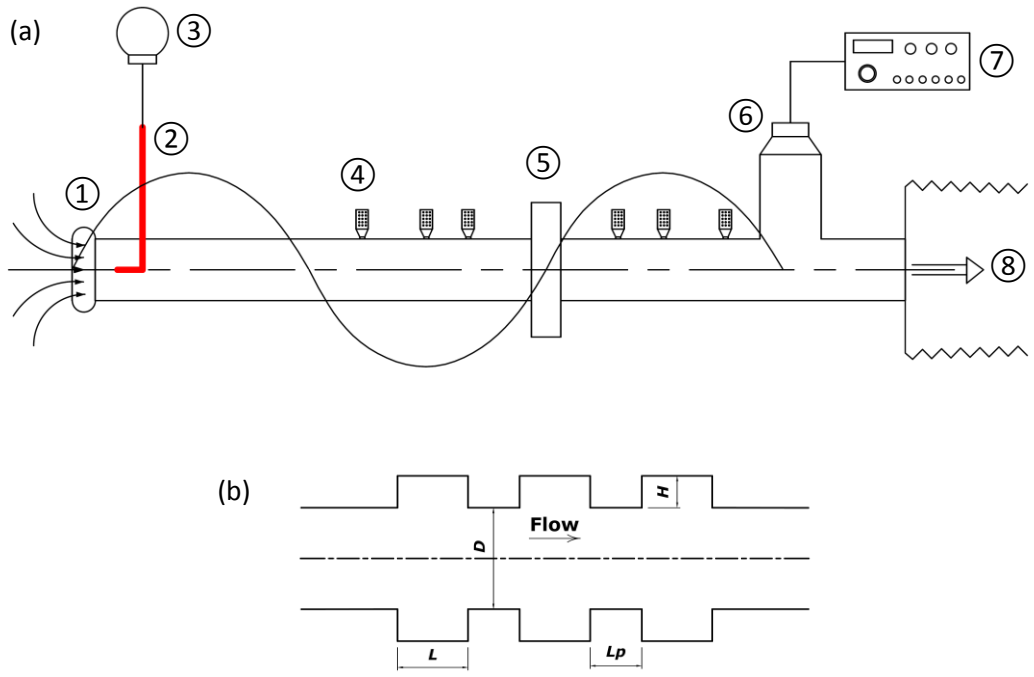

Figure 5.1. (a) Schematic of the SWM setup: ①Bell-mouth entrance, ②Pitot tube, ③Validyne differential pressure transducer, ④ One of six microphones, ⑤Test section, ⑥Speaker, ⑦Function generator with amplifier, ⑧Flexible hose exit to blower, (b) Sketch of the multiple cavities test section

The acoustic standing wave is excited along the duct using a loud speaker that is controlled via a function generator. The function generator provides a sinusoidal excitation with a frequency that matches the resonance frequency of

the system. A power amplifier is used to facilitate achieving high acoustic velocity ratios of about 20% of the mean flow velocity. The 3-phase AC blower motor, controlled by a Variable Frequency Drive (VFD), is used to control flow velocity in the main pipe. The current facility achieves various Strouhal numbers (*St*) ranging from 0.35 up to 1.2 covering the first two modes of the cavity shear layer instability.

Six microphones type G.R.A.S. 40BP, calibrated by G.R.A.S 42AB pistonphone, are used to measure the sound pressure in the main pipe. Fluke 922 pressure reader, with resolution of 1 Pa, is used to calibrate the differential pressure of the Pitot tube which is measured by a Validyne DP103 pressure transducer. The overall propagated uncertainty associated with the measured source, for a general test case of three-cavity configuration, is estimated to be about 2%. For very low source values near the boundaries of the lock-in range, this uncertainty measure is not a good description of the source accuracy. Therefore, an accuracy check procedure is developed that is applicable even for small source values. The Standing wave equation is obtained from the three microphones based on a least square method. The equation is then reused to estimate the acoustic pressure value at each microphone location and is compared to the actual microphone measurement. The percentage deviation, for the same three-cavity configuration, is limited to 0.8% over all the investigated test conditions.

Multiple cavities of 2″ length (L) and 1″ depth (H) in 4" schedule 80 pipes are investigated for a single spacing to cavity length ratio of 0.5. This spacing ratio is within the practical range and yet small to help overcoming the challenge of holding the acoustic velocity constant for the proper application of the SWM as previously discussed. The effect of gradually increasing the number of cavities is investigated up to six cavities. The aeroacoustic source map is measured for each configuration of cavities for wide ranges of Strouhal numbers (0.35 – 1.2) and excitation levels (0.5 % – 20%). The test matrix is achieved by varying the flow velocity up to 12 m/s which corresponds to a Reynolds number of approximately 7×10^4 and a Mach number of approximately 0.03.

5.3 Semi-Empirical Prediction Model

A semi-empirical prediction model is developed based on the building unit cavity source to predict the amplitude of oscillation for a twelve-cavity configuration. Self-excited measurements of the 12-cavity configuration are also performed to validate the model and consequently validate the building unit source methodology. The modelling procedure is based on the approach developed by Shaaban and Ziada (2018). The objective of the model is to predict the peak oscillation amplitude. The Strouhal number corresponding to the peak source from the SWM is used as an input to the model. A sweep of different acoustic velocity ratios is carried out to seek the resonance condition at which the source of the cavities counterbalances the system losses.

The acoustic power generated is computed from the source term as shown by equation (5.2). The acoustic velocity ratio, as a function of the antinode amplitude, is determined corresponding to the location of each cavity assuming a sinusoidal distribution of the acoustic wave. The first three entrance cavities are assigned a three-cavity configuration source with the acoustic velocity ratio considered at the center of the middle cavity. The chosen number of cavities in the entrance section is based on the SWM measurements which will be discussed at the first section of the results. The rest of the cavities are assigned the building unit cavity source, each of which corresponds to the acoustic velocity ratio at the location of the cavity center.

$$\Pi = \frac{1}{2}\,\rho A U\, v^2 * S \tag{5.2}$$

The system acoustic losses are estimated based on of the total impedance difference (ΔZ) at the midspan of the piping system calculated from both the upstream and downstream ends as shown in equation (5.3). The piping entrance radiation impedance is solved analytically using the fourth order formula given by Munjal (1987) based on Levine and Schwinger model (1948). The reflection coefficient of the piping discharge to the flexible hose was measured by Mohamed (2015) for the same setup using the two-microphone method in the presence of mean flow. The inductance effect at the cross-sectional area changes are accounted for based on the study by Kregomard and Garcia (1987). The impedances from both ends are transferred to the mid-section using the acoustic wave equation, given by

equation (5.4), which accounts for the visco-thermal losses in the complex wave number (β). The effect of the presence of the mean flow is taken into consideration by the Mach number (M) terms. Moreover, Shaaban and Ziada (2018) in their previous model have shown the importance of considering the acoustic absorption losses at the cavity edges to accurately estimate the oscillations amplitude. Thus, the absorption impedance loss (Z_{abs}) is considered for each cavity as given by equation (5.5).

$$\Pi_{loss} = \Delta Z * (A\, v)^2, \tag{5.3}$$

$$P(x,t) = \left\{ P^+ \, e^{\frac{-j\,\beta\,x}{(1+M)}} + \, P^- \, e^{\frac{j\,\beta\,x}{(1-M)}} \right\} e^{j\,(2\pi f)t}, \tag{5.4}$$

$$Z_{abs} = \, 570 \, \frac{k\,a}{M}. \tag{5.5}$$

5.4 PIV Experimental Setup

It is desired to extract the individual source of a cavity in a long multiple-cavity section to validate the building unit cavity source. This objective can be achieved by means of Howe's analogy which requires knowledge of the flow field details measured, for example, by means of Particle Image Velocimetry (PIV) laser technique. An acrylic cavity is used to allow for optical access. Nd:YAG laser, with wavelength of 532 nm, is shot horizontally towards the acrylic cavity. Nikon camera is fixed above the cavity in order to capture the laser illuminated plane. The experimental setup is shown schematically in Figure 5.2. The camera has a resolution of 4 MP with 12-bit CCD chip that provides the digital output for the

processing computer. AF Nikkor lens is used with 50 mm focal length. Bis(2-ethylhexyl) sebacate is used to seed the air flow. The seeding particles exiting the aerosol generator are characterized by a mean diameter of 1 μm. Stokes number corresponding to the small size particle is way less than 0.1 which ensures tracing error less than 1% as indicated by Melling (1997) and Tropea et al. (2007).

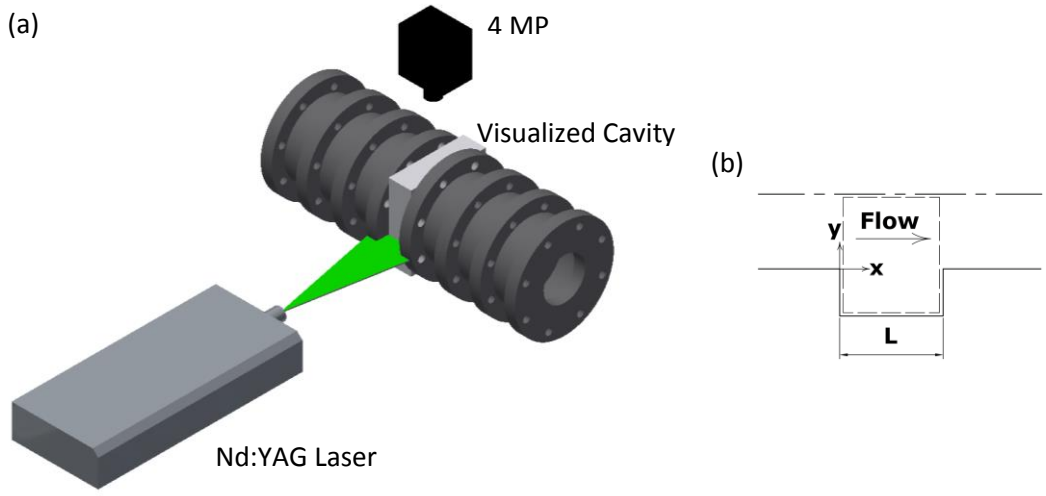

Figure 5.2. (a) Schematic of the PIV experimental setup, (b) The visualized window of the acrylic cavity

The square field of view has a side length of about 80 mm. The coarse interrogation region is 32 × 32 pixels which is further refined to be 16 × 16 pixels. The time difference between the two captured frames is estimated to limit the particles translation to a maximum of 4 pixels, i.e. quarter the size of the interrogation region. The speaker signal is used to trigger the laser pulses to achieve phase locked images. The zero phase corresponds to zero acoustic pressure in the rising portion of the cycle in the upstream duct. TSI LaserPulse Model 610035

synchronizer is used to synchronize the timing of the laser pulses and the captured images. Image processing is done using Insight 4G software. At least 99% good vectors validation rate is achieved for each case study.

A first order deformation grid employing gaussian sub-pixel interpolation has been used for processing the velocity vectors. The maximum streamwise $(\partial u/\partial y)_{max}$ and cross-stream $(\partial v/\partial x)_{max}$ velocity gradients are found to be about 0.029 and 0.007 pixel/pixel, respectively. The uncertainty in the vector processing is estimated based on the study by Scarano and Riethmuller (2000) who used a similar processing approach. Consequently, the uncertainty associated with the aforementioned velocity gradients is less than 4% and 7% for the streamwise and cross-stream directions, respectively.

The source of the ninth cavity in a twelve-cavity configuration is investigated using PIV for the sake of comparison with the building unit source measured by means of the SWM. The Strouhal number is fixed to the value corresponding to the peak aeroacoustic source as determined by the SWM measurements. Five different acoustic velocity ratios are tested ranging from 0.005 to 0.1. For every test case, eight uniformly spaced phases of the acoustic cycle are visualized with 200 images captured per phase.

Finite element analysis using Abaqus is performed to estimate the acoustic velocity field that is then combined with the PIV flow data to compute the acoustic power generated using Howe's Integrand given by equation (5.6). Three-

dimensional axisymmetric model is developed for the piping system housing the twelve-cavity configuration. Large settling chambers, six times the size of the pipe, are included to simulate the acoustic pressure nodes at the boundaries. Triangular meshing elements of size of 0.003 m are used along the duct but this size is refined to 0.0005 m in the twelve-cavity region. Mesh sensitivity analysis is carried out to make sure that the simulated acoustic mode is not affected by the mesh size. The final model included about 800,000 elements. The predicted resonance frequency matches the experimentally measured one with an approximate deviation of 2%. The acoustic pressure amplitude generated by the simulation is unity. This amplitude is then scaled to the proper excitation levels corresponding to the different investigated cases. A Matlab code, based on Euler's equation, is developed to compute the acoustic particle velocity distribution from the acoustic pressure gradients previously estimated from the finite element simulation.

$$\Pi = -\rho \int \omega . (U \times v) \, \mathrm{dV} \tag{5.6}$$

5.5 Results

5.5.1 SWM Measurements for Gradually Increasing Number of Cavities

The aeroacoustic source is shown for gradually increasing number of cavities in Figure 5.3 and Figure 5.4 for acoustic velocity ratios of 0.01 and 0.1 representing small and high excitation levels, respectively. Attention is now focused on the shear layer fundamental mode which is centered on a Strouhal number of 0.6. This is because the aeroacoustic source produced by this shear layer

mode is the strongest and therefore it has the highest potential to cause vibration or noise problems in industrial applications. For the low excitation level case shown in Figure 5.3, increasing the number of cavities generally increases the source strength, but the amount of this change decreases asymptotically until it reaches a constant value starting from the fourth cavity. Similar trends have been observed for the intermediate excitation levels, but the asymptotic contribution of each cavity is found to be more stable and considerably lower in magnitude. High excitation levels exhibit a different correlation between the source strength and the number of cavities. As shown in Figure 5.4, although a discernable contribution is observed upon adding the second cavity, starting from the fourth cavity almost no contribution is added to the generated aeroacoustic source. This phenomenon may be attributed to the vortex damping losses in the added cavity which seems to cancel out the small increase in generated power. Vortex damping have been reported by Ziada (1994) for the case of closed side-branch resonances. The Strouhal number corresponding to the peak source reaches a virtually constant value starting from the fourth cavity being 0.525 for excitation levels less than or equal to 2% and it shifts to 0.55 for higher excitation levels. This fairly matches the values of the peak whistling Strouhal number reported by Nakiboglu et al. (2011) for long corrugated pipes.

The test results of all cases, including the number of cavities and excitation levels, are summarized in Figure 5.5, which shows the change in the peak source value for each additional cavity. The results of different acoustic velocity ratios are

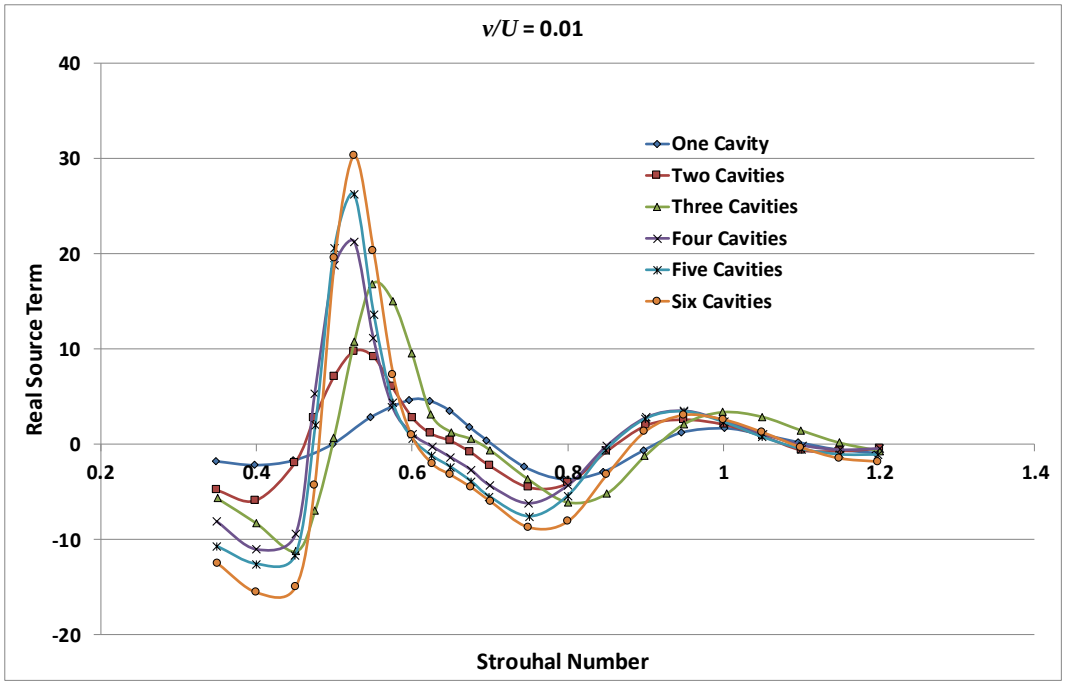

Figure 5.3. Real source vs. Strouhal number for gradually increasing number of cavities with *v/U* = 0.01

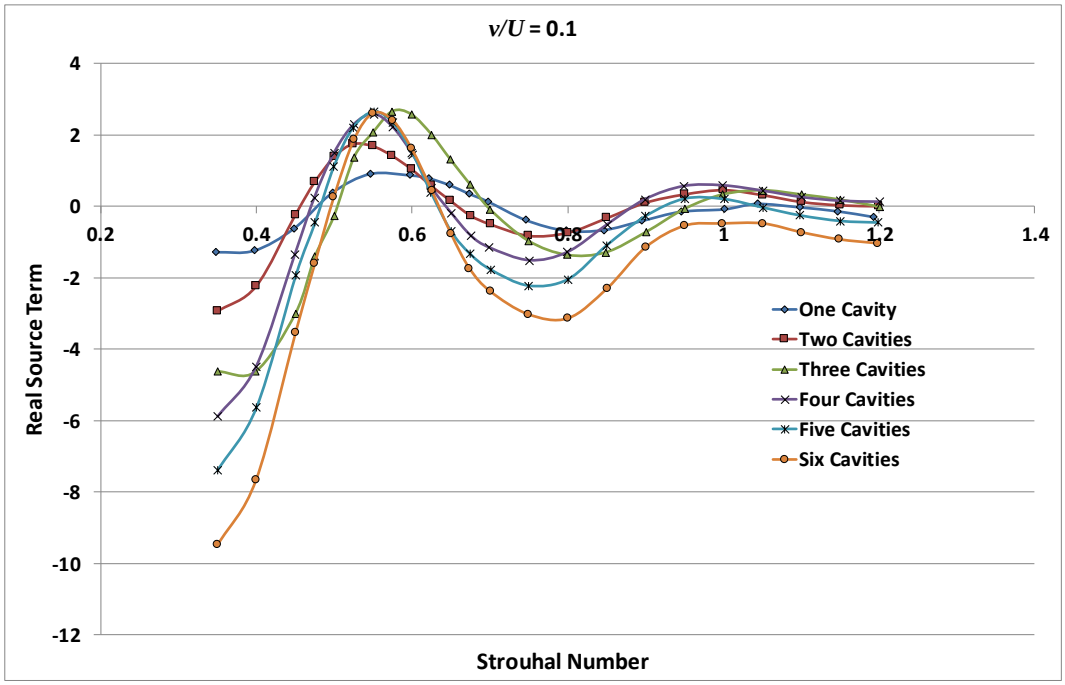

Figure 5.4. Real source vs. Strouhal number for gradually increasing number of cavities with *v/U* = 0.1

shown for the range from 0.005 to 0.1. The change in the peak source value is defined as the source contribution of the added cavity. The main observation here is that, regardless the excitation level, the flow is almost fully developed resulting in a constant source contribution after the fourth cavity for the investigated spacing ratio.

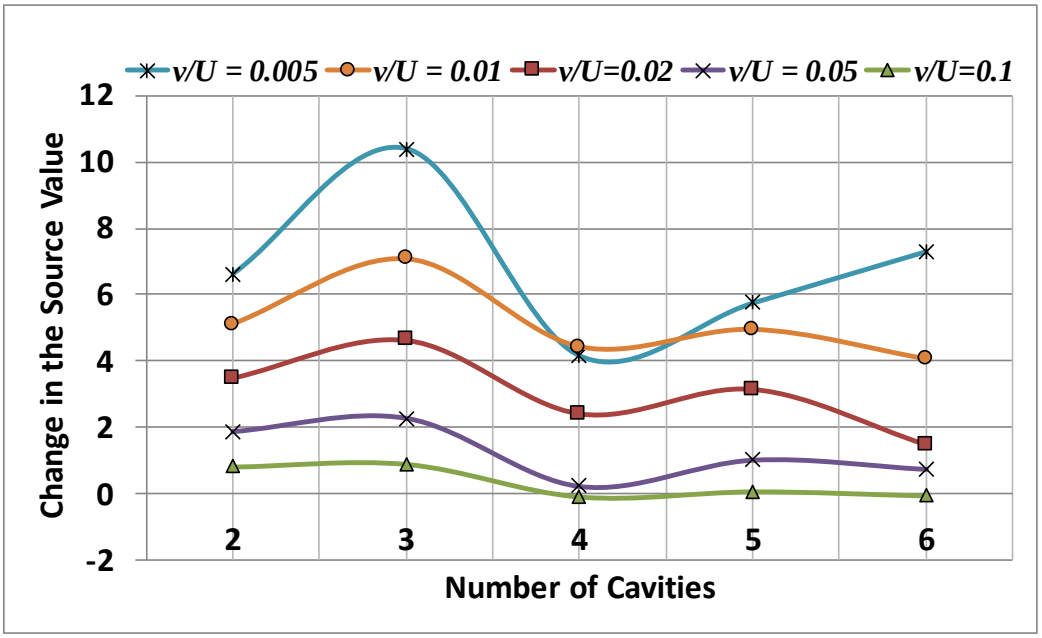

Figure 5.5. Change in the peak source value corresponding to each added cavity for different acoustic velocity ratios

The asymptotic level, computed as the average of the consistent contribution of the fourth, fifth and sixth cavities, is defined as the building unit cavity source which is a function of the excitation level. It eventually vanishes when the excitation level is increased to 10% or higher. Such source is expected to be representative of any cavity in a long multiple-cavity section after the three entrance cavities. This building unit cavity source will be validated using two different

approaches. First, it will be used in a semi-empirical model to predict the self-excited oscillations of a pipe section with 12 cavities and compare the prediction with experimentally measured self-excited oscillation. The second approach of validation uses PIV flow measurements to estimate the source strength of the 9^{th} cavity in an arrangement of 12 cavities. These two validation methods are presented in the next two sections.

5.5.2 Prediction Model Based on the Building Unit Cavity Source

A semi-empirical model is developed to predict the oscillation of a twelve-cavity system positioned between two straight pipes 60 cm each. The model is based on the building unit cavity source. In order to validate the proposed building unit cavity approach, the model prediction is compared to the measured amplitude of the self-excited oscillations. In the semi-empirical model, the first three entrance cavities are assigned the source strength measured for a three-cavity configuration with the same spacing ratio. The acoustic power of the cavities is calculated from the source strength taking into consideration the value of the acoustic particle velocity corresponding to the location of the center of each cavity. A sinusoidal distribution of the acoustic standing wave is assumed along the duct at the resonance frequency. Different types of acoustic losses are calculated from basic principles as previously discussed in the modelling section.

The steady state resonance amplitude is determined by the flow conditions at which the acoustic power produced by the twelve cavities counterbalances the

system acoustic losses as depicted in Figure 5.6. The resonance oscillation amplitude is predicted to be 5.1% of the mean flow velocity. The building unit cavity source has been determined based on the variation of the peak source of a gradually increasing number of cavities. Thus, the predicted amplitude corresponds to the resonance oscillations at a Strouhal number of 0.55 which is consistently observed in the SWM measurements for configurations with four or more cavities at this excitation level. The acoustic absorption losses at the cavity edges are found to be crucial for the accurate prediction of the amplitude of the acoustic pressure oscillations. Without considering such absorption losses, the generated power always exceeds the dissipated energy due to acoustic losses for the whole spectrum of acoustic velocity ratios indicating unrealistic infinite oscillations amplitude. This has clearly pointed towards an underestimation of the acoustic losses of the system.

A self-excited experimental setup is built for the sake of model validation. A sweep of flow velocities is performed using a variable speed blower and the acoustic oscillations amplitude is measured as a function of the flow velocity using a microphone that is situated close to the acoustic pressure anti-node. Such location is determined from the expected resonance mode wavelength which scales with the system physical length. The acoustic frequency remains virtually constant throughout the lock-in range with a slight increase with flow velocity towards the end of the lock-in range. This helps maintaining the synchronization of both the

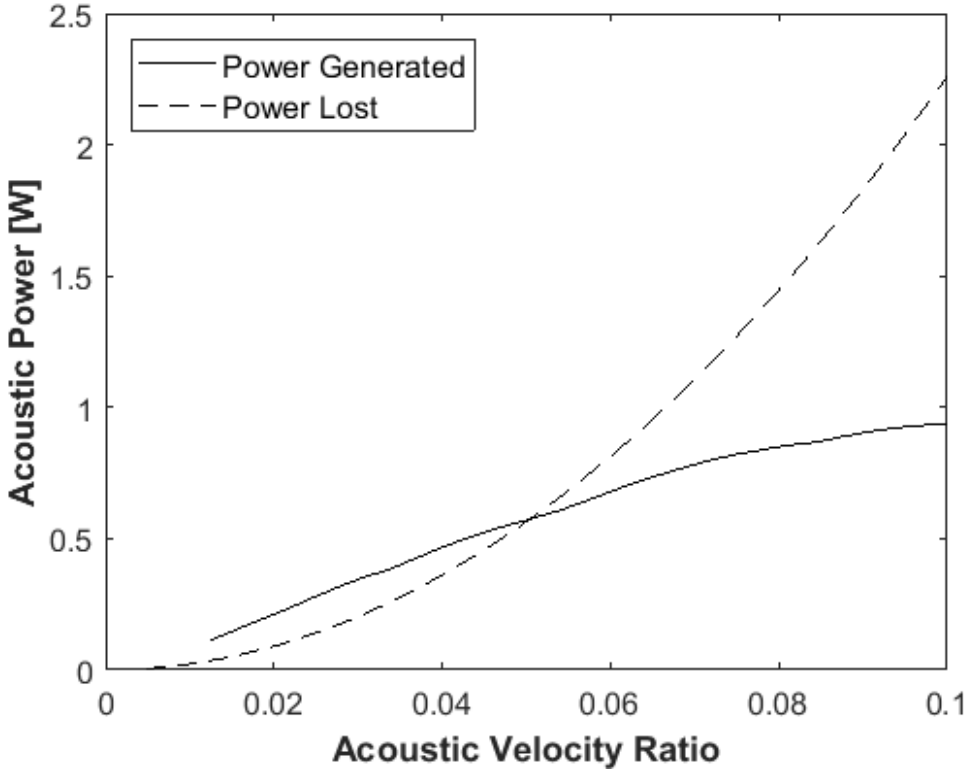

Figure 5.6. Acoustic Power generated by the twelve-cavity section vs. that lost by the system at different acoustic velocity ratios

acoustic and hydrodynamic instability cycles. Similar characteristics have been reported for resonances of closed side-branches in a recent review article by Tonon et al. (2011). The lock-in-range of the self-excited oscillations is presented in Figure 5.7 and is compared with the predicted peak oscillations amplitude based on the building unit cavity source. The deviation between the peak amplitude measured experimentally and that predicted by the model is about 13%. Moreover, the Strouhal numbers corresponding to the peak oscillations in both approaches are virtually the same. This good agreement between the model and the experimental data validates the proposed approach of the building unit cavity source, which is the basic idea of the prediction model.

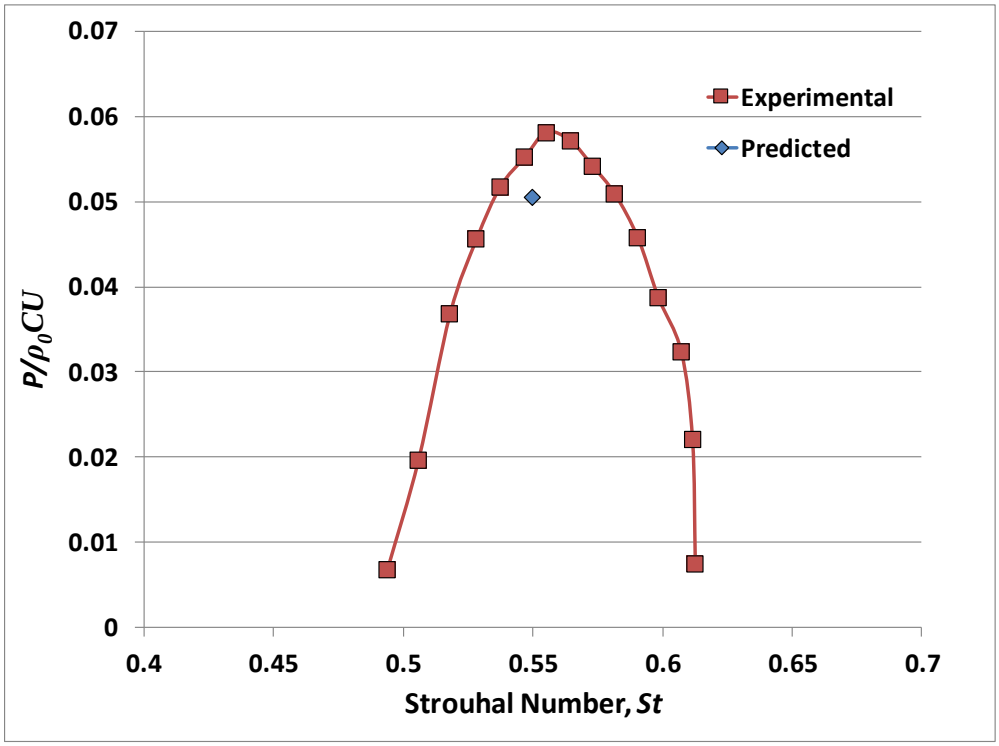

Figure 5.7. Experimental self-excited lock-in range vs. the predicted peak amplitude for the twelve-cavity configuration

5.5.3 Source Measurement of the Ninth Cavity using PIV

Another approach to validate the building unit cavity source is to measure the source of an individual cavity in a long multiple-cavity section. Howe's analogy, which is based on flow field data measured by the PIV system, is adopted here to measure the source strength of a middle cavity in a long multiple-cavity pipe section. To this end, the ninth cavity in a twelve-cavity configuration is investigated. The Strouhal number is kept at the value corresponding to the peak source obtained from the SWM measurements. Different acoustic velocity ratios are tested in the range from 0.005 to 0.1.

The flow is captured at eight uniformly spaced phases of the acoustic cycle, i.e. phase locked PIV images. The general flow characteristics have been found to be similar to those reported by Mohamed and Ziada (2014) for the shear layer flow over a single cavity. The shear layer is formed at the interface between the core flow, characterized with high flow velocity and the cavity domain, where the flow is almost stagnant. The shear layer is associated with high value of vorticity. At low excitation levels, the shear layer vorticity field can be described as a vorticity cloud which is flapping during the acoustic cycle. However, at relatively higher excitation levels, distinct coherent structures start to separate from the vorticity cloud and roll over the cavity mouth. Thus, the vorticity field chosen to be presented in Figure 5.8 is for an intermediate excitation case of 5% where distinct coherent structures can be traced along the different phases of the acoustic cycle.

The flow field data obtained from the PIV measurements are then combined with the acoustic velocity data, estimated from the finite element simulation of the sound field, to compute the acoustic power generated by the cavity. The spatial distribution of the average acoustic power generated by the *ninth* cavity over the whole acoustic cycle is shown in Figure 5.9 for acoustic velocity ratios of 0.005, 0.02 and 0.1 representing low, intermediate and high excitation levels, respectively. The distribution shows two strong sources at the upstream and downstream thirds of the cavity. A sink exists in the middle of the cavity and underneath the upstream source at the beginning of the cavity shear layer. This agrees well with the source distribution for the single cavity case studied by Mohamed and Ziada (2014) and

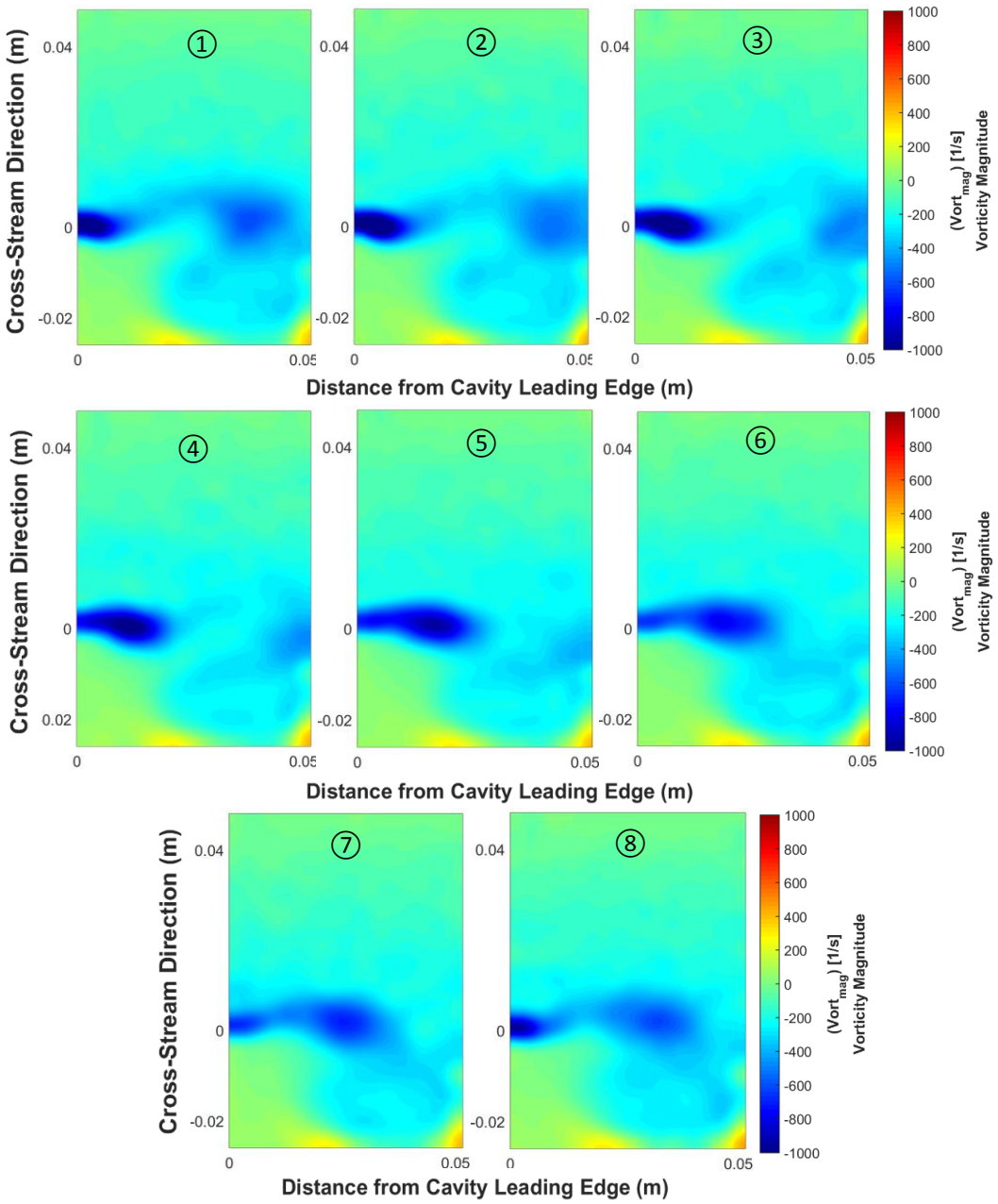

Figure 5.8. Vorticity distribution for the flow over the ninth cavity for *v*/U = 0.05 over the eight points of the acoustic cycle with ① being at θ = 0

for the three-cavity configuration studied by Shaaban and Ziada (2019). However, it can be seen here that the source distribution for the low excitation level case is not as crisp and well organized as the other cases. This will be discussed in more

details later in this section. The acoustic power is seen to increase proportional to the acoustic excitation level as can be observed from the contour values.

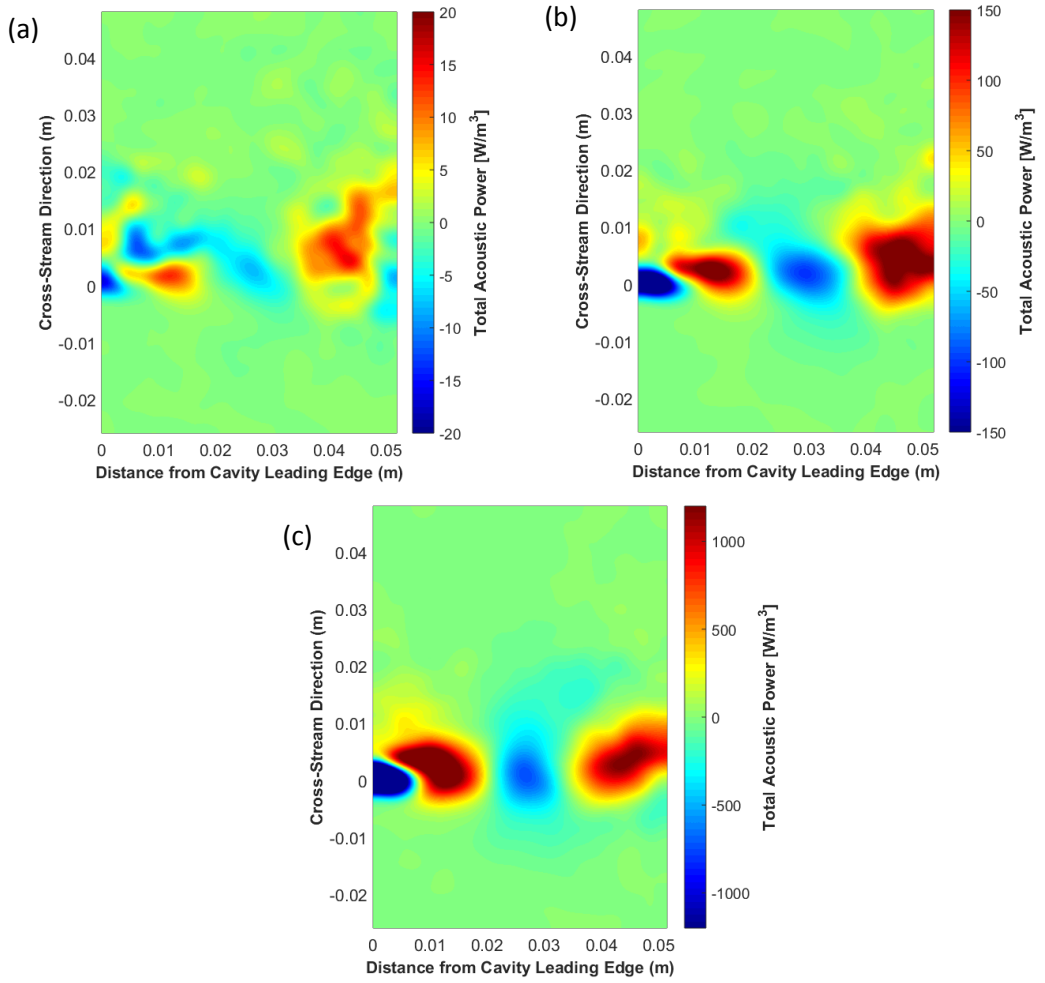

Figure 5.9. Spatial distribution of the average acoustic power over the acoustic cycle for the ninth cavity at different excitation levels: (a) *v/U* = 0.005, (b) *v/U* = 0.02 and (c) *v/U* = 0.1

The next step is to calculate the dimensionless aeroacoustic source based on the acoustic power as given by equation (5.2). A comparison between the ninth cavity source, calculated by applying Howe's analogy to the flow field data, and the building unit cavity source measured by means of the SWM is presented in

Figure 5.10. Fair agreement is found between both source values for excitation levels higher than or equal 2%. This gives support to the validity of the building unit cavity source. However, the source based on the PIV data is underestimated for low excitation levels exhibiting a trend where the source decreases with decreasing acoustic velocity ratio. This contradicts the trend of the building unit cavity source and the general source trends reported in the literature for a single cavity and multiple-cavity arrangements (Nakiboglu et al., 2012; Mohamed et al., 2018; Shaaban and Ziada, 2018). This indicates that some of the assumptions associated with the PIV images are no longer valid at these low excitation levels, as further discussed in the following paragraphs.

The main assumption implied in the PIV measurements is the two-dimensionality of the axisymmetric pipe flow. This assumption may be supported by the fact that the acoustic standing wave along the duct is a plane wave that is also uniform axisymmetrically. However, the background turbulence which is essentially present in the flow field is three-dimensional in nature. Such turbulence is expected to become more dominant and effective as the excitation level decreases to sufficiently low levels. In a previous study by Mohamed and Ziada (2014) for the single cavity source, the maximum deviation between the PIV source and that obtained from the SWM was reported for the minimum excitation level of 0.2%. However, the difference was still within the acceptable limits. Also, Shaaban and Ziada (2019) have not reported large discrepancy between the PIV and the SWM sources for the three-cavity configuration. Therefore, it is worthwhile investigating

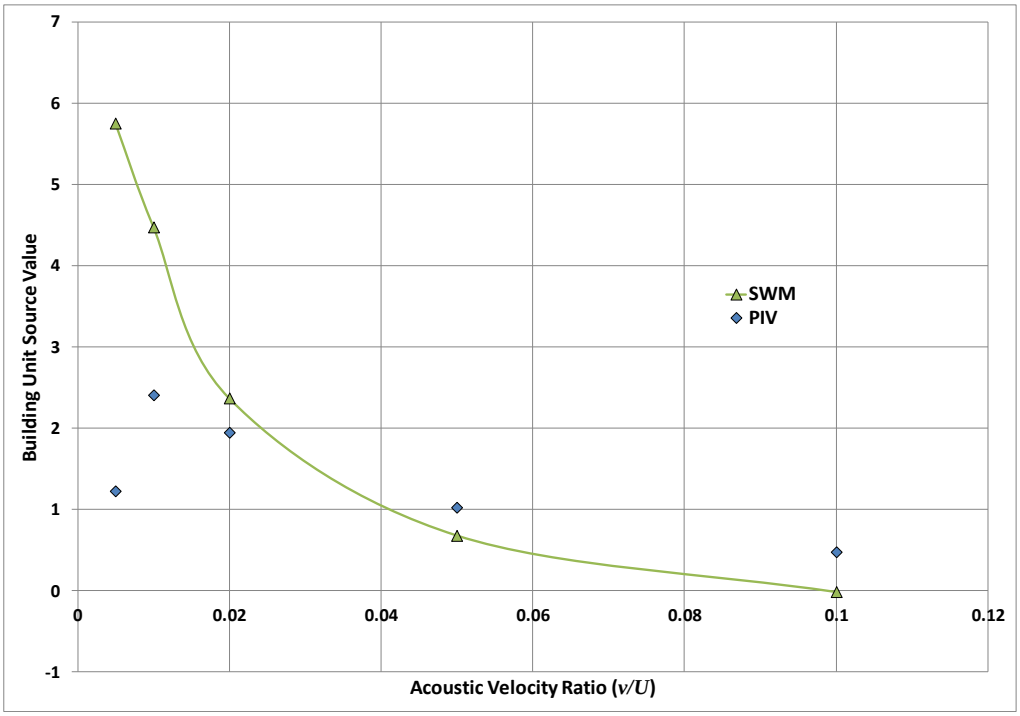

Figure 5.10. Comparison of the building unit source value measured using the SWM vs. that using Howe's analogy based on the PIV data

how the turbulence level evolves from the previously studied three cavities towards the currently investigated ninth cavity.

The streamwise turbulence fluctuations are shown in Figure 5.11 for the first, third and ninth cavities at the same excitation level of 2%. The turbulence level obviously increases for the ninth cavity and spreads over a wider zone. The same conclusion can be deduced from the cross-stream turbulence contours depicted in Figure 5.12 for the same test conditions. However, this comparison is not held at the same exact values of low excitation levels where the source value being underestimated. So, in order to verify that the increase in turbulence level is due to the cavity location and not because of excitation level, the streamwise

turbulence fluctuations are shown in Figure 5.13 for the ninth cavity at low excitation level of 0.5% compared with the first cavity at 0.2% and 2% as slightly lower and higher excitation levels, respectively. It can be noted that regardless the excitation level of the first cavity, the turbulence level of the ninth cavity is much higher because of its location and the flow development rather than the excitation level. Thus, based on this discussion, it can be concluded that the ninth cavity PIV source matches the building unit source except for low excitation levels for which the turbulence level dominates at the ninth cavity. Under these conditions, the PIV measurement technique is inadequate because of the three-dimensional nature of the flow. On the other hand, the SWM is expected to yield a more accurate building unit source because it extracts the integral effect of the source even when the flow is three-dimensional.

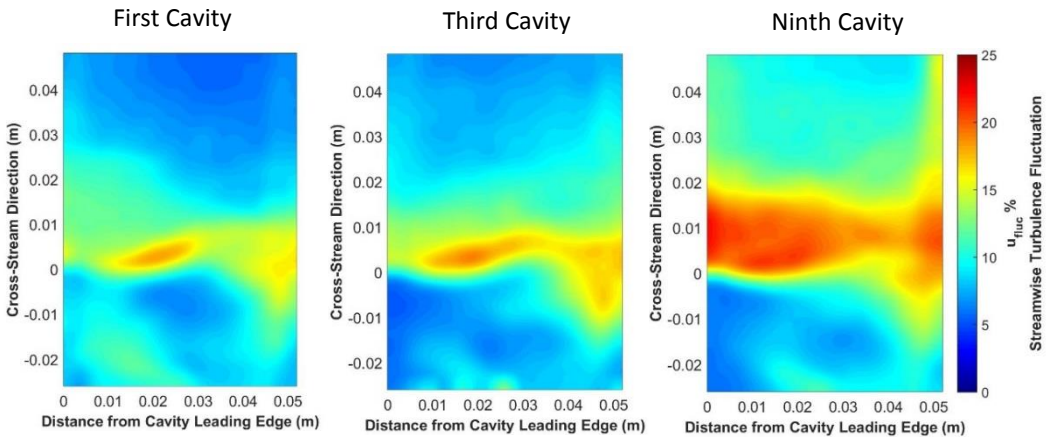

Figure 5.11. Streamwise turbulence fluctuation for the first, third and ninth cavities at v/U = 0.02

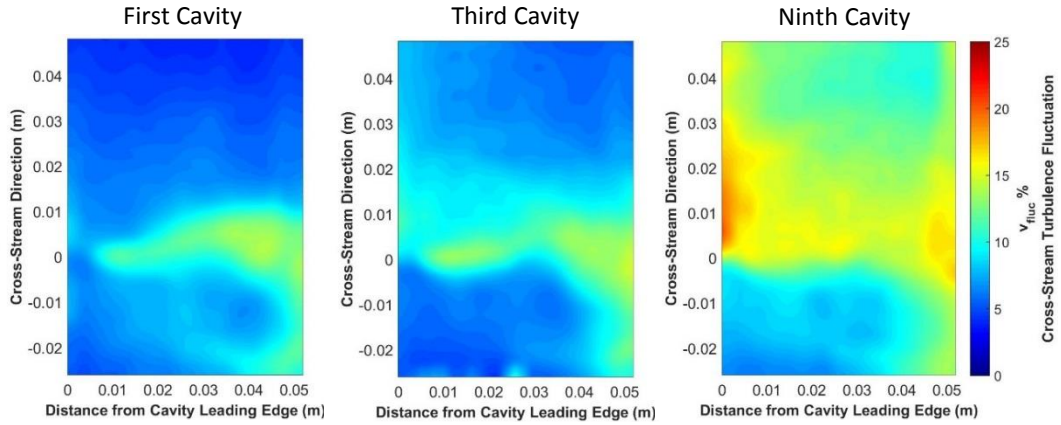

Figure 5.12. Cross-stream turbulence fluctuation for the first, third and ninth cavities at *v/U* = 0.02

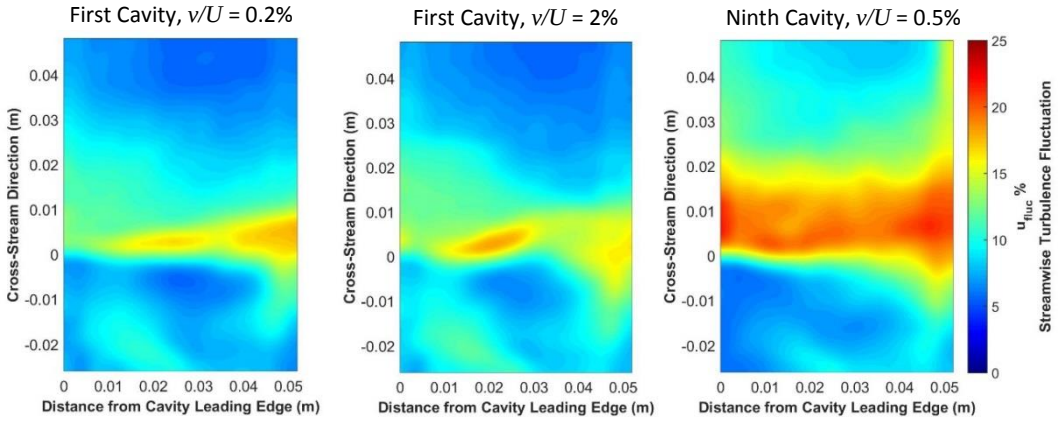

Figure 5.13. Streamwise turbulence fluctuation for the first cavity at *v/U* = 0.002 and 0.02 vs. the ninth cavity at *v/U* = 0.005

5.5.4 Effect of Number of Cavities on the Strouhal Number

During the experiments, the Strouhal number that corresponds to the peak source value is observed to shift towards lower values upon increasing the number of cavities for the low and intermediate excitation levels. It eventually becomes constant for configurations with four or more cavities as has been observed in the SWM results. A physical explanation for this Strouhal shift is sought in this section. The velocity profile approaching the first cavity has been shown by Shaaban and

Ziada (2019) to approximate the fully developed one-sixth power law profile. The Strouhal number corresponding to the peak source at low and intermediate excitation levels was reported to be 0.6 with a dimensionless boundary layer momentum thickness (θ/a) of 0.11. The velocity profile approaching the ninth cavity is compared to that approaching the first cavity in Figure 5.14. The boundary layer momentum thickness for the ninth cavity is obviously thicker with a dimensionless value of 0.13. The thicker boundary layer requires higher flow velocities in order to get excited. This explains the shift of the Strouhal number to 0.525 for long multiple-cavity sections. The Strouhal numbers based on the momentum thickness (St_θ) for both the single cavity and the ninth cavity agree well with a deviation of only 4%. These findings support the hypothesis that the Strouhal shift is caused by the development of the velocity profile approaching the downstream cavities with slightly thicker boundary layer. This Strouhal number shift to a lower value seems to become complete after the four-cavity configuration along with the consistent building unit cavity source.

5.6 Conclusions

The changes in the aeroacoustic source upon gradually increasing number of cavities have been investigated using the SWM. The contribution of each added cavity reaches an asymptotic constant value starting from the fourth cavity indicating fully developed source conditions at the investigated spacing ratio of half. Such consistent contribution is used to define a building unit cavity source that

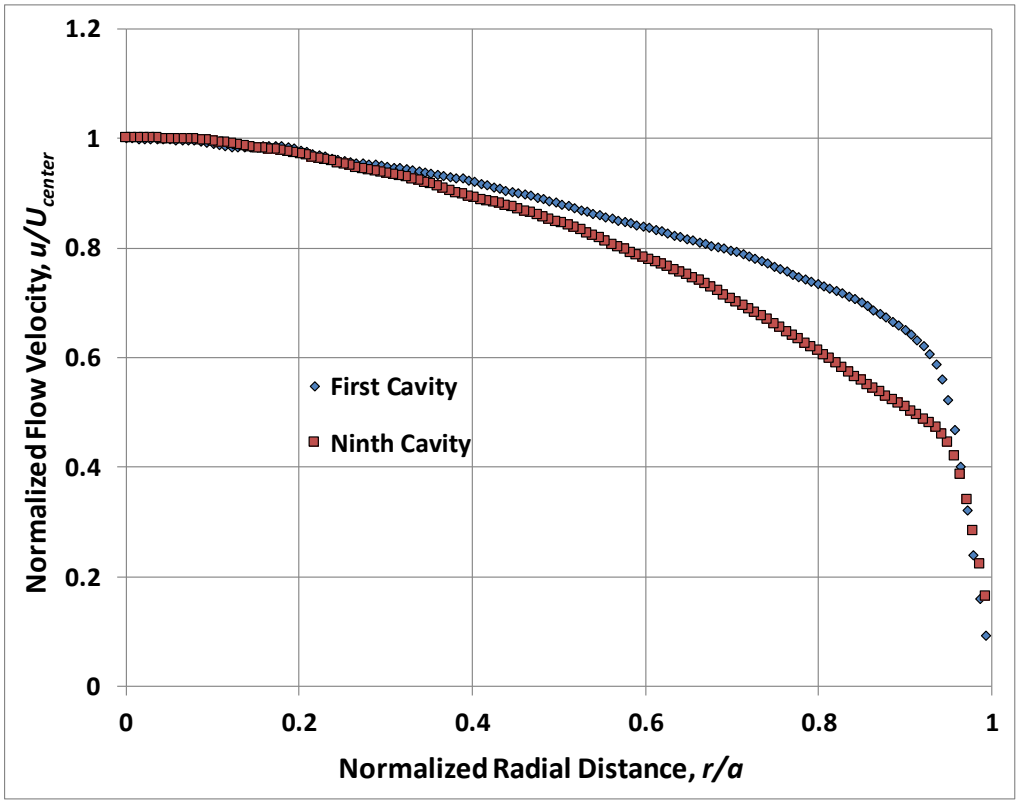

Figure 5.14. Normalized velocity profile over the pipe radius at the cavity entrance for the first and ninth cavities

is representative of a general cavity in a long multiple-cavity section. The strength of the building unit source decreases upon increasing the acoustic velocity ratio and eventually vanishes at an excitation level of 0.1. The Strouhal number corresponding to the peak source becomes consistent starting from the four-cavity configuration as well.

The building unit cavity is validated via two different approaches. First, a semi-empirical prediction model, based on the building unit cavity source, is used to predict the oscillations amplitude of a long twelve-cavity configuration. The predicted amplitude agrees well with the measured one with only 13% deviation.

Including the absorption losses at the cavity edges is essential for accurate model performance. The peak whistling Strouhal number of the self-excited experiment agrees well with the value predicted by the model.

The second validation approach is to measure the building unit cavity source using the flow field data acquired by PIV technique. The ninth cavity in a long twelve-cavity configuration has been chosen for this case study. The source distribution is found to be similar to that obtained from single cavity experiments. The measured source of the ninth cavity is found to agree well with the building unit cavity source for acoustic velocity ratios higher than 0.01. The flow at lower excitation levels has been found to be dominated by the three-dimensional turbulence effects which preclude adequate flow field measurements by means of PIV technique. For this reason, the PIV methodology substantially underestimates the value of the building unit cavity source. In such situations, when three-dimensional effects are present, the SWM is a reliable and efficient methodology to measure aeroacoustic sources in confined flows.

Nomenclature

a	Pipe radius (m)
A	Pipe cross-sectional area (m^2)
f	Resonance frequency (Hz)
H	Cavity depth (m)

k	Wave number (m^{-1})
L	Cavity length (m)
M	Mach number
P	Acoustic pressure (Pa)
S	Normalized aeroacoustic source
St	Strouhal number based on the cavity length
St_θ	Strouhal number based on the momentum thickness
U	Flow velocity (m/s)
v	Acoustic particle velocity (m/s)
ΔZ	Acoustic impedance difference at the piping mid-section (Pa s/m^3)
Z_{abs}	Absorption impedance loss at the cavity edges (Pa s/m^3)
ω	Flow vorticity (1/s)
θ	Momentum boundary layer thickness (m)
Π	Acoustic power (W)
Π_{loss}	Acoustic power losses (W)
β	Complex wave number (m^{-1})

References

Belfroid, S., Shatto, D., and Peters, M., 2007. Flow induced pulsations caused by corrugated tubes. *In*: *Pressure Vessels and Piping Conference*. ASME, 439–447.

Coltman, J., 1968. Sounding mechanism of the flute and organ pipe. *The Journal of the Acoustical Society of America*, 44 (4), 983–992.

Golliard, J., Belfroid, S., Vijlbrief, O., and Lunde, K., 2015. Direct measurements

of acoustic damping and sound amplification in corrugated pipes with flow. *In*: *Pressure Vessels and Piping Conference*. ASME, PVP2015-45494.

Golliard, J., González-Díez, N., Belfroid, S., Nakiboğlu, G., and Hirschberg, A., 2013. U-RANS model for the prediction of the acoustic sound power generated in a whistling corrugated pipe. *In*: *Pressure Vessels and Piping Conference*. ASME, PVP2013-97385.

Graf, H. and Ziada, S., 1992. Flow induced acoustic resonance in closed side branches: an experimental determination of the excitation source. *In*: *International Symposium on Flow-Induced Vibration and Noise*. ASME, 63.

Graf, H. and Ziada, S., 2010. Excitation source of a side-branch shear layer. *Journal of Sound and Vibration*, 329 (14), 2825–2842.

Kergomard, J. and Garcia, A., 1987. Simple discontinuities in acoustic waveguides at low frequencies: critical analysis and formulae. *Journal of Sound and Vibration*, 114 (3), 465–479.

Levine, H. and Schwinger, J., 1948. On the Radiation of Sound from an Unflanged Circular Pipe. *Physical Review*, 73 (4), 383–406.

Melling, A., 1997. Tracer particles and seeding for particle image velocimetry. *Measurement Science and Technology*, 8 (12), 1406–1416.

Mohamed, S., 2015. Sound waves excitation by flow in a pipe housing a shallow cavity. PhD Thesis, McMaster University.

Mohamed, S., Graf, H., and Ziada, S., 2018. Measurement of the Excitation Source of an Axisymmetric Shallow Cavity Shear Layer. *Journal of Pressure Vessel Technology*, doi: 10.1115/1.4039781.

Mohamed, S. and Ziada, S., 2014. PIV Measurements of Aeroacoustic Sources of a Shallow Cavity in a Pipeline. *In*: *Pressure Vessels and Piping Conference*. ASME, PVP2014-28508.

Munjal, M., 1987. *Acoustics of ducts and mufflers with application to exhaust and ventilation system design*. First edition. John Wiley & Sons.

Nair, K. and Sarkar, S., 2016. Large Eddy Simulation of Self-Sustained Cavity Oscillation for Subsonic and Supersonic Flows. *Journal of Fluids Engineering*, 139 (1), 11102.

Nakiboglu, G., Belfroid, S., Golliard, J., and Hirschberg, A., 2011. On the whistling of corrugated pipes: effect of pipe length and flow profile. *Journal of Fluid*

Mechanics, 672, 78–108.

Nakiboglu, G., Belfroid, S., Willems, J., and Hirschberg, A., 2010. Whistling behavior of periodic systems: Corrugated pipes and multiple side branch system. *International Journal of Mechanical Sciences*, 52 (11), 1458–1470.

Nakiboglu, G., Manders, H., and Hirschberg, A., 2012. Aeroacoustic power generated by a compact axisymmetric cavity: prediction of self-sustained oscillation and influence of the depth. *Journal of Fluid Mechanics*, 703, 163–191.

Oshkai, P., Yan, T., Velikorodny, A., and VanCaeseele, S., 2008. Acoustic Power Calculation in Deep Cavity Flows: A Semiempirical Approach. *Journal of Fluids Engineering*, 130 (5), 51203.

Popiel, C., Kozak, M., Małecka, J., and Michalak, A., 2013. Friction Factor for Transient Flow in Transverse Corrugated Pipes. *Journal of Fluids Engineering*, 135 (7), 74501.

Rajavel, B. and Prasad, M., 2014. Parametric studies on acoustics of corrugated tubes using large eddy simulation (LES). *Noise Control Engineering Journal*, 62 (4), 218–231.

Rayleigh, Lord, 1879. On the instability of jets. *In*: *Proc. London Math. Soc 10*. 4–13.

Rockwell, D. and Naudascher, E., 1978. Review—self-sustaining oscillations of flow past cavities. *Journal of Fluids Engineering*, 100 (2), 152–165.

Scarano, F. and Riethmuller, M., 2000. Advances in iterative multigrid PIV image processing. *Experiments in Fluids*, 29, S051–S060.

Shaaban, A. and Ziada, S., 2018. Acoustic Response of Multiple Shallow Cavities and Prediction of Self-Excited Acoustic Oscillations. *Journal of Fluids Engineering*, 140 (9), 91203.

Shaaban, A. and Ziada, S., 2019. Effect of the Separation Distance on the Aeroacoustic Source of Multiple Shallow Cavities. *Journal of Fluids Engineering*, 141 (1), 011102.

Stel, H., Morales, R., Franco, A., Junqueira, S., Erthal, R., and Gonçalves, M., 2010. Numerical and Experimental Analysis of Turbulent Flow in Corrugated Pipes. *Journal of Fluids Engineering*, 132 (7), 71203.

Tonon, D., Hirschberg, A., Golliard, J., and Ziada, S., 2011. Aeroacoustics of pipe

systems with closed branches. *International Journal of Aeroacoustics*, 10 (2–3), 201–275.

Tropea, C., Yarin, A., and Foss, J., eds., 2007. *Springer Handbook of Experimental Fluid Mechanics*. First edition. Berlin, Heidelberg: Springer.

Williams, J. and Hawkings, D., 1969. Sound generation by turbulence and surfaces in arbitrary motion. *Philosophical Transactions of the Royal Society of London A: Mathematical, Physical and Engineering Sciences*, 264 (1151), 321–342.

Ziada, S., 1994. A flow visualization study of flow-acoustic coupling at the mouth of a resonant side-branch. *Journal of Fluids and Structures*, 8 (4), 391–416.

CHAPTER 6
SUMMARY AND CONCLUSIONS

6.1 Thesis Summary

In the current research, work has been accomplished towards investigating the phenomenon of sound generation by flow over multiple consecutive axisymmetric shallow cavity configurations, with the ultimate goal of predicting pulsation amplitude in corrugated pipes. Multiple cavity configurations can provide a model for corrugated pipes widely used in gas and oil offshore fields. The first phase of the project investigates the aeroacoustic source of one, two and three-cavity configurations. The standing wave method (SWM) is adopted in the current experimental work as an efficient and simple method to accurately measure the source generated by the cavity configurations. The trends observed for the source are compared with the characteristics of the self-excited resonance of similar multiple cavity configurations. The measured source is eventually utilized in a semi-empirical model to predict the self-excited oscillations amplitude. The resonance occurs at the conditions where the power generated by the multiple cavity section, based on the measured aeroacoustic source, counterbalances the system acoustic losses, modelled from basic principles.

The second phase of the research project studies the effect of the plateau separation distance between neighbouring cavities on the global value of the

generated source. The spacing ratio is a new geometrical parameter distinctive to multiple cavity configurations that was fundamentally absent in the single cavity rich literature. The spacing ratio is varied across a practical range and the corresponding aeroacoustic source is measured using the SWM for both two and three-cavity configurations. The cases with enhanced acoustic power generation, i.e. constructive hydrodynamic interference, are further investigated by visualizing the flow field using PIV. A comparison is held between the global source measured by the SWM and that obtained by summing up the individual cavity sources computed from the PIV data.

The third phase of the project assesses the development of the source over an extended number of multiple cavities and whether fully developed conditions would eventually be attained after a certain number of entrance cavities. The asymptotically persistent source contribution of the downstream cavities can be representative of a general cavity within a long corrugated pipe and defines a building unit cavity source. This is an essential concept to link the lab measured source of a relatively compact multiple cavity configuration to a corrugated pipe that extends for several kilometers. The building unit cavity source is compared with that of the ninth cavity in a twelve-cavity configuration extracted using PIV technique. Finally, a semi-empirical model is developed based on the building unit source. The model performance is then assessed through resonance amplitude prediction of a twelve-cavity configuration.

6.2 Conclusions

- The aeroacoustic source of multiple cavity configurations non-linearly increases with the number of cavities.
  - The non-linearity indicates the presence of a hydrodynamic coupling between the neighbouring cavities.
  - The general source trends fairly agree with the self-excited oscillations amplitude of corresponding multiple cavity configurations.
- The collapse of the lock-in ranges of multiple cavity configurations backs up using the cavity length as the proper length scale for the Strouhal number.
- A semi-empirical model, based on the measured source values, successfully predicts the self-excited oscillation amplitude of a piping system housing multiple cavity configurations.
  - This is a step to broaden the applicability of the lab measured source to industrial systems with different geometries and boundary conditions.
  - The model fairly predicts the pulsations amplitude with a maximum deviation of 17% for the tested one, two and three-cavity configurations.
- Including the absorption losses at the cavity edges is crucial for accurate amplitude prediction indicating the absence of edge losses in the cavity source determined by the SWM.
- The separation distance substantially affects the hydrodynamic coupling between neighbouring cavities.

- At low and intermediate excitation levels, extremum spacing ratios of 0.5 and 1.375 are associated with strong source values indicating constructive interference conditions. The source of the two-cavity configurations exceeds double that of the single cavity, while the source of the three-cavity configurations exceeds triple that of the single one.
- At high excitation levels the source slightly but consistently decreases with increasing the spacing ratio.
- The consistent constructive interference spacing ratios reflect favourable conditions where each cavity enhances the oscillations of the downstream neighbouring cavity. This is backed up by analysis of the convection speeds of disturbances in the pipe spacing and along the cavity shear layer.
- The destructive interference spacing ratio is a function of the number of cavities indicating a more complicated mechanism.

- Flow visualization of constructive interference cases shows strong vorticity at each of the cavities with obvious synchronization between the coherent structures throughout the acoustic cycle.
- The spatial source distribution in each of the cavities is characterized with two sources near the cavity edges with a sink in the middle and another small sink underneath the upstream corner resembling that reported for a single cavity.
- The most downstream cavity contributes the largest share of the total source at low excitation levels. This trend is reversed for high excitation levels.

- The summation of the individual cavity sources, based on the PIV data and applying Howe's analogy, is in a good agreement with the global SWM source.
- The cavity source contribution reaches asymptotically a constant value starting from the fourth cavity, at the investigated spacing ratio of half, with a consistent Strouhal number corresponding to the peak source. Such a persistent source contribution defines a building unit cavity source.
  - The building unit cavity source is function of the acoustic excitation level.
- The building unit cavity source agrees well with the ninth cavity source in a twelve-cavity configuration extracted using the PIV technique.
- A model, based on the building unit cavity source, fairly predicts the oscillation amplitude of a twelve-cavity configuration with a good agreement regarding the Strouhal number corresponding to the peak amplitude.
  - This validates the model and consequently the building unit source which is the basis for it.

6.3 Novel Research Contributions

A list of the novel contributions which the present research has added to the current state of knowledge, regarding the sound generation by flow over multiple shallow cavities, can be summarized in the following:

1. A semi-empirical model has been developed which successfully predicts the amplitude of self-excited oscillations of piping systems housing multiple

cavities utilizing the measured source. Moreover, the model demonstrates the importance of considering the absorption losses at the cavity edges.

2. The spacing ratios between consecutive cavities corresponding to constructive hydrodynamic interference have been indicated showing its consistency regardless the number of encountered cavities. On the other hand, the destructive interference spacing ratio is found to be dependent on the number of cavities reflecting a more complicated interaction mechanism.

3. The effect of the acoustic excitation level on the hydrodynamic interaction between neighbouring cavities has been revealed.

4. Different hydrodynamic interaction patterns have been analytically interpreted based on the convection speeds of disturbances in the pipe spacing and along the cavity shear layer.

5. Flow visualization of constructive interference conditions has been performed showing strong, highly synchronized, vortical structures in each of the investigated cavities. Moreover, the source distribution and each cavity contribution to the total of the source have been revealed. Good agreement is achieved between both measurement methodologies of the SWM and Howe's analogy based on the PIV data.

6. The number of entrance cavities after which the source of subsequent cavities achieves fully developed conditions has been indicated defining the building

unit cavity source. This building unit source is further validated via fair agreement with the PIV measured source of a general cavity in a long multiple cavity section.

7. A model, based on the building unit cavity source, has been developed which is capable of accurately predicting the oscillations amplitude of a piping system housing a long multiple cavity section. This validates the building unit source concept, which can be further developed to predict the response of corrugated pipes.

6.4 Recommendations for Future Work

The current research work improved our level of understanding of the hydrodynamic coupling between consecutive multiple cavities and the associated sound generation as a model for long corrugated pipes. It sheds some light on the development of the source until achieving the fully developed conditions. Also, prediction models are developed, which utilize the measured sources during the investigation, to accurately estimate the oscillations amplitude of different multiple cavity configurations. However, there are still some areas for suggested future work which would have a potential contribution and can be summarized in the following topics:

- Developing a prediction model that combines the single cavity source trends for different cavity geometrical parameters (e.g. cavity volume, length to

depth ratio), previously reported in the literature, with the separation distance analysis accomplished in the current investigation. Such a model should be capable of predicting the self-excited oscillations amplitude for multiple cavity configurations whose source have not been experimentally measured.

- Testing the effect of the separation distance ratio on the number of entrance cavities to achieve fully developed source conditions which have been measured in the current investigation.

- Investigating different practical countermeasures to alleviate the pulsations amplitude in corrugated pipes relying on our enhanced understanding of the phenomenon.

- Applying the standing wave method on more complex structures with complicated geometries. The method is based on black box analysis of compact aeroacoustic sources without simplifying the tested configurations. Actual gate and control valves are good candidates as they are characterized with complex geometries while being extensively used pipe fittings.

REFERENCES

Aly, K. and Ziada, S., 2010. Flow-excited resonance of trapped modes of ducted shallow cavities. *Journal of Fluids and Structures*, 26 (1), 92–120.

Amielh, M., Anselmet, F., Jiang, Y., Kristiansen, U., Mattei, P., Mazzoni, D., and Pinhède, C., 2014. Aeroacoustic source analysis in a corrugated flow pipe using low-frequency mitigation. *Journal of Turbulence*, 15 (10), 650–676.

Belfroid, S., Korst, H., Nielsen, K., and Bendiksen, E., 2011. Application of a new carcass design for prevention of singing behaviour in flexible risers. *In*: *Pressure Vessels and Piping Conference*. ASME, 319–327.

Belfroid, S., Shatto, D., and Peters, M., 2007. Flow induced pulsations caused by corrugated tubes. *In*: *Pressure Vessels and Piping Conference*. ASME, 439–447.

Bolduc, M., Ziada, S., and Lafon, P., 2016. Flow-Excited Acoustic Resonance of Trapped Modes of a Ducted Rectangular Cavity. *Journal of Pressure Vessel Technology*, 138 (3), 31303.

Bruggeman, J., Hirschberg, A., Van Dongen, M., Wijnands, A., and Gorter, J., 1991. Self-sustained aero-acoustic pulsations in gas transport systems: experimental study of the influence of closed side branches. *Journal of Sound and Vibration*, 150 (3), 371–393.

Coleman, H. and Steele, W., 2009. *Experimentation, validation, and uncertainty analysis for engineers*. Third edition. John Wiley & Sons.

Coltman, J., 1968. Sounding mechanism of the flute and organ pipe. *The Journal of the Acoustical Society of America*, 44 (4), 983–992.

Davies, P., 1981. Flow-acoustic coupling in ducts. *Journal of Sound and Vibration*, 77 (2), 191–209.

DeBoo, G., Ramsden, K., Gesior, R., and Strub, B., 2007. Identification of Quad Cities main steam line acoustic sources and vibration reduction. *In*: *Pressure Vessels and Piping Conference*. ASME, 485–4891.

Dequand, S., Hulshoff, S., and Hirschberg, A., 2003. Self-sustained oscillations in a closed side branch system. *Journal of Sound and Vibration*, 265 (2), 359–386.

Finnegan, S., Meskell, C., and Ziada, S., 2010. Experimental investigation of the acoustic power around two tandem cylinders. *Journal of Pressure Vessel Technology*, 132 (4), 41306.

Freymuth, P., 1966. On transition in a separated laminar boundary layer. *Journal*

of Fluid Mechanics, 25 (4), 683–704.

Golliard, J., Belfroid, S., Diez, N., Bendiksen, E., and Frimodt, C., 2013. On the whistling of corrugated pipes with narrow cavities. *In*: *Pressure Vessels and Piping Conference*. ASME, PVP2013-97340.

Golliard, J., Belfroid, S., Vijlbrief, O., and Lunde, K., 2015. Direct measurements of acoustic damping and sound amplification in corrugated pipes with flow. *In*: *Pressure Vessels and Piping Conference*. ASME, PVP2015-45494.

Golliard, J., González-Díez, N., Belfroid, S., Nakiboğlu, G., and Hirschberg, A., 2013. U-RANS model for the prediction of the acoustic sound power generated in a whistling corrugated pipe. *In*: *Pressure Vessels and Piping Conference*. ASME, PVP2013-97385.

Graf, H. and Ziada, S., 1992. Flow induced acoustic resonance in closed side branches: an experimental determination of the excitation source. *In*: *International Symposium on Flow-Induced Vibration and Noise*. ASME, 63.

Graf, H. and Ziada, S., 2010. Excitation source of a side-branch shear layer. *Journal of Sound and Vibration*, 329 (14), 2825–2842.

Harrington, M. and Dunham, W., 1960. Studies of the Mechanism for the Flow-Induced Cavity Resonance. *The Journal of the Acoustical Society of America*, 32 (7), 921.

Howe, M., 1980. The dissipation of sound at an edge. *Journal of Sound and Vibration*, 70 (3), 407–411.

Kriesels, P., Peters, M., Hirschberg, A., Wijnands, A., Iafrati, A., Riccardi, G., Piva, R., and Bruggeman, J., 1995. High amplitude vortex-induced pulsations in a gas transport system. *Journal of Sound and Vibration*, 184 (2), 343–368.

Lafon, P., Caillaud, S., Devos, J., and Lambert, C., 2003. Aeroacoustical coupling in a ducted shallow cavity and fluid/structure effects on a steam line. *Journal of Fluids and structures*, 18 (6), 695–713.

Melling, A., 1997. Tracer particles and seeding for particle image velocimetry. *Measurement Science and Technology*, 8 (12), 1406–1416.

Michalke, A., 1965. On spatially growing disturbances in an inviscid shear layer. *Journal of Fluid Mechanics*, 23 (3), 521–544.

Michaud, S., Ziada, S., and Pastorel, H., 2001. Acoustic fatigue of a steam dump pipe system excited by valve noise. *Journal of Pressure Vessel Technology*, 123 (4), 461–468.

Miksad, R., 1972. Experiments on the nonlinear stages of free-shear-layer transition. *Journal of Fluid Mechanics*, 56 (4), 695–719.

Mohamed, S., 2015. Sound waves excitation by flow in a pipe housing a shallow cavity. PhD Thesis, McMaster University.

Mohamed, S., Graf, H., and Ziada, S., 2018. Measurement of the Excitation Source of an Axisymmetric Shallow Cavity Shear Layer. *Journal of Pressure Vessel Technology*, doi: 10.1115/1.4039781.

Mohamed, S. and Ziada, S., 2014. PIV Measurements of Aeroacoustic Sources of a Shallow Cavity in a Pipeline. *In*: *Pressure Vessels and Piping Conference*. ASME, PVP2014-28508.

Mohamed, S. and Ziada, S., 2015. Effect of Cavity Volume on the Flow-Excited Acoustic Resonance of a Shallow Cavity in a Pipe-Line. *In*: *Pressure Vessels and Piping Conference*. ASME, PVP2015-45205.

Nair, K. and Sarkar, S., 2016. Large Eddy Simulation of Self-Sustained Cavity Oscillation for Subsonic and Supersonic Flows. *Journal of Fluids Engineering*, 139 (1), 11102.

Nakiboglu, G., Belfroid, S., Golliard, J., and Hirschberg, A., 2011. On the whistling of corrugated pipes: effect of pipe length and flow profile. *Journal of Fluid Mechanics*, 672, 78–108.

Nakiboglu, G., Belfroid, S., Willems, J., and Hirschberg, A., 2010. Whistling behavior of periodic systems: Corrugated pipes and multiple side branch system. *International Journal of Mechanical Sciences*, 52 (11), 1458–1470.

Nakiboglu, G. and Hirschberg, A., 2012. Aeroacoustic power generated by multiple compact axisymmetric cavities: Effect of hydrodynamic interference on the sound production. *Physics of Fluids*, 24 (6), 67101.

Nakiboglu, G., Rudenko, O., and Hirschberg, A., 2013. Hydrodynamic interference in corrugated pipes. *In*: *ICSV 20*. 865–872.

Nakiboglu, G., Manders, H., and Hirschberg, A., 2012. Aeroacoustic power generated by a compact axisymmetric cavity: prediction of self-sustained oscillation and influence of the depth. *Journal of Fluid Mechanics*, 703, 163–191.

Nelson, P., Halliwell, N., and Doak, P., 1983. Fluid dynamics of a flow excited resonance, Part II: Flow acoustic interaction. *Journal of Sound and Vibration*, 91 (3), 375–402.

NRC, 2002. Failure of Steam Dryer Cover Plate After a Recent Power Uprate. NRC Information Notice 2002-26, US Nuclear Regulatory Commission, Washington, D.C.

Oshkai, P. and Yan, T., 2008. Experimental investigation of coaxial side branch resonators. *Journal of Fluids and Structures*, 24 (4), 589–603.

Petrie, A. and Huntley, I., 1980. The acoustic output produced by a steady airflow through a corrugated duct. *Journal of Sound and Vibration*, 70 (1), 1–9.

Popiel, C., Kozak, M., Małecka, J., and Michalak, A., 2013. Friction Factor for Transient Flow in Transverse Corrugated Pipes. *Journal of Fluids Engineering*, 135 (7), 74501.

Radavich, P., Selamet, A., and Novak, J., 2001. A computational approach for flow–acoustic coupling in closed side branches. *The Journal of the Acoustical Society of America*, 109 (4), 1343–1353.

Raffel, M., Willert, C., Wereley, S., and Kompenhans, J., 2007. *Particle image velocimetry: a practical guide*. Second. Springer.

Rajavel, B. and Prasad, M., 2014. Parametric studies on acoustics of corrugated tubes using large eddy simulation (LES). *Noise Control Engineering Journal*, 62 (4), 218–231.

Rayleigh, Lord, 1879. On the instability of jets. *In*: *Proc. London Math. Soc 10*. 4–13.

Rockwell, D., 1977. Prediction of Oscillation Frequencies for Unstable Flow Past Cavities. *Journal of Fluids Engineering*, 99 (2), 294–299.

Rockwell, D., 1983. Oscillations of impinging shear layers. *AIAA Journal*, 21 (5), 645–664.

Rockwell, D. and Naudascher, E., 1978. Review—self-sustaining oscillations of flow past cavities. *Journal of Fluids Engineering*, 100 (2), 152–165.

Rockwell, D. and Schachenmann, A., 1982. The organized shear layer due to oscillations of a turbulent jet through an axisymmetric cavity. *Journal of Sound and Vibration*, 85 (3), 371–382.

Scarano, F. and Riethmuller, M., 2000. Advances in iterative multigrid PIV image processing. *Experiments in Fluids*, 29, S051–S060.

Stel, H., Morales, R., Franco, A., Junqueira, S., Erthal, R., and Gonçalves, M., 2010. Numerical and Experimental Analysis of Turbulent Flow in Corrugated Pipes. *Journal of Fluids Engineering*, 132 (7), 71203.

Tam, C. and Block, P., 1978. On the tones and pressure oscillations induced by flow over rectangular cavities. *Journal of Fluid Mechanics*, 89 (2), 373–399.

Tropea, C., Yarin, A., and Foss, J., eds., 2007. *Springer Handbook of Experimental Fluid Mechanics*. First edition. Berlin, Heidelberg: Springer.

Williams, J. and Hawkings, D., 1969. Sound generation by turbulence and surfaces in arbitrary motion. *Philosophical Transactions of the Royal Society of London A: Mathematical, Physical and Engineering Sciences*, 264 (1151), 321–342.

Ziada, S., 1994. A flow visualization study of flow-acoustic coupling at the mouth of a resonant side-branch. *Journal of Fluids and Structures*, 8 (4), 391–416.

Ziada, S., Bühlmann, E., and Bolleter, U., 1989. Flow impingement as an excitation source in control valves. *Journal of Fluids and structures*, 3 (5), 529–549.

Ziada, S. and Lafon, P., 2014. Flow-Excited Acoustic Resonance Excitation Mechanism, Design Guidelines, and Counter Measures. *Applied Mechanics Reviews*, 66 (1), 10802.

Ziada, S. and Shine, S., 1999. Strouhal numbers of flow-excited acoustic resonance of closed side branches. *Journal of Fluids and Structures*, 13 (1), 127–142.

APPENDIX A
SWM UNCERTAINTY ANALYSIS

Uncertainty analysis is done on the different acoustic measurements encountered in this investigation using the SWM. First, the basic uncertainties of the measurement equipment which are used is presented and then the propagation of these uncertainties towards the final measured quantities is discussed in details. G.R.A.S. 40BP microphones are characterized by acoustic pressure measurement uncertainty ($\delta p/p$) of 0.7%. Frequency resolution uncertainty ($\delta f/f$) is 0.25%. Temperature sensor uncertainty ($\delta T/T$) is 0.33%. The uncertainty in the Validyne differential pressure transducer ($\delta P/P$) is 0.25%. The cavities dimensions are machined with uncertainty ($\delta L/L$) of 0.24%.

The propagation of these uncertainties towards the final quantities is calculated using Kline McClintock approach (Coleman and Steele, 2009). The error in a single experiment can be computed using the first order Taylor series expansion and the uncertainty can be optimally expressed as the root mean square of error components. The general mathematical formula can be expressed as follows:

$$Y = fn\,(X_1, X_2, \ldots., X_i, \ldots., X_n), i = 1{:}n \tag{A.1}$$

$$\delta Y = \left[\sum_{i=1}^{n}\left(\frac{\partial Y}{\partial X_i}\,\delta X_i\right)^2\right]^{1/2} \tag{A.2}$$

Therefore, the uncertainty of the flow velocity ($\delta U/U$) is 0.125%, the speed of sound is ($\delta c/c$) 0.17%, the dimensionless acoustic velocity amplitude ($\delta[v/U]/[v/U]$) is 0.73% and the uncertainty of Strouhal number ($\delta St/St$) is 0.37%. The uncertainty of the differential acoustic pressure across the test section ($\delta\Delta p/\Delta p$) is calculated, for the three-cavity configuration at an intermediate excitation level of 0.032 and Strouhal number of 0.6, having a value of 1.9%. Finally, the uncertainty propagated towards the real aeroacoustic source ($\delta S/S$) is evaluated to be 2%.

$$U = \sqrt{\frac{2P}{\rho}} \longrightarrow \frac{\delta U}{U} = \frac{1}{U}\sqrt{\left(\sqrt{\frac{2}{\rho}}\,\frac{1}{2\sqrt{P}}\,\delta P\right)^2} = \frac{1}{2}\,\frac{\delta P}{P} = 0.125\% \quad \text{(A.3)}$$

$$c = \sqrt{\gamma\, R\, T} \longrightarrow \frac{\delta c}{c} = \frac{1}{2}\,\frac{\delta T}{T} = 0.17\% \quad \text{(A.4)}$$

If, $Y = \frac{X_1 X_2}{X_3}$

$$\therefore \frac{\delta Y}{Y} = \frac{1}{Y}\sqrt{\left(\frac{X_2}{X_3}\delta X_1\right)^2 + \left(\frac{X_1}{X_3}\delta X_2\right)^2 + (X_1 X_2 \delta X_3)^2} = \sqrt{\left(\frac{\delta X_1}{X_1}\right)^2 + \left(\frac{\delta X_2}{X_2}\right)^2 + \left(\frac{\delta X_3}{X_3}\right)^2} \quad \text{(A.5)}$$

$$\frac{v}{U} = \frac{p}{\rho C U} \longrightarrow \delta[v/U]/[v/U] = \sqrt{\left(\frac{\delta p}{p}\right)^2 + \left(\frac{\delta c}{c}\right)^2 + \left(\frac{\delta U}{U}\right)^2} = 0.73\% \quad \text{(A.6)}$$

$$St = \frac{f\,L}{U} \longrightarrow \frac{\delta St}{St} = \sqrt{\left(\frac{\delta f}{f}\right)^2 + \left(\frac{\delta L}{L}\right)^2 + \left(\frac{\delta U}{U}\right)^2} = 0.37\% \quad \text{(A.7)}$$

$$S = \frac{\Delta p/(0.5\rho U^2)}{v/U} = \frac{2\,\Delta p}{\rho\, U\, v} \longrightarrow \frac{\delta S}{S} = \sqrt{\left(\frac{\delta \Delta p}{\Delta p}\right)^2 + \left(\frac{\delta U}{U}\right)^2 + \left(\frac{\delta v}{v}\right)^2} = 2\% \quad \text{(A.8)}$$

Applying the same methodology, the uncertainty is further investigated for more test conditions. The real aeroacoustic source term is plotted against different

Strouhal numbers for an intermediate excitation level of 0.02 in Figure A.1 for the three-cavity configuration including the corresponding error bars. The uncertainty at the peak source is found to be 1.4%, while the average uncertainty is about 4.2%. There is an expected trend of increasing uncertainty as the absolute value of the source decreases. Moreover, the peak source value is shown for different acoustic excitation levels in Figure A.2 with the corresponding uncertainty. The average uncertainty was 3.2% with the maximum value, at the highest acoustic velocity ratio, corresponding to the minimum source.

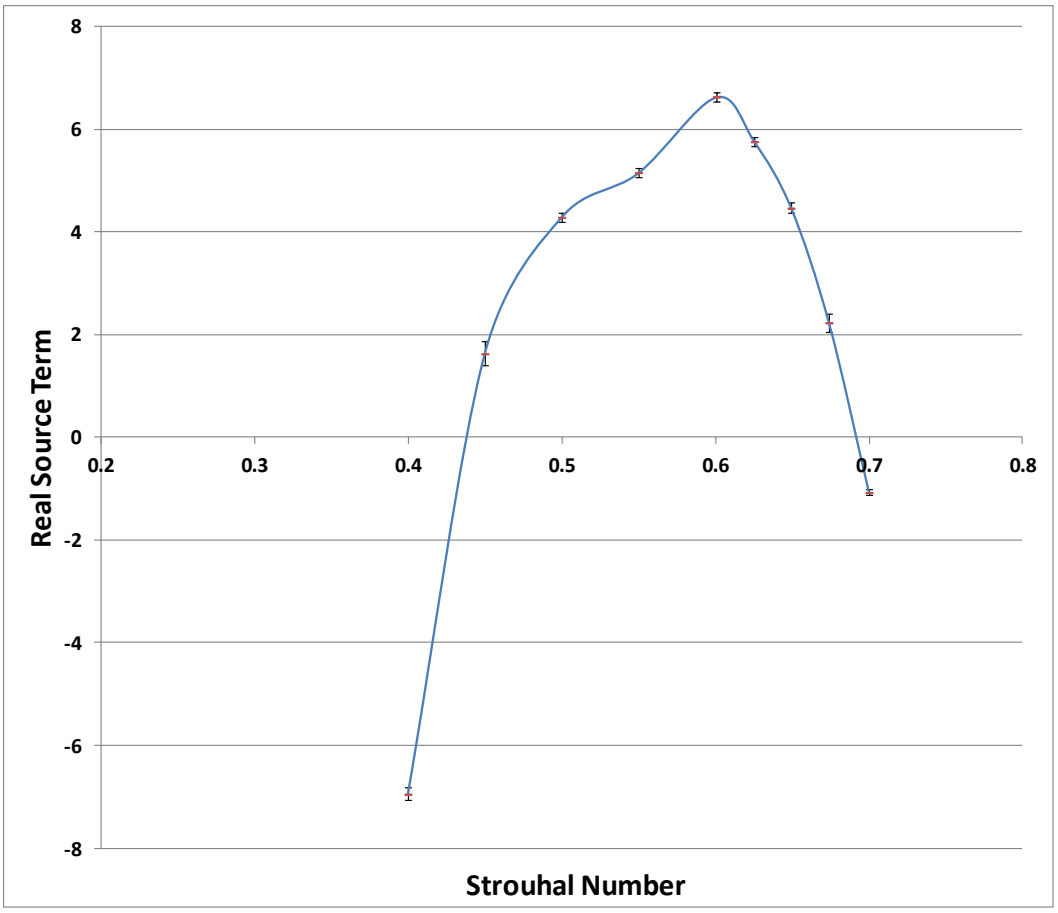

Figure A.1. Real source term vs. Strouhal number for the three-cavity configuration for an intermediate excitation level (v/U = 0.02) including the error bars

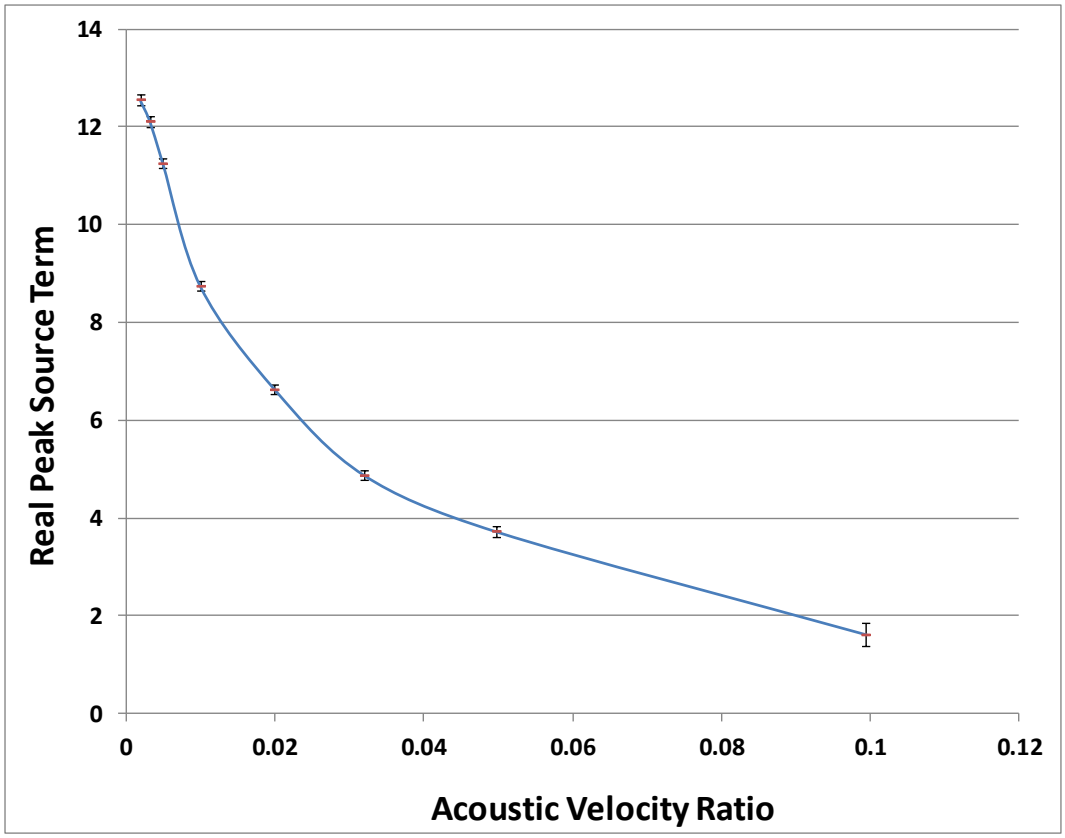

Figure A.2. Real peak source term vs. acoustic velocity ratio (*v/U*) for the three-cavity configuration showing the error bars

APPENDIX B
PIV UNCERTAINTY ANALYSIS

Tracking error is one of the common sources of uncertainty in the PIV flow visualization which reflects that the seeding particles do not perfectly follow the investigated flow field. The seeding particles, emitted by the used aerosol generator in the current study, are characterized with a small mean diameter of 1 μm. Such a small particle size results in a stokes number much smaller than 0.1 and consequently a tracking error of less that 1% (Melling, 1997; Tropea et al., 2007). Image processing of the PIV raw images to estimate the flow field parameters is also associated with uncertainty. The objective of this section is to quantify the associated uncertainty with the velocity and vorticity fields, measured using PIV, as a result of the image processing technique.

The vector processing scheme used in the current investigation is similar to the one adopted by Scarano and Riethmuller (2000). To quantify the uncertainty of the processing scheme, Scarano and Reithmuller used predefined raw images and compared the known input with the processed output flow field. In their investigation, a correlation is found between the velocity gradient values and the associated uncertainty for different sets of interrogation region sizes. The fine interrogation region size currently used is 16 × 16 pixels. A typical flow field for the visualized cavities in the separation distance analysis involves a maximum

streamwise velocity gradient $(\partial u/\partial y)_{max}$ of about 0.041 pixel/pixel at the shear layer near the upstream edge of the cavity. On the other hand, the maximum cross-stream velocity gradient $(\partial v/\partial x)_{max}$ is about 0.007 pixel/pixel. Based on Scarano and Reithmuller's correlations, the absolute uncertainty in the particle displacement for both the streamwise (ε_u) and cross-stream (ε_v) directions are estimated to be 0.015 and 0.005 pixels, respectively. Consequently, the uncertainty in the streamwise and cross-stream velocity components is less than 1% and 2%, respectively. The corresponding uncertainty in the velocity gradients is estimated based on equations (B.1) and (B.2). The factor "0.7" results from the central differencing technique employed while computing the velocity gradients (Raffel et al., 2007). The values of Δx and Δy are 8 pixels based on the analyzed velocity vector array. Eventually, the maximum uncertainty in the vorticity components is less than 4% and 6% for the streamwise and cross-stream directions, respectively. The summary of the uncertainty analysis is presented in Table B.1. Another uncertainty analysis is done for the visualized ninth cavity tested at a slightly different Strouhal number. However, the uncertainty percentages don't vary much being less than 4% and 7 % for the streamwise and cross-stream velocity gradients, respectively.

$$\varepsilon(\partial u/\partial y) = 0.7\ \frac{\varepsilon_u}{\Delta y} \tag{B.1}$$

$$\varepsilon(\partial v/\partial x) = 0.7\ \frac{\varepsilon_v}{\Delta x} \tag{B.2}$$

Table B.1. Summary of the uncertainty parameters for the PIV measured velocity and vorticity fields of a typical visualized cavity in the separation distance analysis

Maximum streamwise velocity gradient $(\partial u/\partial y)_{max}$	0.041 pixel/pixel
Maximum cross-stream velocity gradient $(\partial v/\partial x)_{max}$	0.007 pixel/pixel
Absolute uncertainty in streamwise displacement (ε_u)	0.015 pixels
Absolute uncertainty in cross-stream displacement (ε_v)	0.005 pixels
Relative uncertainty in streamwise velocity (ε_u/u)	0.4%
Relative uncertainty in cross-stream velocity (ε_v/v)	1.6%
Absolute uncertainty in streamwise gradient $(\varepsilon(\partial u/\partial y))$	1.31×10^{-3} pixel/pixel
Absolute uncertainty in cross-stream gradient $(\varepsilon(\partial v/\partial x))$	4.38×10^{-4} pixel/pixel
Relative uncertainty in streamwise gradient $(\varepsilon(\partial u/\partial y)/(\partial u/\partial y)_{max})$	3.2%
Relative uncertainty in cross-stream gradient $(\varepsilon(\partial v/\partial x)/(\partial v/\partial x)_{max})$	5.9%

APPENDIX C
Additional Measured Data

This section is dedicated to providing additional measured data supplementary to the results in chapters 3 – 5 presented in the sections C.1 – C.3, respectively.

C.1 Additional Data to Chapter (3)

The cavities investigated in this section are of 2″ length (L) and 1″ depth (H) with separation distance to cavity length ratio (L_p/L) of 1.0.

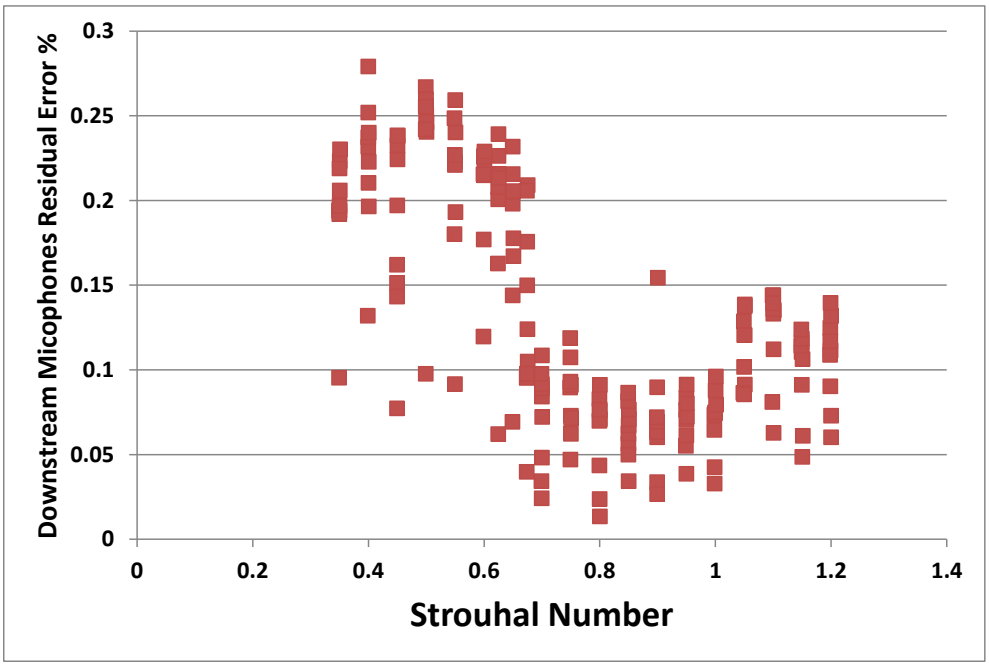

Figure C.1. The residual error percentage for downstream microphones at different Strouhal numbers for the three-cavity configuration. Data points at the same Strouhal number represent different excitation levels.

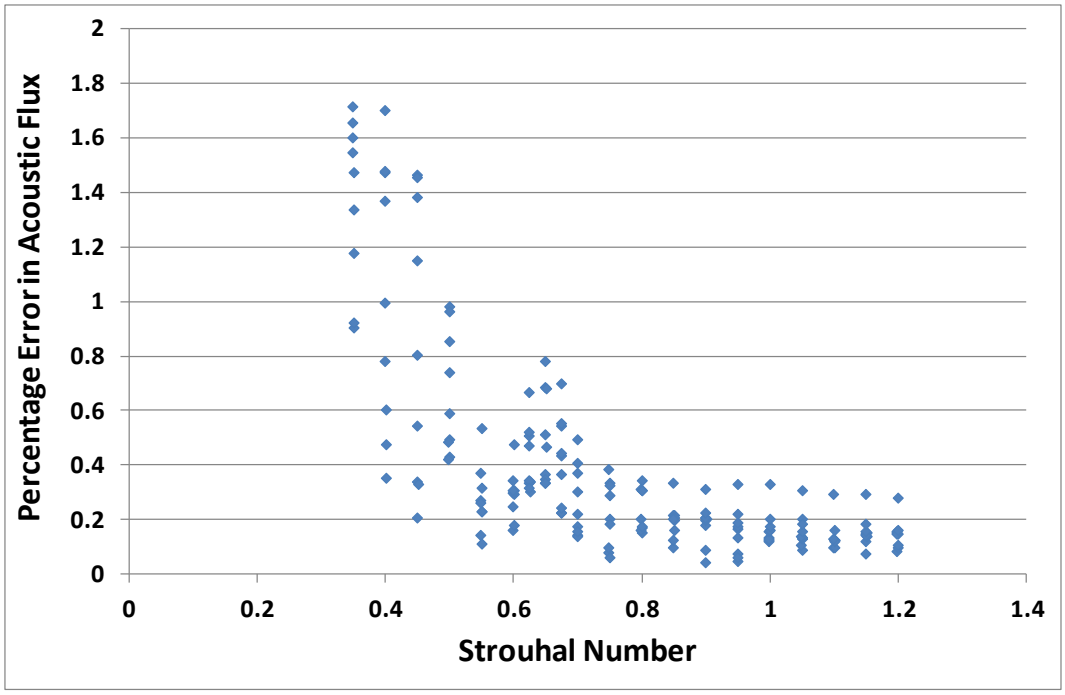

Figure C.2. The percentage error in the acoustic flux at the cavity center for different Strouhal numbers for the three-cavity configuration. Data points at the same Strouhal number represent different excitation levels.

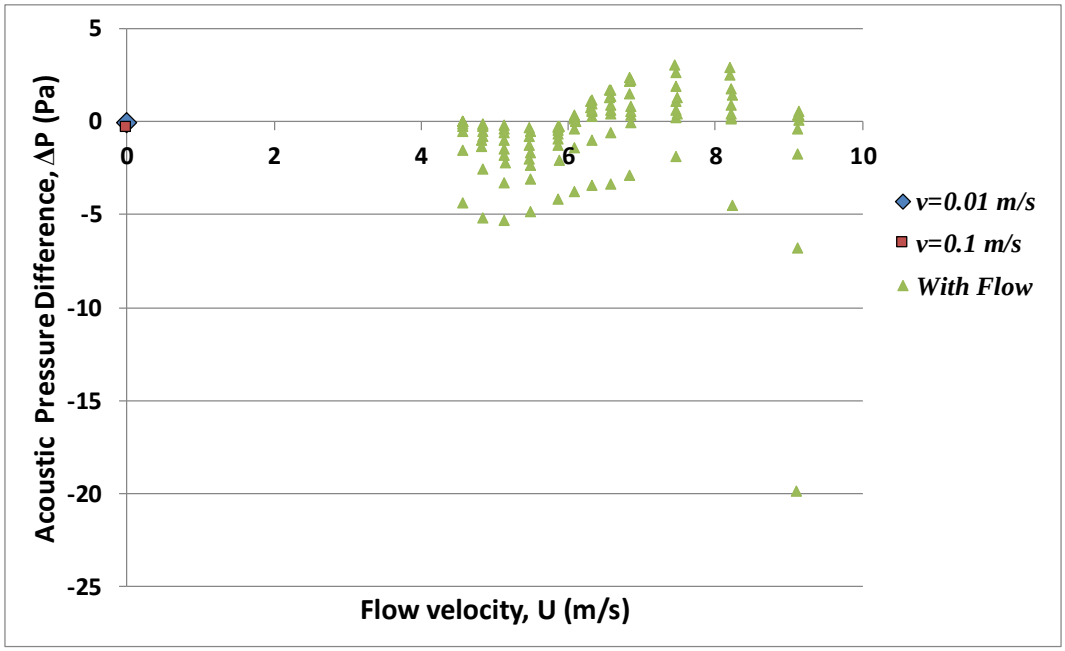

Figure C.3. Acoustic pressure difference across the three-cavity test section for different flow velocities including two no-flow cases. Data points at the same flow velocity represent different excitation levels.

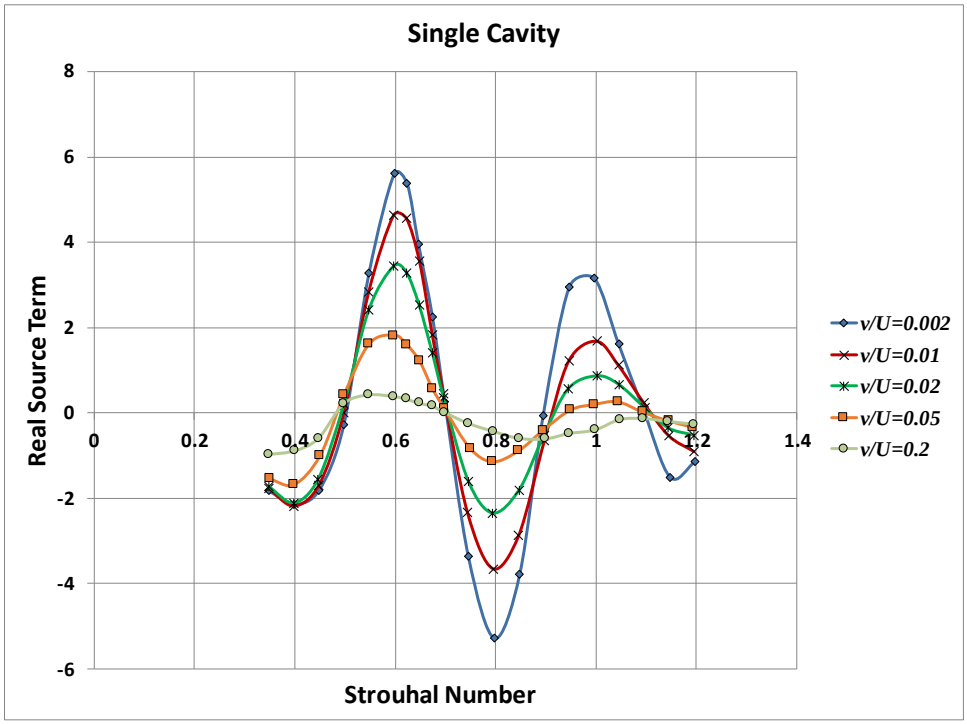

Figure C.4. Real source term vs. Strouhal number for different acoustic velocity ratios for the single cavity configuration

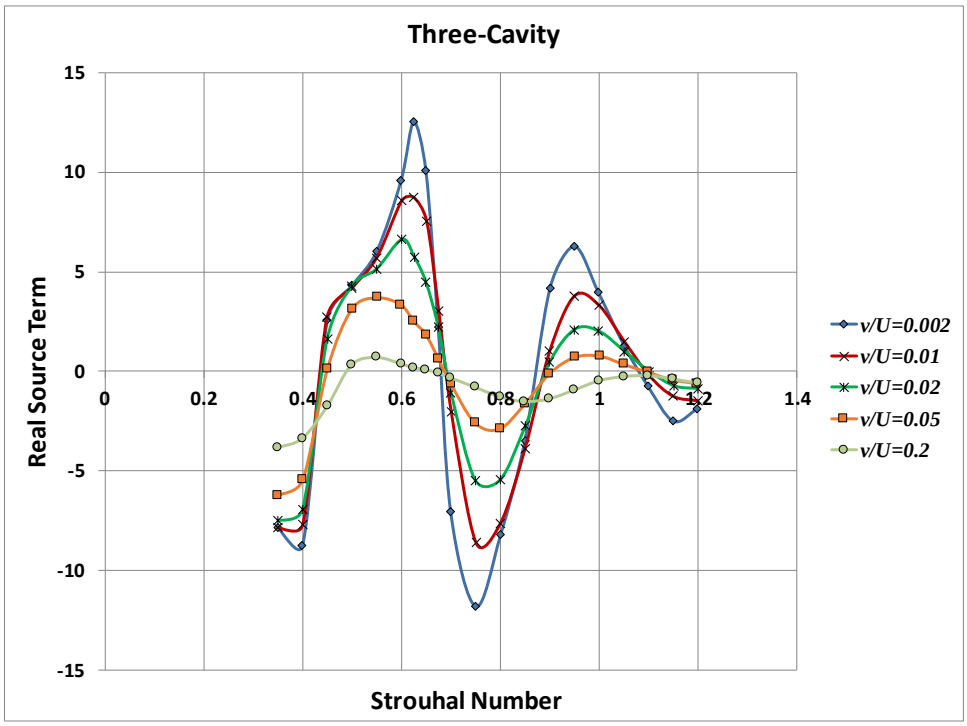

Figure C.5. Real source term vs. Strouhal number for different acoustic velocity ratios for the three-cavity configuration

C.1.1 Absorption Losses at the Cavity Edges

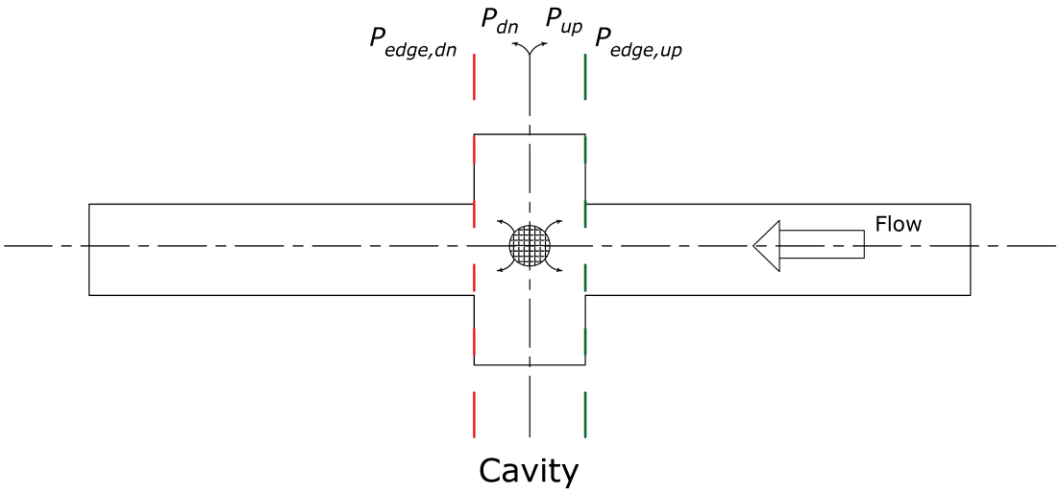

Figure C.6. Schematic of the acoustic pressure before and after the cavity for the SWM calculations

Figure C.6 aims at presenting the acoustic pressure parameters before and after the cavity that is involved in the SWM calculations. The target of this section is to show that the estimated cavity aeroacoustic source is an undamped source, i.e. does not account for the absorption losses at the cavity edges. Consequently, the absorption losses at cavity edges should be included in the prediction model to ensure accurate estimation of the pulsations amplitude. This is in contrast to other measurement techniques which rely on tracing a travelling acoustic wave and the changes occurring as it passes through the cavity section (e.g. Golliard et al., 2015). For these techniques, the measurements reflect all the sources and losses in the passage of the travelling wave. Thus, the measured source in that case is a damped one, i.e. includes the damping losses.

$P_{edge,up}$ and $P_{edge,dn}$ represents the acoustic pressure values at the cavity upstream and downstream edges, respectively, estimated from the corresponding acoustic standing wave measured using three microphones. P_{up} and P_{dn} represents the acoustic pressure values at the center line of the cavity section estimated from the upstream and downstream sides. The difference between P_{up} and P_{dn} gives the ΔP term which is used to calculate the source as previously shown by equation (3.1). The transfer of the real value of the acoustic pressure from the edges to the center line in the current experimental methodology only involved an extrapolation of the acoustic wave equation without accounting for the cavity absorption losses. However, accounting for these losses would yield $\Delta P'$ which should eventually be equal to ΔP, assuming symmetric losses at both edges, as shown by equations C.1 and C.2. Thus, the measured ΔP term is the same as the $\Delta P'$ that recovers the loss terms, i.e. the measured source is undamped. It may be argued that one edge is slightly more affected by absorption as compared to the other edge considering the direction of the flow. However, such effect is minimal, given the low Mach number flows encountered, and consequently is not considered in this discussion.

$$\Delta P = P_{up} - P_{dn} \tag{C.1}$$

$$\Delta P' = P_{up}{}' - P_{dn}{}' = (P_{up} + P_{absorp,loss}) - (P_{dn} + P_{absorp,loss})$$

$$= P_{up} - P_{dn} = \Delta P \tag{C.2}$$

C.2 Additional Data to Chapter (4)

The cavities investigated in this section are of 2″ length (L) and 1″ depth (H) with separation distance to cavity length ratio (L_p/L) varying from 0.5 to 1.375.

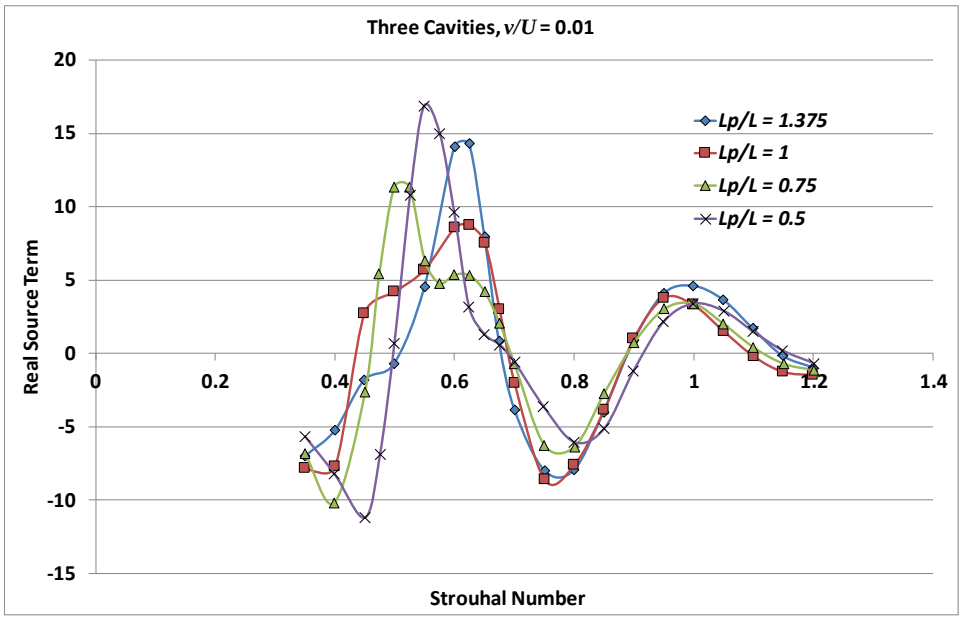

Figure C.7. Real source term vs. Strouhal number for different separation distances for the three-cavity case at v/U = 0.01

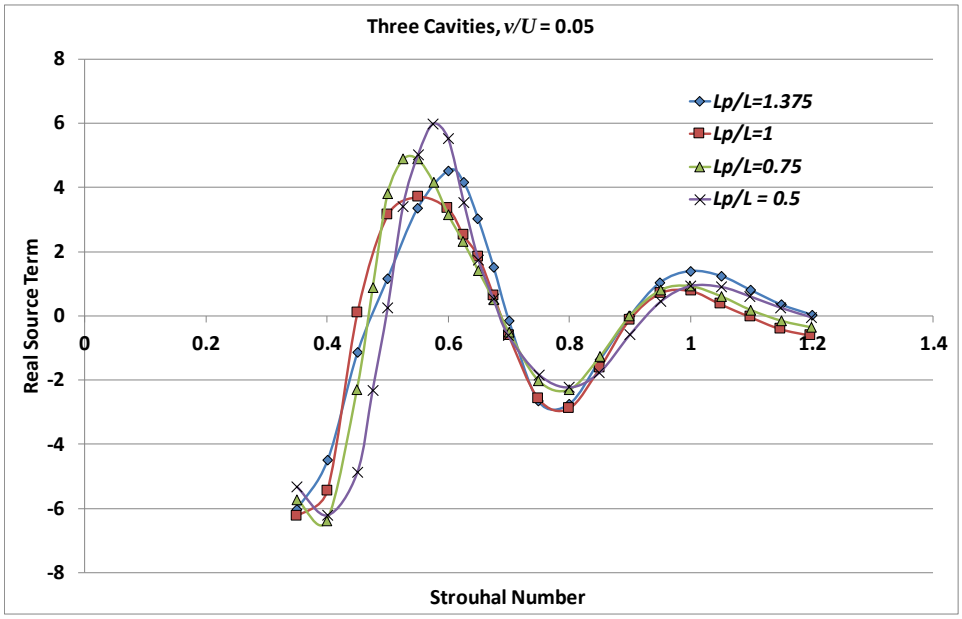

Figure C.8. Real source term vs. Strouhal number for different separation distances for the three-cavity case at v/U = 0.05

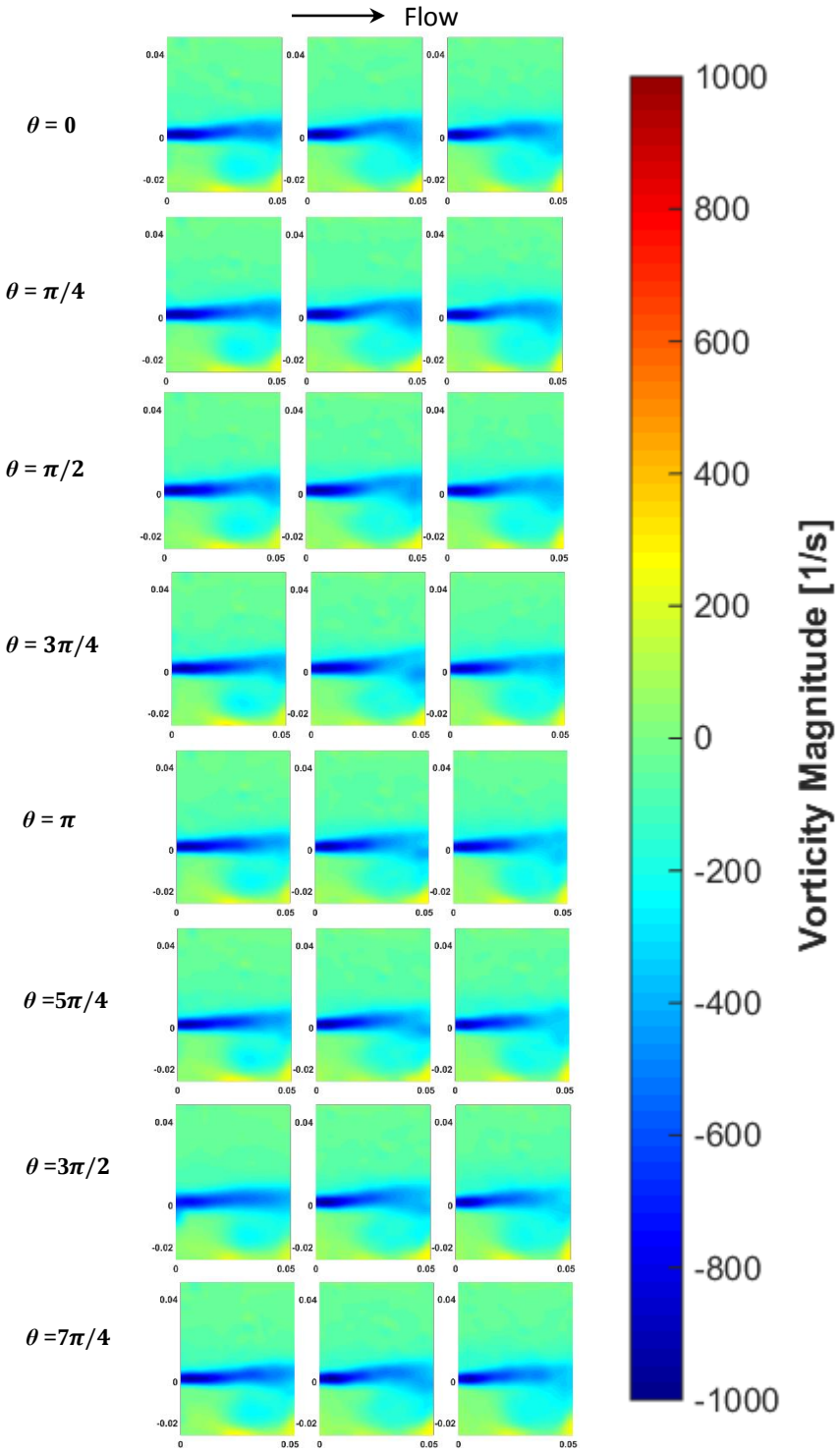

Figure C.9. Vorticity distribution for the flow over the three cavities at *v/U* = 0.002 over the eight points of the acoustic cycle

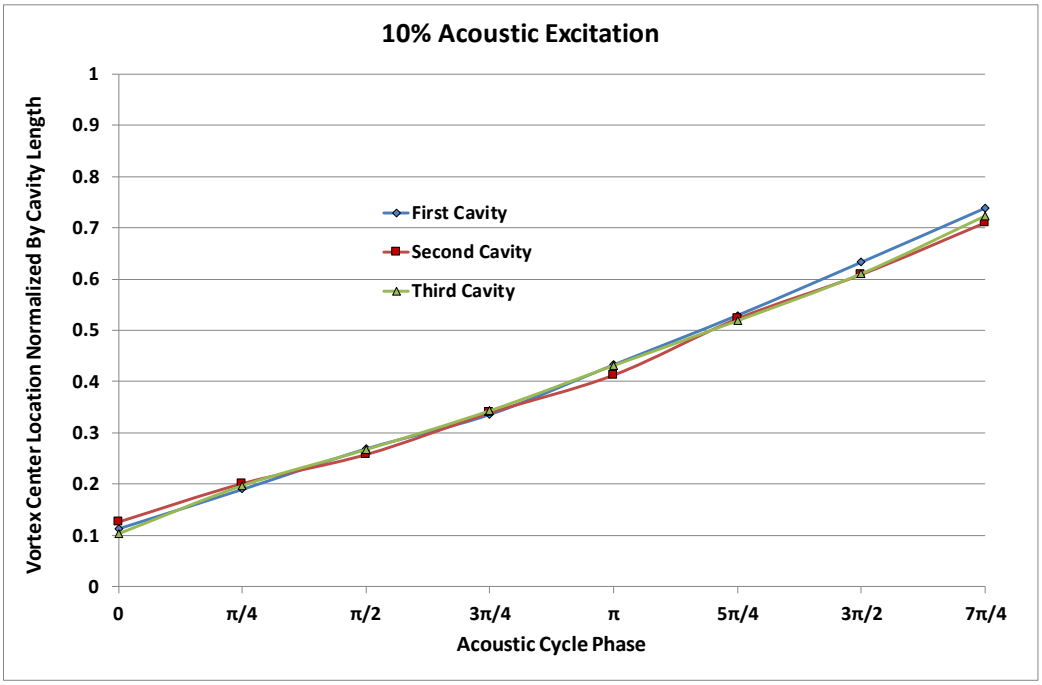

Figure C.10. Vortex center location normalized by cavity length for each of the three cavities over the eight points of the acoustic cycle at v/U = 0.1

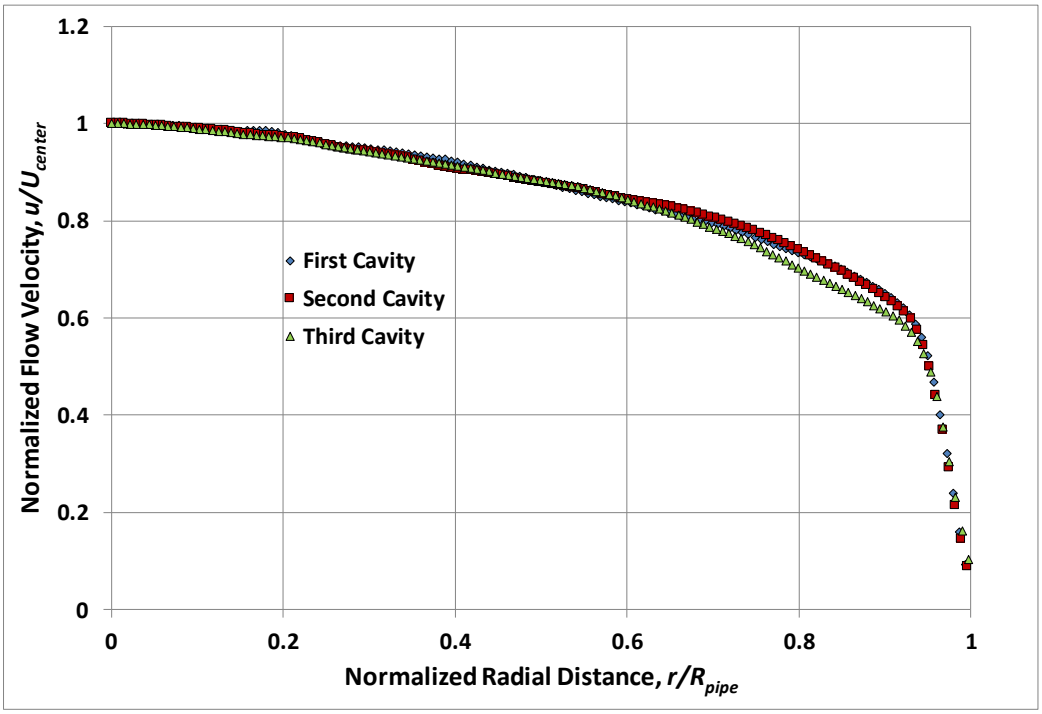

Figure C.11. Normalized velocity profile over the pipe radius at the cavity entrance for the first, second and third cavities for the low excitation level case

C.3 Additional Data to Chapter (5)

The cavities investigated in this section are of 2″ length (L) and 1″ depth (H) with separation distance to cavity length ratio (L_p/L) of 0.5.

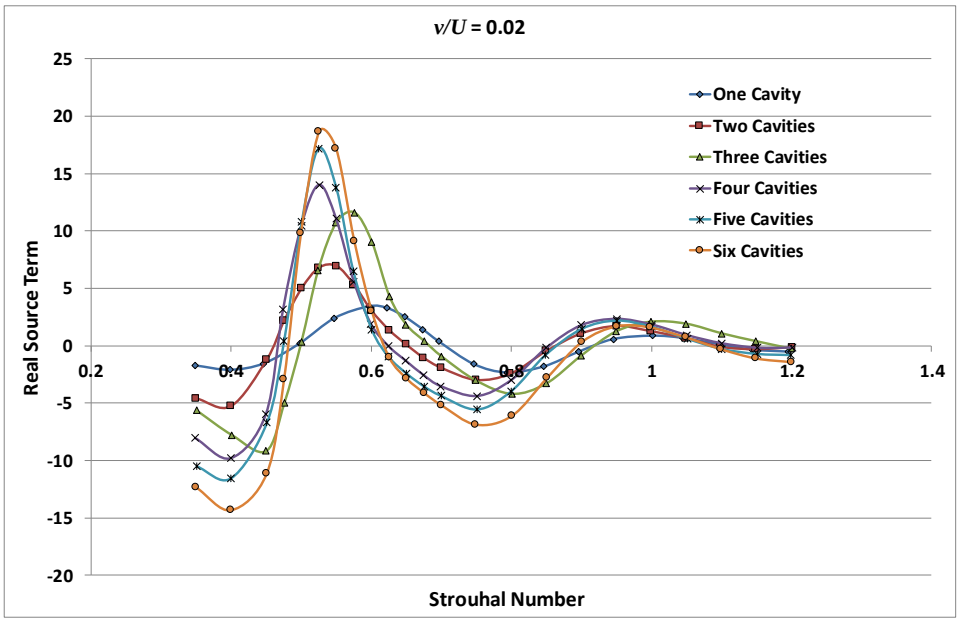

Figure C.12. Real source vs. Strouhal number for gradually increasing number of cavities with v/U = 0.02

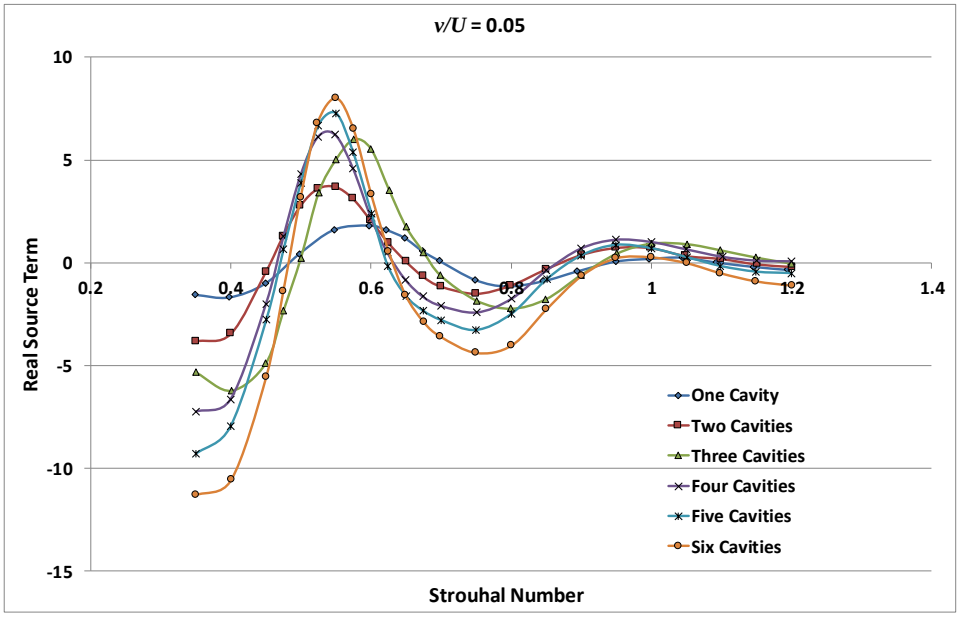

Figure C.13. Real source vs. Strouhal number for gradually increasing number of cavities with v/U = 0.05

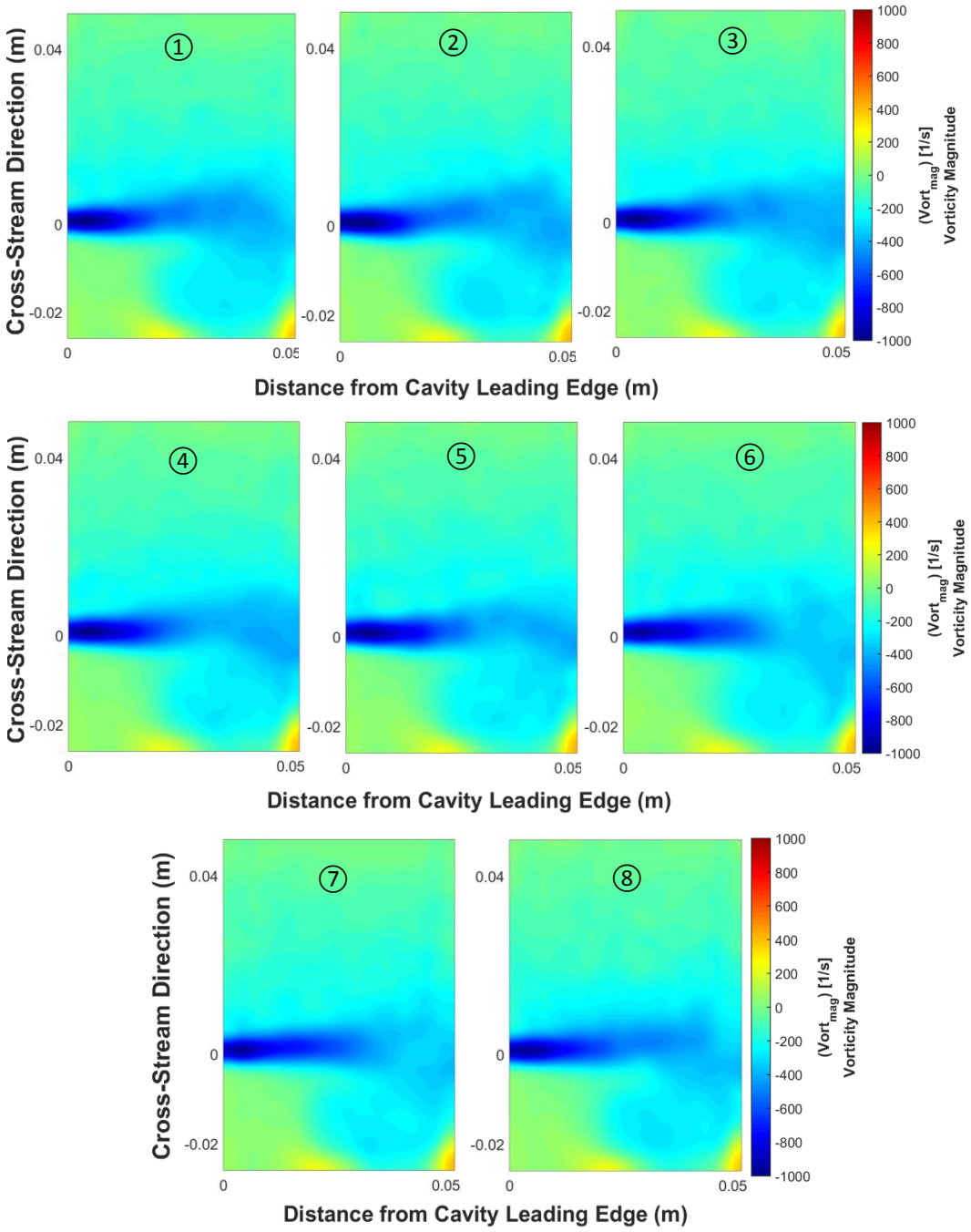

Figure C.14. Vorticity distribution for the flow over the ninth cavity for v/U = 0.005 over the eight points of the acoustic cycle with ① being at θ = 0

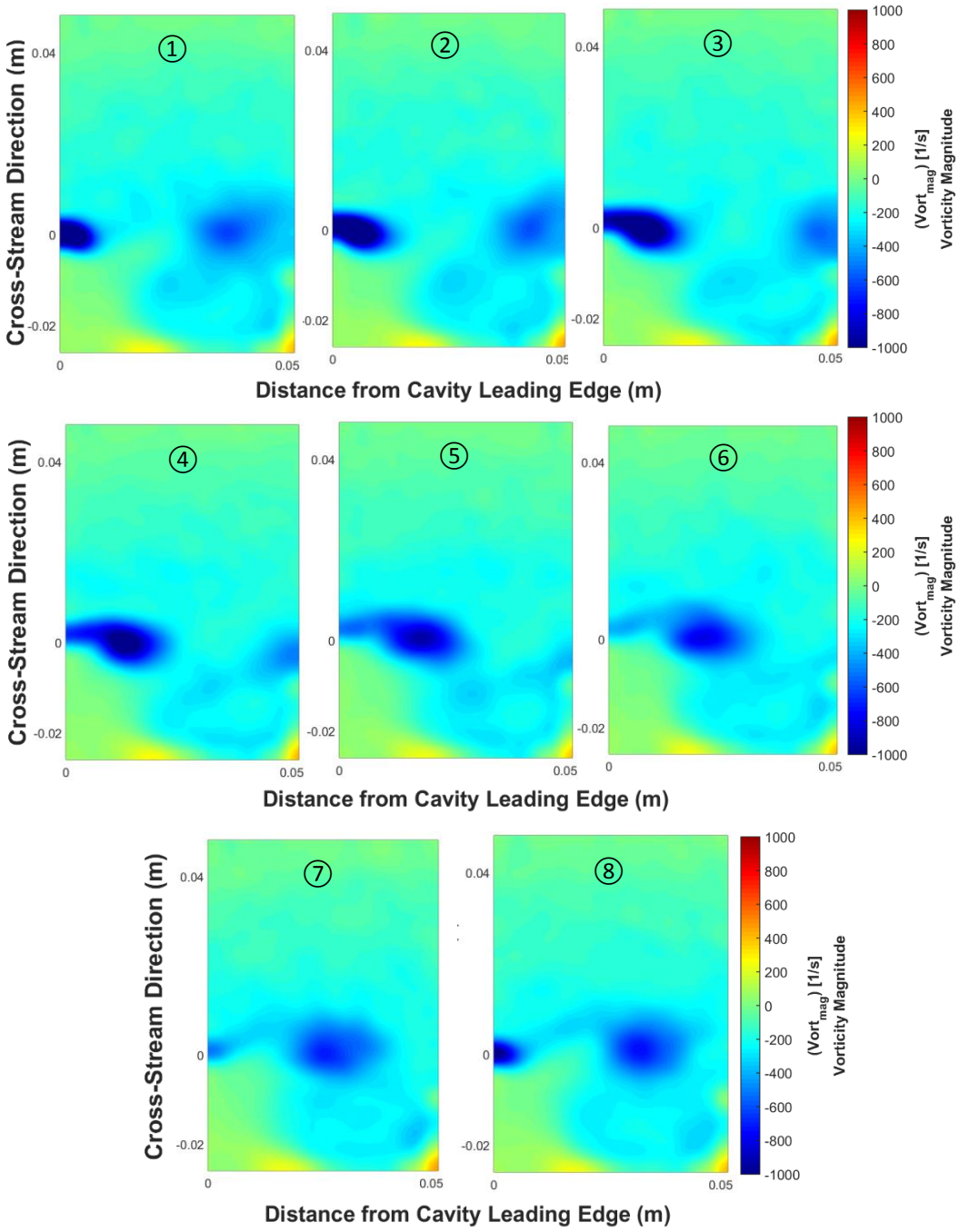

Figure C.15. Vorticity distribution for the flow over the ninth cavity for *v*/U = 0.1 over the eight points of the acoustic cycle with ① being at $\theta = 0$

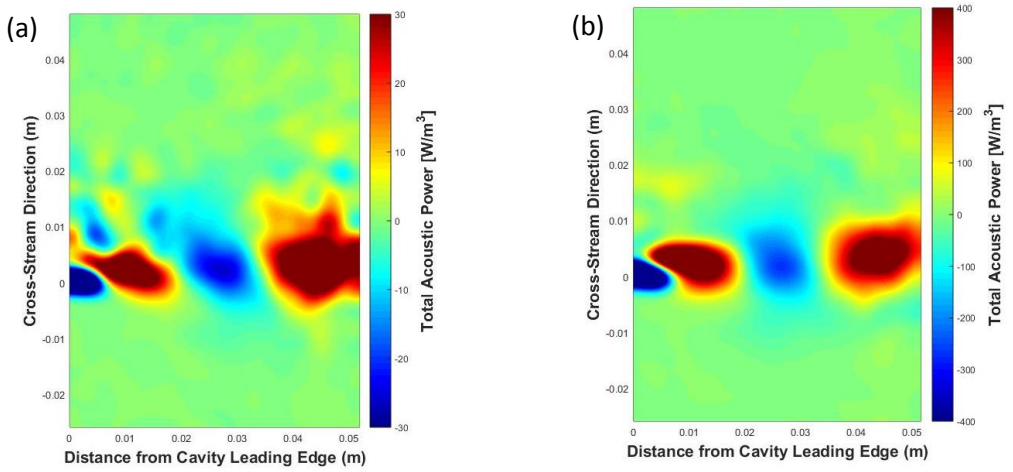

Figure C.16. Spatial distribution of the average acoustic power over the acoustic cycle for the ninth cavity at different excitation levels: (a) *v/U* = 0.01 and (b) *v/U* = 0.05

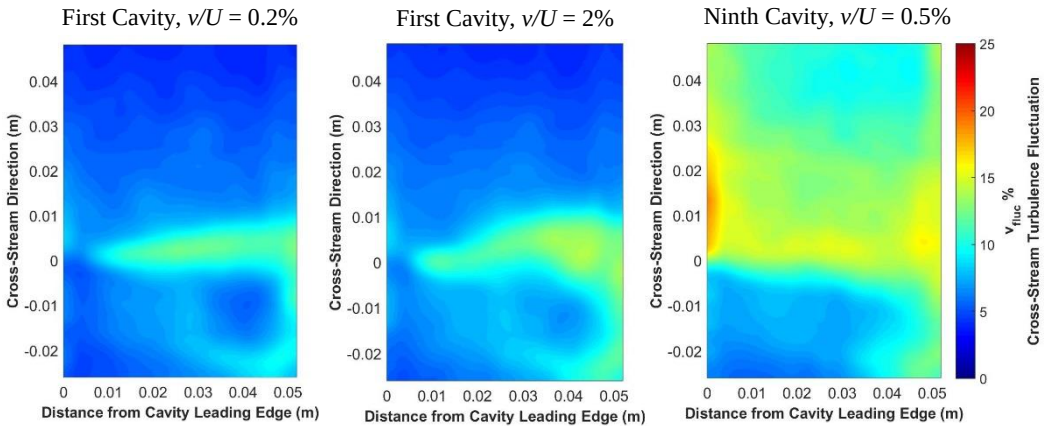

Figure C.17. Cross-stream turbulence fluctuation for the first cavity at *v/U* = 0.002 and 0.02 vs. the ninth cavity at *v/U* = 0.005